Development and Application of a High Throughput Methodology to Characterize and Formulate Protein-Based Therapeutics

By

Lei Hu

Submitted to the graduate degree program in Pharmaceutical Chemistry and the Graduate Faculty of the University of Kansas in partial fulfillment of the requirements for the degree of Doctor of Philosophy.

_____

Chairperson Dr. Russ Middaugh

_____

Dr. David Volkin

_____

Dr. Jennifer Laurence

_____

Dr. Susan Lunte

_____

Dr. Carey Johnson

Date Defended: 10/22/2012

The Dissertation Committee for Lei Hu

certifies that this is the approved version of the following dissertation:

Development and Application of a High Throughput Methodology to Characterize and Formulate Protein-Based Therapeutics

_____

Chairperson Dr. Russ Middaugh

_____

Dr. David Volkin

_____

Dr. Jennifer Laurence

_____

Dr. Susan Lunte

_____

Dr. Carey Johnson

Date Approved: 10/22/2012

Abstract

The conformational stability of a protein is a fundamental concern in formulating protein drug products, and development of analytical methods for stability characterization is critical for this purpose. Because of the complexity, relatively lower stability and variety of degradation pathways of protein molecules, the selection of appropriate analytical methods is important and needs to meet specific requirements for stability testing, screening formulations, as well as for product release. To characterize the stability of proteins comprehensively, the conformational stability of proteins is typically investigated using a variety of biophysical measurements as a function of environmental stresses such as pH and temperature. These multiple techniques typically require a variety of single function instruments. Each technique, however, provides information on only a particular aspect of a protein's higher order structural integrity (secondary, tertiary, and quaternary). The combination of different techniques provides a better understanding of the overall conformational stability of a protein, although these measurements typically require large sample quantities and long experimental times. Therefore, the development of high throughput methods to comprehensively characterize protein stability with a single multifunctional instrument is needed to save both materials and time.

In the first part of my work (Chapters 2-4), a new methodology is developed to obtain protein conformational stability data simultaneously, including UV absorption, light scattering, and near- and far- UV CD by employing a multimodal spectrometer (Chapter 2). Fluorescence spectral data are also collected on the same instrument although not

simultaneously. The method is developed by examining the thermal and pH stability of four model proteins. Results show reproducible and accurate data using this single instrument, and data collection is rapid with minimal protein sample requirements. This study also illustrates the application of this method for generating empirical phase diagrams (EPDs) to better characterize the overall conformational stability of proteins. This new approach facilitates the rapid characterization of protein structure and stability data in a single instrument. It is useful for analysis of unknown proteins, as well as screening of solution conditions to optimize stability for protein therapeutic drug candidates.

I also describe the application of this new method (Chapter 2) to characterize the stability of the recombinant anthrax protective antigen (rPA) and its 2-fluorohistidine (2-FHis) labeled analogue (Chapter 3). Protective antigen (PA) is a key, non-toxic component of the anthrax toxin. It is also a primary antigenic component of the current formaldehyde inactived anthrax vaccine. An analogue of PA has been recently shown to block key steps in pore formation in the process of inducing cytotoxicity in cells. Thus, it can potentially be used as an antitoxin or a vaccine. This analogue is synthesized by incorporating the unnatural amino acid 2-fluorohistidine (2-FHis). In this study, the effects of 2-FHis labeling on rPA antigen stability and its dynamic properties are investigated by various experimental techniques. Physical stability profiles of the two proteins (rPA and 2-FHis rPA) are created by using the empirical phase diagram (EPD) approach, and stability differences between them are identified. Results show that rPA and 2-FHis rPA have similar stability at pH 7-8. With decreasing pH, however, 2-FHis rPA is found to be more stable. Intramolecular dynamics sensitive measurements of the proteins at pH 5 find that 2-FHis rPA has increased internal

mobility under acidic pH conditions. The stability and dynamics characterization data provide information useful for the formulation development of 2-FHis rPA as a more stable antigen for vaccine development.

In addition, the new multimodal spectrometer method (Chapter 2) is coupled to other techniques such as SDS-PAGE, static light scattering, dynamic light scattering, isoelectric focusing, size-exclusion liquid chromatography as well as micro flow imaging to characterize the stability of dominant-negative inhibitor (DNI) protein (Chapter 4). DNI is a translocation-deficient mutant of PA with double mutations of K397D and D425K. It is a promising candidate for treatment or prevention of anthrax disease, which can potentially provide high immunogenicity in vaccines and therapeutic activity in antitoxic therapy. The lyophilized protein formulated with common excipients was stored for about 8 years at refrigerated temperature. In my study, samples were placed at two selected temperatures (40 and 70 ℃) for one to four weeks, and analyzed by the above mentioned methods. The chemical stability (deamidation) was also evaluated using capillary isoelectric focusing (cIEF). Results show that the thermally stressed DNI protein retained its native conformation at temperatures as high as 70 ℃ for one month. The long-term stability of DNI was also demonstrated for samples stored at 4 ℃ for about 8 years. These data provide valuable and encouraging information for development of an alternative recombinant anthrax vaccine using a mutated anthrax protective antigen.

In the second part of my work (Chapters 5, 6), the research focuses on stability characterization and formulation of a pneumolysin mutant (L460D), a candidate for a

pneumococcal vaccine (Chapter 5), and two virus-like particles (VLPs) as candidates for use against human filovirus infection (Ebola and Marburg, Chapter 6). In these studies, a three step experimental design is employed in the characterization and formulation processes. First, the conformational stability of the pneumolysin mutant and VLPs are characterized under stressed environmental conditions (pH 3-8 and temperature 10-87.5 ℃) by different analytical methods. Second, different types of biophysical data are summarized by using the empirical phase diagram (EPD) method, which is also used to define conditions for an excipients screening study. Finally, the pharmaceutical excipients are screened and potential stabilizers are identified by appropriate assays. In these studies, critical parameters (such as solution pH, temperature, ionic strength and stabilizers) affecting the stability of proteins are defined. These studies provide a basis for selection of optimized solution conditions for further long-term stability studies of pneumococcal antigens and Ebola and Marburg virus-like particles, and illustrate the utility of the multimodal spectrometer and EPD analysis for vaccine formulation development.

Lovingly dedicated to

my parents Sulan Lin and Zhongxiao Hu and my wife Shan Huang

ACKNOWLEDGEMENTS

Frist of all I want to express my sincere gratitude to my advisor **Dr. Russ Middaugh** for offer me the valualbe opportunity to study in his laboratory. With your tremendous help, instructions and patience for me, I learn and improve so much in the scientific area. Your eminent guidance and lectures went through my work and has made this thesis the way it looks like today.

I also want to give my sincere and grateful thanks to **Dr. Sangeeta Joshi** for her outsanding guidance, suggestions and help during the process of my study and life at KU. Unlimited thanks to the **Dr. David Volkin** for his constructive guidance and offer to share his invaluable practical and theoretical knowledge in the area of protein science.

I sincerely thank Dr. David Volkin, Dr. Jennifer Laurence, Dr. Carey Johnson, and Dr. Susan Lunte, my dissertation committee members for their valuable suggestions, time and help.

Thanks to all of the past and present lab members of the Middaugh and Volkin groups for thier help and friendship. Special thanks go to the Dr. Chris Olsen and Dr. Yuhong Zeng for their help and critical suggestions during the course of this work. Their furitful knowledge and strict science attitude impressed me very much.

I wish to extend my appreciation to all staff members, colleagues of the Department of Pharmaceutical Chemistry at KU and friends for their tireless help and support in one way or another.

Last but most importanly, I would like to express my most heartful thanks to my parents and my wife for their encouragement and moral support and beloved friends for their tireless and permanent help. To my daughters Bonnie and Claire, all of you make me life so wonderful!

TABLE OF CONTENTS

Chapter 1 Introduction 1

1.1 Overview of protein formulation 2

1.2 Specific aims and chapter summaries 5

1.2.1 Development of a high throughput method for biophysical characterization of protein stability 5

1.2.2 Application of the high throughput method for the biophysical characterization of protein stability. 8

1.2.3 Analytical characterization and adjuvant studies of dominant negative inhibitor as an anthrax vaccine 10

1.2.4 Physical characterization and formulation development of a recombinant pneumolysin mutant protein based pneumococcal vaccine 11

1.2.5 Biophysical characterization and conformational stability of Ebola and Marburg virus-like particles 12

1.3 References 12

Chapter 2 Development of a High Throughput Method for Biophysical Characterization of Protein Stability 15

2.1 INTRODUCTION 16

2.2 EXPERIMENTAL SECTION 19

2.2.1 Materials. 19

2.2.2 Instrumentation and Instrumental Conditions. 19

2.2.3.1 Optimization and Collection of Near UV CD Spectra of BSA. 20

2.2.3.2 Optimization and Collection of Near-far UV CD Spectra of Four Model Proteins. 20

2.2.3.3 Simultaneous Collection of CD and UV Absorbance Data to Determine the T_m of Four Model Proteins. 21

2.2.3.4 Collection of Intrinsic Fluorescence Thermal Data of Four Model Proteins. 21

2.2.4 Collection of Spectroscopic Data from Separate Instruments. 22

2.2.5 Empirical Phase Diagram 22

2.3 RESULTS AND DISCUSSION 23

2.3.1 Optimization and Collection of Near UV CD Spectra of BSA 23

2.3.2 Optimization and Simultaneous Collection of Near and Far UV CD Spectra of Model Proteins. 25

2.3.3 CD Thermal Unfolding Measurements. 27

2.3.4 Simultaneous UV Absorbance Measurements. 30

2.3.5 Intrinsic Fluorescence Measurements. 31

2.3.6 Empirical Phase Diagrams 32

2.4 CONCLUSIONS 33

2.5. ASSCOCIATED CONTENT 35

2.6 REFERENCES 35

Chapter 3 Application of the high throughput method for the biophysical characterization of protein stability 49

3.1 INTRODUCTION 50

3.2 MATERIALS AND METHODS 52

3.2.1 Materials 52

3.2.2 Biophysical Characterization 53

3.2.2.1 Far and Near UV Circular Dichroism Spectroscopy 53

3.2.2.2 Optical Density Measurements 54

3.2.2.3 Intrinsic Fluorescence Spectroscopy 54

3.2.2.4 Extrinsic Fluorescence Spectroscopy 54

3.2.2.5 Empirical Phase Diagram (EPD) 55

3.2.3 Dynamic Properties Measurements 55

3.2.3.1 High Resolution Ultrasonic Spectroscopy 55
3.2.3.2 Density 56
3.2.3.3 Red-Edge Excitation Shifts 56
3.3 RESULTS 57
3.3.1 Biophysical Characterization 57
3.3.1.1 Near and Far UV Circular Dichroism Spectroscopy 57
3.3.1.2 Intrinsic Fluorescence Spectroscopy 59
3.3.1.3 Optical Density Measurements 63
3.3.1.4 Extrinsic Fluorescence Spectroscopy 63
3.3.1.5 Empirical Phase Diagrams 65
3.3.2 Dynamic Properties Measurements 67
3.3.2.1 High Resolution Ultrasonic Spectroscopy (HR-US) 67
3.3.2.2 Red-Edge Excitation 68
3.4 DISCUSSION 70
3.5 ASSCOCIATED CONTENT 73
3.6 REFERENCES 73
Chapter 4 Analytical Characterization and Adjuvant Studies of Dominant Negative Inhibitor as an Anthrax Vaccine 80
4.1. INTRODUCTION 81
4.2 MATERIALS AND METHODS 83
4.2.1 Materials 83
4.2.2 Analytical Characterization 84
4.2.2.1 SDS-PAGE 84
4.2.2.2 Far and Near UV Circular Dichroism Spectroscopy 84
4.2.2.3 Intrinsic Fluorescence Spectroscopy 85

4.2.2.4 Optical Density Measurements 85
4.2.2.5 Static Light Scattering 86
4.2.2.6 Dynamic Light Scattering 86
4.2.2.6 Deamidation studies using capillary isoelectric focusing (cIEF) 86
4.2.2.7 Size-Exclusion Liquid Chromatography 87
4.2.2.8 Micro flow imaging 87
4.2.2 Adjuvant-Antigen study 88
4.3. Results 88
4.3.1 Anlytical Characterization 88
4.3.1.1 SDS-PAGE 88
4.3.1.2 Near and Far UV Circular Dichroism Spectroscopy 90
4.3.1.3 Intrinsic Fluorescence Spectroscopy 96
4.3.1.4 Optical density measurements 98
4.3.1.4 Static Light Scattering 100
4.3.1.5 Dynamic Light Scattering 100
4.3.1.6 Deamidation studies using capillary isoelectric focusing (cIEF) 102
4.3.1.7 Size-Exclusion Liquid Chromatography 105
4.3.1.8 Micro flow imaging 107
4.3.2 Adjuvant-Antigen study 107
4.3.2.1 Adsorption studies 107
4.3.2.2 Stability of DNI on the surface of Alhydrogel 110
4.4 CONCLUSIONS 111
4.5 REFERENCES 112
Chapter 5 Physical Characterization and Formulation Development of a Recombinant Pneumolysoid Protein based Pneumococcal Vaccine 113

5.1 Introduction 114
5.2 MATERIALS AND METHODS 116
5.2.1 Materials 116
5.2.2 Physical Characterization 117
5.2.2.1 Far-UV Circular Dichroism Spectroscopy 117
5.2.2.2 Intrinsic Fluorescence Spectroscopy 117
5.2.2.3 Extrinsic Fluorescence Spectroscopy 118
5.2.2.4 Static Light Scattering 118
5.2.2.5 Data Visualization Techniques 119
5.2.3 Excipient Screening 121
5.2.4 Adjuvant-Antigen Studies 122
5.2.4.1 Adsorption Study 122
5.2.4.2 Stability of L460D Pneumolysoid on the Surface of the Aluminum Hydrogel 123
5.3 Results 124
5.3.1 Physical Characterization 124
5.3.1.1 Far-UV Circular Dichroism Spectroscopy 124
5.3.1.2 Intrinsic Fluorescence Spectroscopy 124
5.3.1.3 Static Light Scattering 126
5.3.1.4 Extrinsic Fluorescence Spectroscopy 126
5.3.1.5 Data Visualization Techniques 127
5.3.2 Excipient Screening 128
5.3.3 Adjuvant-Antigen studies 136
5.3.3.1 Adsorption Study 136

5.3.3.2 Stability of L460D pneumolysoid on the Surface of the Aluminum Hydroxide Adjuvant....137

5.4 Summary and Discussion....140

5.5. ASSCOCIATED CONTENT....143

5.6 REFERENCES....143

Chapter 6 Biophysical Characterization and Conformational Stability of Ebola and Marburg Virus-like Particles....154

6.1 INTRODUCTION....155

6.2 MATERIALS AND METHODS....158

6.2.1 Generation of VLPs....158

6.2.2 Preparation of virus-like particles for biophysical analysis....158

6.2.3 Electron microscopy....159

6.2.4 Far-UV Circular Dichroism Spectroscopy....159

6.2.5 Intrinsic Fluorescence Spectroscopy....160

6.2.6 Extrinsic Fluorescence Spectroscopy....160

6.2.7 Static Light Scattering....161

6.2.8 Dynamic Light Scattering....161

6.2.9 Empirical Phase Diagrams....162

6.3 RESULTS....163

6.3.1Biophysical Characterization of Purified VLPs Produced in Insect Cells....163

6.3.2 Dynamic Light Scattering....166

6.3.3 Static Light Scattering....168

6.3.4 Far-UV Circular Dichroism Spectroscopy....170

6.3.5 Intrinsic Fluorescence....175

6.3.6 Extrinsic (Laurdan) Fluorescence....180

6.3.7 Empirical Phase Diagrams....183
6.4 DISCUSSION....185
6.5 REFERENCES....190
Chapter 7 Conclusions....195
7.1 Summary and Conclusions....196
7.2 Future Directions....201
7.3 References....204

Chapter 1 Introduction

1.1 Overview of protein formulation

Biopharmaceutical products represent a significant and growing proportion of the pharmaceutical industry, with more than 200 biopharmaceutical products presently on the market. The total global market for protein-based therapeutics is estimated to grow between 7% and 15% annually over the next several years.[1] Recombinant therapeutic proteins and monoclonal antibody-based (mAb-based) products represent the two biggest protein drugs categories, with an estimated market size of $61 billion for recombinant therapeutic proteins and $38 billion for mAb-based products in 2009.[2,3] These drugs are used to treat nearly 150 diseases, including cancer, infectious diseases, autoimmune diseases and AIDS/HIV1.[4] In 2010, 240 mAb products and 120 recombinant proteins were evaluated in clinical trials. Protein-based products are likely to represent four of the five top-selling drugs globally by 2013.[3,5] With the rapid increase in the biopharmaceutical market, the development of stable protein-based dosage forms is critical and a major challenge for pharmaceutical scientists.

One of the greatest challenges in the formulation development of protein products is minimizing their physical and chemical instabilities during manufacturing, storage, and administration. The structural complexity of protein drugs has a significant impact on the development of stable protein-based therapeutics and vaccines. Proteins differ from conventional small molecule chemically synthesized drugs with respect to many properties, such as size, shape, conformation, amphotericity and heterogeneity of structures.[6] The complexity of protein molecules means that there are many potential physical and chemical degradation pathways such as conformational changes including unfolding and aggregation, as well as chemical changes such as hydrolysis, deamidiation and oxidation, all of which can

shorten the drug's shelf life and decrease its potency.[7] Physical and chemical stresses such as temperature, pH, agitation, light, pressure, oxidants and certain solutes can all cause degradation of proteins, and hence, protein-based drugs.

To maintain the stability and activity of protein-based drugs during pharmaceutical development processes, a procedure name as "formulation" is performed. During this process, the protein of interest at the appropriate concentration is mixed with certain pharmacologically inactive ingredients (known as "excipients" when they are actually included in a formulation), which are used to enhance stability and solubility of drugs. Protein drugs are usually formulated in liquid solution or solid-state (e.g. lyophilized or spray drying) forms. The simplest and most economical way, however, is to develop a solution formulation. During liquid formulation development, the protein of interest is mixed with certain excipients in selected solution conditions. Formulation studies should address the effects of various factors such as temperature, solution pH, buffer ion, salt, protein concentration and excipients on stability, as well as their effects on solubility.[8] Although not addressed in the present work, other studies including photostability, agitation, and freeze-thaw cycling are also usually performed to evaluate the effect of other stresses. Preservative studies are also performed if the protein product is intended for multidose use with the preservative used to prevent microbial growth. Finally, material compatibility studies must be performed with containers or delivery or other medical devices to test the adsorption potential of a protein to surface present.[8,9] The stabilizing effects of the above factors can be monitored by a wide variety of different analytical methods. Because proteins are complex molecules and a variety of environmental stresses can produce instability in proteins, a

number of separate analytical methods such as described below must be applied for protein characterization and formulation processes.

An extensive physicochemical characterization of a protein forms the basis for the development of a stable formulation by using different analytical methods. The development of analytical methods usually starts with studies referred to as "preformulation". Preformulation studies are used to understand the physico-chemical characteristics of a protein molecule and better understand which formulation conditions would be most suitable to maintain the stability of proteins.[10] During preformulation, a wide variety of methods such as spectroscopic, hydrodynamic, calorimetric, electrophoretic, chromatography and mass spectrometry techniques are used to characterize the macromolecule systems. The selection of methods used for an individual protein is determined by the properties of the protein and the design criteria for the formulation.[10] This analysis should detect the most common degraded forms of proteins, such as an unfolded protein, soluble and insoluble aggregates, and chemical modified proteins through reactions such as hydrolysis, deamidation and oxidation. The wide range of the methods selected for such analyses will provide different types of information. Typical physical and biological properties monitored include[6,10]:

- Size: Studied by methods such as sodium dodecyl sulfate-polyacrylamide gel electrophoresis (SDS-PAGE), size exclusion chromatography (SEC), light scattering, analytical ultracentrifugation (AUC), and mass spectrometry (MS).
- Charge: Studied by methods such as isoelectric focusing (IEF), ion exchange chromatography (IEC) and Zeta-potential measurement.

- Conformation: Studied by methods like circular dichroism (CD), FTIR, ultra-violet (UV) absorbance, fluorescence, differential scanning calorimeter (DSC), SEC and MS.
- Biological activity: Studied by various types of bioassays and specific binding assays to molecular and cellular targets.

Changes in chemical properties can also be monitored by various analytical techniques. For example, deamidation of asparagine (Asn) and/or glutamine (Gln) side-chains is a common chemical change that can be monitored by IEF, IEC and MS techniques. Similarly, the oxidation of methionine and other amino acid residues can be detected by reverse-phase chromatography, hydrophobic interaction chromatography and MS techniques. Both types of analyses can now usually performed by a combination of LC and MS after proteolysis of a protein (peptide mapping). In summary, different techniques are used to characterize the stability of proteins comprehensively, and the selection of appropriate methods is critical for the development of stable drug formulations.

1.2 Specific aims and chapter summaries

1.2.1 Development of a high throughput method for biophysical characterization of protein stability

As described above, for preformulation studies, the physical stability of macromolecules is often investigated by a combination of various techniques that can provide insight into different types of protein structure (primary, secondary, tertiary and quaternary), although any one technique can only offer a limited amount of the desired information. Therefore, several techniques are usually combined to obtain a better understanding of the system. Commonly

used spectroscopic techniques include UV absorbance, near and far UV CD, FTIR spectroscopy, intrinsic and extrinsic fluorescence as well as various forms of light scattering measurements. These measurements of protein stability are often performed as a function of environmental stresses such as temperature, pH or unfolding agents. Under these stressed conditions, an accelerated stability study will provide useful information on the stability of proteins with respect to these stresses. These accelerated stability studies can help us evaluate the long-term stability of protein drugs under selected formulation, storage and processing conditions.

Spectroscopic experiments are typically performed on individual, single function instruments which can be quite expensive to purchase and maintain, and require large quantities of sample, and often result in long total data acquisition times. With the development of new technologies, multifunctional instruments are currently being developed by several vendors. One such instrument is the Applied Photophysics Chirascan-plus circular dichroism spectrometer which can acquire CD, UV absorption/optical density and fluorescence spectra. There is, however, no analytical method currently available to simultaneously acquire these spectroscopic data due to methodological constraints. For example, collecting both near and far UV CD data in a single spectroscopic scan has not been performed previously since the aromatic CD signals are much weaker than those in the peptide-sensitive far UV region.[11,12,13] Thus, near UV CD spectrum acquisition typically requires higher protein concentration and longer cell path lengths. Successful simultaneous collection of near and far UV CD, UV absorbance and fluorescence spectra would therefore require a suitable cell path length, protein concentration and instrument parameter settings.

Therefore, a new analytical method needs to be developed to collect different types of biophysical data simultaneously and thus save experimental sample and time.

In chapter 2, I propose a sensitive method using the Chirascan-plus instrument and a modest amount of protein sample to investigate protein stability by simultaneous collection of different types of data as a function of temperature (10-87.5^{o}C) and pH (3-8). The method was developed by examining the thermal and pH stability of four model proteins (bovine serum albumin (BSA), lysozyme, α-chymotrypsin and aldolase).[14] This method permits the collection of high quality near-far UV CD, UV absorption and optical density data simultaneously in a single sample run. Fluorescence emission spectra were also collected using this instrument in a subsequent experiment. Results demonstrate reproducible and accurate results from this single instrument, with rapid data collection and minimal protein sample requirements. The resulting method was sensitive, reproducible and robust when used to investigate the physical stability of proteins.

I also illustrate the application of this method to the generation of empirical phase diagrams (EPDs) to better characterize the overall conformational stability of proteins. The empirical phase diagram (EPD) was constructed as described previously[15-16] to summarize and facilitate the analysis of the complex data sets obtained. The EPD is used to identify coherent parameter regions that define protein structural states as a function of solution variables (temperature and pH in this case). The EPD approach has previously been applied to various macromolecule systems (e.g., proteins, DNA, viruses, and virus-like particles).[16] In brief, the normalized experimental data at each coordinate (i.e., at specific temperature and pH combinations) are first converted into an *N*-dimensional vector, where *N* refers to the

number of variables included (i.e., number of different types of data). The complete data sets from all measurements are then defined as multi-dimensional vectors in a temperature/pH phase space. Projectors of each individual vectors are calculated and summed into an $N \times N$ density matrix. By definition, an $N \times N$ matrix has N sets of eigenvalues and eigenvectors. By applying the principal components analysis, the individual vectors at each coordinate are truncated into 3-dimensional vectors and re-expanded into a new basis set consisting of the three eigenvectors corresponding to the three largest eigenvalues. The resultant 3-dimensional vectors are used to construct an empirical phase diagram using a red, green, and blue (RGB) color system. Regions of similar color indicate similar protein conformational states under the investigated conditions.

The newly developed methodology using simultaneous data collection linked to EPD analysis permits evaluation of protein conformational stability in a single process. The rapidly acquired data set provides a more complete assessment of a biomolecule's physical stability, including effects on secondary and tertiary structure as well as aggregation behavior, as a function of a variety of environmental stresses. This new approach facilitates the rapid characterization of protein structure and stability in a single procedure. It is useful for analysis of unknown proteins as well as for screening of solution conditions to optimize stability for protein therapeutic drug candidates.

1.2.2 Application of the high throughput method for the biophysical characterization of protein stability.

After successful method development in section 1.2.1, the multi-measurement method is used to characterize the stability of several macromolecular systems, including (1) anthrax

recombinant protective antigen (rPA) and its 2-fluorohistidine (2-FHis) labeled analogue (2-FHis rPA); (2) ricin toxin A-chain (RTA) and 22 of its single, double and triple mutants. My colleague Justin Thomas and I applied this new approach successfully to characterize the stability and differentiate stability differences between RTA and many of its mutants. Detailed information and results will be presented in future papers. The successful application of the method to the characterization of these vaccine candidates demonstrates the utility of the method for analysis of unknown proteins. The reproducibility, sensitivity and robustness of the method are also demonstrated.

Protective antigen (PA) is non-toxic but a key component of the anthrax toxin. It forms pores within the low pH environment of host endosomes, which is crucial for the pathogenesis of anthrax.[15,16,17] It is also a primary component of current and developing anthrax vaccines. A novel analogue of PA designated 2-fluorohisidine protective antigen was recently found to have the capability to block the key step of pore formation. The analogue was synthesized by incorporating the unnatural amino acid 2-fluorohistidine (2-FHis) into rPA.[18] This replacement was found to block low pH-induced pore formation with cells protected from the lethal effects of the toxin[19,20], suggesting that the 2-FHis rPA could potentially be used as an antitoxin or a vaccine to treat or prevent anthrax infections. In this study, we examined the effect of 2-fluorohistidine labeling of rPA on its stability and dynamics by the various spectroscopic and light scattering techniques described in section 1.2.1. Physical stability profiles of the two proteins (rPA and 2-FHis rPA) were created by using the empirical phase diagram (EPD) approach, and the stability differences between them were identified. Sensitive dynamic measurements of the proteins at pH 5 were also

performed using red edge excitation and high resolution ultrasonic spectroscopy techniques. The stability and dynamic characterization data provided information to better understand the similarities and differences of properties between the two proteins. These data were used to further the formulation development of the potential vaccine and/or antitoxin candidate 2-FHis rPA with regards to selection of optimized solution conditions.

1.2.3 Analytical characterization and adjuvant studies of dominant negative inhibitor as an anthrax vaccine

In Chapter 4, the stability of a dominant-negative inhibitor (DNI) based on rPA was characterized under stressed conditions at elevated temperatures. DNI is a translocation-deficient mutant of PA with double mutations of K397D and D425K.[21] This mutant strongly inhibits toxin action in cell culture and in an animal intoxication model, and is more immunogenic than PA in a mice study.[22] These previous results suggest that DNI has the potential to be used as an antitoxin and/or as a potent immunnogen for anthrax therapy. To evaluate the structural integrity of DNI after eight years of storage, an accelerated stability study was performed. In this study, samples were placed at two selected temperatures (40 and 70 ℃) for one to four weeks, and analyzed by different techniques. The lyophilized DNI proteins were reconstituted with water and then prepared in citrate phosphate buffers for biophysical characterization. Analytical methods include the techniques developed in section 1.2.1 and others such as SDS-PAGE, static light scattering, dynamic light scattering as well as micro flow imaging techniques. Results showed that the thermally stressed DNI protein retained completely native conformation to temperatures as high as 70 ℃ for one month. Long-term stability of DNI was also demonstrated after refrigerated storage for about 8 years.

Studies of DNI with aluminum adjuvants were further performed to study antigen/adjuvant interactions and the stability of DNI on the surface of the adjuvant. Because purified recombinant proteins are usually not highly immunogenic, an adjuvant is usually used to boost their immunogenicity.

1.2.4 Physical characterization and formulation development of a recombinant pneumolysin mutant protein based pneumococcal vaccine

In Chapter 5, the characterization and formulation development of a recombinant pneumolysin mutant protein was performed. *Streptococcus pneumoniae* (pneumococus) is a major cause of death, especially in children, due to fatal infections.[23,24,25] Pneumococus has more than 90 known serotypes, which vary by geographical location. Pneumolysin, a sulfhydryl-activated cytolytic toxin, is produced by all invasive strains of *S.pneumoniae* and considered a putative virulence factor.[26,27,28,29] It has been shown to be immunogenic[30,31] and has the potential to be used as a vaccine. To develop a stable pneumolysin vaccine, the conformational stability of a recombinant pneumolysin (L460D) was characterized by various spectroscopic and light scattering techniques over a wide pH and temperature range. Temperature/pH empirical phase diagrams (EPDs) of the pneumolysin was constructed to summarize the large volume of data generated. Excipient screening to identify protein stabilizers was performed using intrinsic fluorescence, static light scattering and differential scanning calorimetry (DSC). The stability of pneumolysin on the surface of alhydrogel was also examined in the presence and absence of excipients. Finally, an optimal formulation was identified which balances the physical stability of pneumolysin with its solution osmolality. This suggested formulation is now being used in animal studies.

1.2.5 Biophysical characterization and conformational stability of Ebola and Marburg virus-like particles

The filoviruses, Ebola (EBOV) and Marburg (MARV), cause severe hemorrhagic fever with up to 90% human mortality.[32,33,34] Virus-like particles of EBOV (eVLPs) and MARV (mVLPs) are attractive vaccine candidates, because they are safe, nonreplicating, easy to produce and can be used directly as immunogens.[35,36,37] To further the development of stable version of these vaccines, the conformational stability of these two enveloped VLPs produced in insect cells was characterized by various spectroscopic techniques over a wide range pH and temperature. Temperature-induced aggregation of the VLPs at various pH values was monitored by light scattering. Temperature/pH empirical phase diagrams (EPDs) of the two VLPs were constructed to summarize the large volume of data generated. The characterization data and conformational stability profiles from these studies provide a basis for selection of optimized solution conditions for further vaccine formulation and stability studies of Ebola and Marburg VLPs.

1.3 References

1. Hiller, A., Fast growth foreseen for protein therapeutics. *Genetic Engineering News* **2009,** *29*, 153-155.
2. Evers, P., The Future of the Biological Market *Bussiness Insights* **2010**.
3. Walsh, G., Biopharmaceutical benchmarks 2010. *Nature biotechnology* **2010,** *28* (9), 917-924.
4. Frokjaer, S.; Otzen, D. E., Protein drug stability: a formulation challenge. *Nature Reviews Drug Discovery* **2005,** *4* (4), 298-306.
5. Goodman, M., Market watch: Sales of biologics to show robust growth through to 2013. *Nature Reviews Drug Discovery* **2009,** *8* (11), 837-837.
6. McNally, E. J.; Hastedt, J. E., *Protein Formulation and Delivery* 2ed.; Informa Healthcare USA, Inc: New York 2007; Vol. 175, p 73-107.
7. Manning, M. C.; Chou, D. K.; Murphy, B. M.; Payne, R. W.; Katayama, D. S., Stability of protein pharmaceuticals: an update. *Pharmaceutical research* **2010,** *27* (4), 544-575.
8. McNally, E. J.; Hastedt, J. E., *Protein Formulation and Delivery* 2ed.; Informa Healthcare USA, Inc: New York 2007; Vol. 175, p 133-151.

9. Rathore, N.; Rajan, R. S., Current perspectives on stability of protein drug products during formulation, fill and finish operations. *Biotechnology progress* **2008,** *24* (3), 504-514.
10. McNally, E. J.; Hastedt, J. E., *Protein Formulation and Delivery*. 2 ed.; Informa Healthcare USA, Inc: New York 2007; Vol. 175, p 109-132.
11. Strickland, E. H.; Beychok, S., Aromatic contributions to circular dichroism spectra of protein. *Critical Reviews in Biochemistry and Molecular Biology* **1974,** *2* (1), 113-175.
12. Kahn, P. C., The interpretation of near-ultraviolet circular dichroism. *Methods in enzymology* **1979,** *61*, 339-378.
13. Kelly, S. M.; Price, N. C., The use of circular dichroism in the investigation of protein structure and function. *Current protein and peptide science* **2000,** *1* (4), 349-384.
14. Hu, L.; Olsen, C. M.; Maddux, N. R.; Joshi, S. B.; Volkin, D. B.; Middaugh, C. R., Investigation of Protein Conformational Stability Employing a Multimodal Spectrometer. *Analytical chemistry* **2011,** 83, 9399-9405.
15. Petosa, C.; Collier, R. J.; Klimpel, K. R.; Leppla, S. H.; Liddington, R. C., Crystal structure of the anthrax toxin protective antigen. *Nature* **1997,** 85, 833-838.
16. Collier, R. J.; Young, J. A. T., Anthrax toxin. *Annual review of cell and developmental biology* **2003,** *19* (1), 45-70.
17. Brey, R. N., Molecular basis for improved anthrax vaccines. *Advanced drug delivery reviews* **2005,** *57* (9), 1266-1292.
18. Eichler, J. F.; Cramer, J. C.; Kirk, K. L.; Bann, J. G., Biosynthetic incorporation of fluorohistidine into proteins in E. coli: a new probe of macromolecular structure. *ChemBioChem* **2005,** *6* (12), 2170-2173.
19. Wimalasena, D. S.; Cramer, J. C.; Janowiak, B. E.; Juris, S. J.; Melnyk, R. A.; Anderson, D. E.; Kirk, K. L.; Collier, R. J.; Bann, J. G., Effect of 2-fluorohistidine labeling of the anthrax protective antigen on stability, pore formation, and translocation. *Biochemistry* **2007,** *46* (51), 14928-14936.
20. Wimalasena, D. S.; Janowiak, B. E.; Lovell, S.; Miyagi, M.; Sun, J.; Zhou, H.; Hajduch, J.; Pooput, C.; Kirk, K. L.; Battaile, K. P., Evidence that histidine protonation of receptor-bound anthrax protective antigen is a trigger for pore formation. *Biochemistry* **2010,** *49*, 6973-6983.
21. Sellman, B. R.; Mourez, M.; Collier, R. J., Dominant-negative mutants of a toxin subunit: an approach to therapy of anthrax. *Science* **2001,** *292* (5517), 695-697.
22. Aulinger, B. A.; Roehrl, M. H.; Mekalanos, J. J.; Collier, R. J.; Wang, J. Y., Combining anthrax vaccine and therapy: a dominant-negative inhibitor of anthrax toxin is also a potent and safe immunogen for vaccines. *Infection and immunity* **2005,** *73* (6), 3408-3414.
23. Gray, B. M.; Converse, G. M.; Dillon, H. C., Epidemiologic studies of Streptococcus pneumoniae in infants: acquisition, carriage, and infection during the first 24 months of life. *Journal of infectious diseases* **1980,** *142* (6), 923-933.
24. Johnston Jr, R. B., Pathogenesis of pneumococcal pneumonia. *Review of Infectious Diseases* **1991,** *13* (Supplement 6), S509-S517.
25. O'Brien, K. L.; Wolfson, L. J.; Watt, J. P.; Henkle, E.; Deloria-Knoll, M.; McCall, N.; Lee, E.; Mulholland, K.; Levine, O. S.; Cherian, T., Burden of disease caused by Streptococcus pneumoniae in children younger than 5 years: global estimates. *The Lancet* **2009,** *374* (9693), 893-902.

26. Rubins, J. B.; Janoff, E. N., Pneumolysin: a multifunctional pneumococcal virulence factor. *Journal of Laboratory and Clinical Medicine* **1998,** *131* (1), 21-27.
27. Jedrzejas, M. J., Pneumococcal virulence factors: structure and function. *Microbiology and molecular biology reviews* **2001,** *65* (2), 187-207.
28. Mitchell, A.; Mitchell, T., Streptococcus pneumoniae: virulence factors and variation. *Clinical Microbiology and Infection* **2010,** *16* (5), 411-418.
29. Molloy, S., Bacterial pathogenicity: Pneumolysin: stimulating protection. *Nature Reviews Microbiology* **2010,** *9* (1), 4-4.
30. Paton, J. C.; Lock, R. A.; Hansman, D. J., Effect of immunization with pneumolysin on survival time of mice challenged with Streptococcus pneumoniae. *Infection and immunity* **1983,** *40* (2), 548-552.
31. Lock, R. A.; Hansman, D.; Paton, J. C., Comparative efficacy of autolysin and pneumolysin as immunogens protecting mice against infection by Streptococcus pneumoniae. *Microbial pathogenesis* **1992,** *12* (2), 137-143.
32. Feldmann, H.; Klenk, H. D., Marburg and Ebola viruses. *Advances in Virus Research* **1996,** *47*, 1-52.
33. Sanchez, A.; Khan, A.; Zaki, S.; Nabel, G.; Ksiazek, T.; Peters, C., Filoviridae: Marburg and Ebola viruses. *Fields virology* **2001,** *1*, 1279-1304.
34. Feldmann, H.; Jones, S.; Klenk, H.; Schnittler, H., Ebola virus: from discovery to vaccine. *Nature Reviews Immunology* **2003,** *3* (8), 677-685.
35. Warfield, K.; Swenson, D.; Demmin, G.; Bavari, S., Filovirus-like particles as vaccines and discovery tools. *Expert Review of Vaccines* **2005,** *4* (3), 429-440.
36. Yang, C.; Ye, L.; Compans, R., Protection against filovirus infection: virus-like particle vaccines. *Expert Review of Vaccines* **2008,** *7* (3), 333-344.
37. Bukreyev, A.; Collins, P., Filovirus vaccines: what challenges are left? *Expert Review of Vaccines* **2010,** *9* (1), 5-8.

Chapter 2 Development of a High Throughput Method for Biophysical Characterization of Protein Stability

2.1 INTRODUCTION

One of the greatest challenges in the formulation development of protein-based therapeutics and vaccines is minimizing their physical and chemical instabilities during manufacturing, storage and administration.[1,2] Protein instability can lead to problems such as aggregation and chemical degradation that can shorten the drug's shelf life and decrease potency. The physical stability of macromolecules is often investigated by a combination of various spectroscopic and calorimetric techniques that each provides a certain insight into the behavior of different types of protein higher-order structure (secondary, tertiary and quaternary). Therefore, several techniques are usually combined to obtain a better understanding of the overall conformational stability of a protein. Commonly used spectroscopic techniques include ultra-violet (UV) absorbance, near and far UV circular dichroism (CD), FTIR spectroscopy, intrinsic and extrinsic fluorescence as well as various forms of light scattering measurements. These measurements of protein stability are often performed as a function of environmental stresses such as temperature, pH or unfolding agents.

Spectroscopic experiments are typically performed on individual, single function instruments which can be quite expensive to purchase and maintain, require large quantities of sample, and often result in long total data acquisition times. With the development of new analytical technologies, however, measurements previously performed on separate instruments can now potentially be performed on a single device. Such multifunctional instruments are currently being developed by several vendors. One such instrument is the Applied Photophysics Chirascan-plus circular dichroism spectrometer, which can acquire CD,

UV absorption/optical density and fluorescence spectra, although currently it is primarily used for CD applications.

There is, however, no currently available method to simultaneously acquire these spectroscopic data due to methodological constraints. For example, collecting both near and far UV CD data in a single spectroscopic scan has not been performed previously since the aromatic CD signals are much weaker compared to the peptide-sensitive far UV region.[3-5] Thus, near and far CD measurements must be performed separately. Typical cell path lengths used for far UV CD measurements are in the range of 0.01 to 0.1 cm with protein concentrations between 0.1 to 1.0 mg/ml. In contrast, the near UV region requires a typical path length of 0.5 to 2 cm and protein concentrations of 0.5 to 2.0 mg/ml.[4]

Successful simultaneous collection of near and far UV CD, UV absorbance and fluorescence measurements would therefore require a suitable cell path length, protein concentration and instrument parameter settings. In principal, it is difficult to find an acceptable tradeoff between concentration and cell path length, because both parameters have the same effect on absorbance. Longer path lengths and higher concentrations produce excess absorbance, which can lead to photomultiplier tube saturation and absorption flattening among other potential problems. In contrast, shorter path lengths and lower concentrations yield too little signal to permit collection of quality near UV CD and UV absorbance spectra. In fact, simultaneously collected near and far UV CD spectra during a single spectral run have never been successfully accomplished to the best of our knowledge.

In this work, we propose a sensitive method using the Chirascan-plus instrument and a modest amount of protein sample to investigate protein stability by simultaneous data

collection of different types of information as a function of temperature and pH. This method permits the collection of high quality CD data in the near and far UV regions in a single sample run. We also use this method to simultaneously collect high resolution UV absorption spectra and light scattering data by measuring the optical density at 350 nm. Fluorescence emission spectra were also collected using this instrument in a subsequent experiment. The large sets of data obtained were combined into an "empirical phase diagram" (EPD) that summarizes all of the data collected into a form of colored diagram which displays structural changes induced by environmental stresses such as pH, temperature, protein concentration and solution ionic strength. The EPD approach has previously been applied to various macromolecule systems (e.g., proteins, DNA, viruses, and virus-like particles).[6] The newly developed methodology using simultaneous data collection linked to EPD data analysis permits evaluation of protein conformational stability in a single process, enabling the acquisition of maximal information from a minimum amount of sample and experimental time. This rapidly acquired data set provides a more complete assessment of a biomolecule's physical stability, including effects on secondary and tertiary structure as well as aggregation behavior, as a function of a variety of environmental stresses. The collection and evaluation of large data sets of lower-resolution biophysical data by high throughput methods offers an alternative, more generally accessible practical approach to rapidly evaluate protein structural integrity compared to higher resolution techniques such as X-ray crystallography and NMR. From a pharmaceutical perspective, this approach also offers the advantages of examining protein conformational stability in different formulation buffers in a high throughput manner with low sample requirements.

2.2 EXPERIMENTAL SECTION

2.2.1 Materials.

Four well characterized model proteins were used including bovine serum albumin (BSA), lysozyme (chicken egg white), α-chymotrypsin (bovine pancreas) and aldolase (rabbit muscle). Their secondary structure contents range from α-helix dominant to β-structure rich and their thermal transition temperatures vary from high to low (Supplemental Table 1). Proteins were purchased from Sigma-Aldrich (St. Louis, MO). Protein samples were prepared in 20 mM citrate phosphate buffer ranging from pH 3 to 8, at one pH unit intervals with the exception of aldolase which was prepared in the same buffer ranging from pH 5 to 8 (due to irreversible unfolding at pH values less than 4.5[7,8]). The ionic strength of the solutions was adjusted to 0.15 with sodium chloride. Samples of lysozyme, α-chymotrypsin and aldolase were dialyzed at 4 ^{o}C using Slide-A-Lyzer dialysis cassettes (Thermo Scientific, Rockford, IL) with a 3.5 kDa MW cutoff before measurements. BSA samples were prepared by dissolving sample into a specific pH citrate phosphate buffer, because of its high purity (≥98%).

2.2.2 Instrumentation and Instrumental Conditions.

CD, UV absorbance, optical density (OD) at 350 nm and fluorescence measurements were performed with the Chirascan-plus Circular Dichroism Spectrometer (Applied Photophysics Ltd, Leatherhead UK). The design features of the Chirascan-plus include a unique F/7 dual polarizing double prism monochromator and a solid state detector which permit higher light throughput and better detector quantum efficiency. Both of these factors contribute to improved signal to noise ratios. This instrument is equipped with a Peltier temperature controller and a 4-position cuvette holder. UV absorption spectra, light scattering

(OD at 350 nm), as well as near and far UV CD data were collected simultaneously. In a separate experiment, fluorescence emission spectra were also collected on this instrument.

2.2.3.1 Optimization and Collection of Near UV CD Spectra of BSA.

Instrument and sample parameters were investigated to optimize cell path length and protein concentration (Supplemental Table 2). Near UV CD spectra of BSA were collected in the range of 250-320 nm with a sampling time per wavelength of 4 sec and step size of 0.5 nm. Filters were placed in front of the CD cell holders on the incident light direction. Criteria for spectra improvement included evaluation of peak resolution and signal to noise ratios. The initial optimized parameters obtained from BSA were selected as a starting point for evaluation of the other model proteins. Buffer blank scans were subtracted from BSA sample scans for linearity calculations. For the simultaneous near-far UV CD measurements described below, buffer blanks were not used since fluctuations in signal intensity from buffer scans may obscure some of the weak, finely structured peaks in the near UV region.[5]

2.2.3.2 Optimization and Collection of Near-far UV CD Spectra of Four Model Proteins.

To optimize protein concentration (0.2, 0.3, 0.4 and 0.5 mg/mL), the near and near-far UV CD spectra of BSA, lysozyme and α-chymotrypsin were collected separately at pH 7. Two instrumental parameters (step size and sampling time per wavelength) were optimized to reduce the measurement time without loss in reproducibility of the finely structured peak information in the near UV. The CD spectra of protein at pH 7 were recorded as a function of temperature (10 to 87.5 ℃) at 2.5 ℃ intervals. Further optimization of sampling time, step size, and protein concentration was carried out by evaluating the thermal transition midpoint temperature (T_m) of the model proteins. T_m values were calculated using a Boltzmann function to produce a

sigmoidal curve using Origin 8.1 software.

2.2.3.3 Simultaneous Collection of CD and UV Absorbance Data to Determine the T_m of Four Model Proteins.

Near and far UV CD spectra of BSA (0.55 mg/mL), lysozyme (0.4 mg/mL), α-chymotrypsin (0.4 mg/mL) and aldolase (0.5 mg/mL) were collected from 200 to 360 nm using a 0.2 cm path length cuvette. An optimized sampling time of 3 sec, bandwidth of 1 nm, and step size of 1 nm were used, along with a heating rate of 1 ℃/min and equilibration time of 1 min at each temperature. The CD spectrum of each protein was recorded in triplicate as a function of temperature (10 to 87.5 ℃) and pH (3 to 8), except for aldolase samples which were measured from pH 5 to 8. In the data analysis, specific CD signals (peaks) in the near and far UV regions were monitored and smoothed using the Savitsky-Golay method (window size 3) using the Pro-Data Chirascan 4.1 (Applied Photophysics Ltd.) software. The T_m value was calculated using a non-linear curve fit (Boltzmann function) of thermal unfolding curves executed in *Origin 7.0* software. The UV absorbance spectrum and light scattering data (OD 350 nm) were obtained simultaneously with the CD spectrum using the same experimental parameters.

2.2.3.4 Collection of Intrinsic Fluorescence Thermal Data of Four Model Proteins.

The Chirascan-plus Circular Dichroism Spectropolarimeter has a fluorescence detector mounted at 90^o that can measure emission spectra. In separate experiments, the intrinsic fluorescence of the four model proteins was monitored using the same concentrations and temperature ramp program used in the CD measurements (section 2.3.3). Dual path length quartz fluorometer cells with an interior width (2 mm) and length (10 mm)

were used, and excitation of the proteins was carried out along the shorter path length axis (2 mm). Samples were measured in triplicate using an excitation wavelength of 295 nm (>95% tryptophan emission). Emission spectra were collected from 310 to 400 nm using a 1nm step size. The excitation and emission slits were set at 3 and 9 nm, respectively. The position of the emission wavelength maximum was determined using a polynomial derivative fitting method executed in *Origin 7.0* software.

2.2.4 Collection of Spectroscopic Data from Separate Instruments.

Various spectroscopic data from individual instruments were collected with BSA over the same temperature and pH ranges, and protein concentration (0.55 mg/ml), as employed above. Far-UV CD spectra were collected with a Jasco-810 Spectrophotometer (Jasco Inc., Easton, MD). Near-UV CD data were collected in the Chirascan-plus instrument. The intrinsic fluorescence spectra of BSA were measured using QuantaMaster Spectrofluorometer (Photon Technology International Inc., Birmingham, NJ). Optical density measurements were obtained using a Cary 100 UV-Visible Spectrophotometer (Varian Inc., Palo Alto, CA) with a cell path length of 1 cm. The same cells were used in the Chirascan experiments to minimize cell variability.

2.2.5 Empirical Phase Diagram

Empirical phase diagrams (EPDs) can be used to summarize the large amounts of data generated from multiple techniques and to visualize macromolecular stability as a function of various stress variables. A detailed description of EPD construction and interpretation is described elsewhere.[6] EPDs are used to identify coherent parameter regions that define similar structural states. Regions of similar color correlate similar protein structures such as

native, molten globule, or aggregated states. Transitions between states are manifested as changes in colors; apparent phase boundaries can be identified based on color changes. Specific colors, however, do not possess meaning other than to identify areas of different protein behavior.

2.3 RESULTS AND DISCUSSION

2.3.1 Optimization and Collection of Near UV CD Spectra of BSA

Optimization of concentration, path length and other instrumental parameters was first performed with BSA to obtain high-quality near CD spectra. Typical near UV CD spectra of BSA at different protein concentrations (0.2, 0.4, 0.6, 0.8 and 1.0 mg/ml) and cell path lengths (10, 4, and 2 mm) are shown in Figures 1A and 1C, respectively. There are two distinct minima at 261.5 and 268.5 nm observed in the near UV CD spectrum of BSA. These peaks arise from phenylalanyl side chains.[9,10] As expected, CD signals decrease with decreasing protein concentration and cell path length. Although the near UV CD bands are weak, they are well resolved (Figure 1D). The repeatability of the triplicate measurements showed spectral overlap with each other after data smoothing. Similar experiments were also performed at 0.2 mg/ml BSA in a 2 mm (Figure 1B) and 0.4 mg/ml BSA in a 1 mm path length cell, but CD bands under these conditions were not always adequately resolved and had poor reproducibility. Signal to noise ratio was also low (e.g. CD peak at 268.5 nm in Figure 1B).

The linearity of the CD signals at different BSA concentrations using the 2 mm path length cell (Figures 1E and 1F) was excellent (r^2= 0.997, at both 261.5 and 268.5 nm). The linearity of the CD signals at different cell path lengths using 0.4 mg/ml BSA (Figures 1G and

1H) was also excellent (r^2= 0.999, at both 261.5 and 268.5 nm). Increases in bandwidth had no apparent effect on the intensity of the CD signal, but some differences in spectral shape were observed. For example, the CD spectrum using a 4 nm bandwidth lost fine structure compared with that using a smaller bandwidth, while decreasing the bandwidth to 0.5 nm decreased the signal to noise ratio (Supplemental Figure 1).

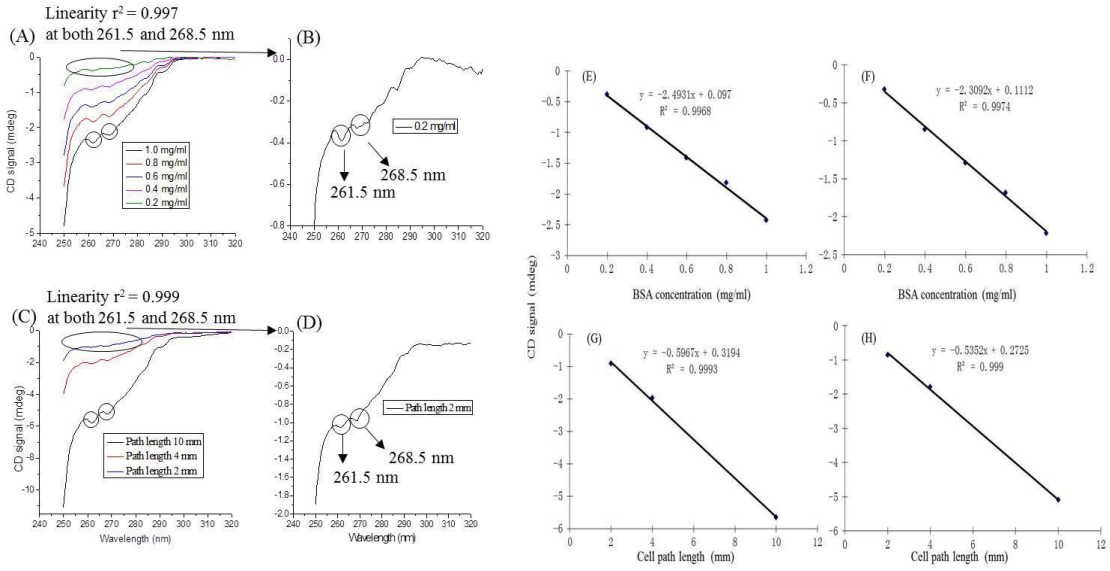

Figure 1. Near-UV CD spectra of BSA. (A): Different BSA concentrations with 2 mm cell path length. (B): 0.2 mg/ml BSA shown separately with an expanded view. (C): Different cell path lengths at 0.4 mg/ml BSA. (D): 0.4 mg/ml BSA using 2 mm cell path length shown separately with an expanded view. The linearity plots are shown from Figures 1E to 1H. The bandwidth was 1 nm. Linearity was calculated from data as described in text.

Based on these results, the experimental parameter combination of protein concentration (0.4 mg/ml), cell path length (2 mm), sampling time (4 sec), step size (0.5 nm) and 1 nm bandwidth produced optimally well-resolved and reproducible CD peaks (Figure 1D). Although higher protein concentrations and longer cell path lengths can increase the CD signal in the near UV region, these changes negatively impact the far UV CD signal due to high absorption.

2.3.2 Optimization and Simultaneous Collection of Near and Far UV CD Spectra of Model Proteins.

Besides tertiary structural information obtained in the near UV CD data described above, the far UV region of a CD spectrum (190-250 nm) primarily contains signals from peptide bond absorption and thus provides information about the secondary structure of a protein.[4] The combined near and far UV CD spectra of three model proteins (BSA, lysozyme and α-chymotrypsin) at different concentrations (0.2, 0.3, 0.4 and 0.5 mg/ml) were collected using the optimized experimental parameters described above. At the lowest concentration tested (0.2 mg/ml), the CD signals for each protein were not always well resolved (data not shown). At higher protein concentrations, good quality CD spectra were obtained covering both far and near UV regions in a single run, although lysozyme and α-chymotrypsin possessed lower signal-to-noise ratios (in the range of 200-210 nm at 0.5 mg/ml).

Two instrumental parameters (sampling time per wavelength and step size) were also further optimized to reduce overall scanning times. When sampling time was changed from 4 to 3 to 2 seconds (at 1 mg/ml protein), protein thermal transition (T_m) values for three model proteins were both precise and accurate (data not shown). At lower protein concentrations (0.4 or 0.3 mg/ml), T_m values of the three model proteins were reproducible with the exception of the 2 second integration times (data not shown). After choosing a suitable sampling time (3 sec), the effect of increasing the step size from 0.5 to 1.0 nm was investigated. Two different protein concentrations were compared for BSA (0.6 and 0.5 mg/ml) and lysozyme and α-chymotrypsin (0.3 and 0.4 mg/ml). Reproducibility of results was not lost by decreasing sampling time and increasing step size, and overall results showed CD signals had excellent precision at lower protein concentrations. Typical protein stability (T_m) results for BSA with these different

experimental variables are summarized in Supplemental Table 3.

After optimization, final parameters are as follows: cell path length of 2 mm, sampling time of 3 sec, step size of 1 nm, and bandwidth of 1 nm. The concentration may vary from 0.4 to 0.6 mg/ml depending on the value of a protein's extinction coefficient. Typical near-far UV CD spectra of the four model proteins at 0.4 or 0.5 mg/ml and 10 ℃ are shown in the Figure 2. In the far UV region (190-250 nm), CD spectra of both BSA and aldolase (Figures 2A and G) manifest a strong double minimum at approximately 222 and 208-210 nm, consistent with both proteins containing the predicted significant amounts of α-helix. Lysozyme (Figure 2C) also showed two negative CD bands at 222 and 209 nm, but the 209 nm band has a larger intensity than the 222 nm signal suggesting the presence of both α-helices and β sheets.[11,12] The CD spectrum of α-chymotrypsin (Figure 2E) contains two negative CD bands near 207 and 230 nm, which are characteristic of β-II proteins.[11,13] α-chymotrypsin belongs to the β-II protein class and contains a significant amount of β-sheet structure which is either highly distorted or made up of short, irregular β strands.

In the near UV region (250-320 nm), contributions of aromatic side chains are often utilized as sensitive probes of protein conformation. Additionally, distinctive vibronic fine structures make it possible in many cases to assign specific features in the near-UV CD to particular types of amino acid residues. In Figure 2 (Figures 2B, D, F, H), several distinct CD bands of the four model proteins are present in this near UV region. Generally, the CD bands at 262, 266 and 269 nm arise from the phenylalanyl side chains and the band near 282 nm from tyrosyl residues. The CD bands at 288 and 289 nm can be attributed to tryptophanyl and/or tyrosyl side chains while the CD band near the 296 nm arises from indole groups.[5]

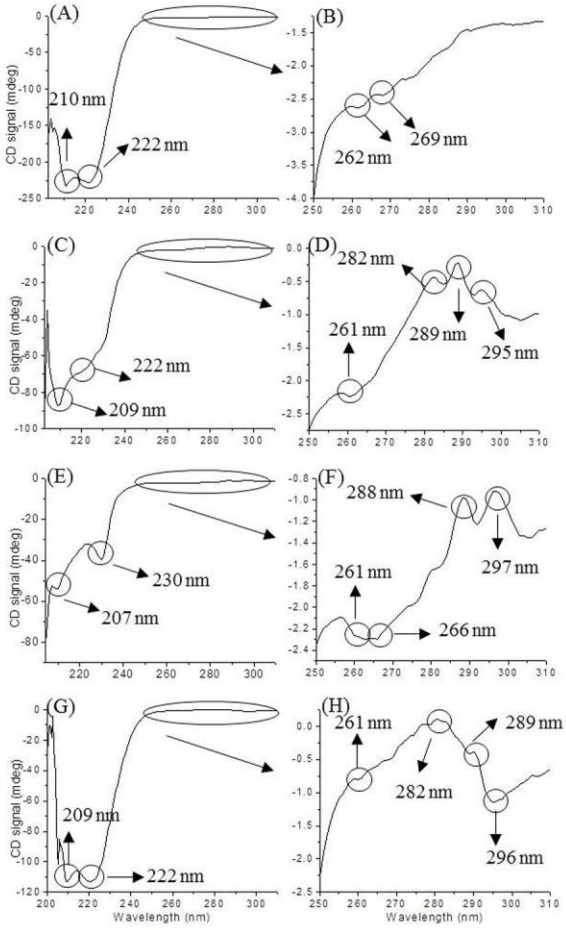

Figure 2. Near and far UV CD spectra for four model proteins collected simultaneously. Near-far UV CD spectra of (A) 0.55 mg/ml BSA and (B) expanded view of its near UV region; (C) 0.4 mg/ml lysozyme and (D) expanded view of its near UV region; (E) 0.4 mg/ml chymotrypsin and (F) expanded view of its near UV region; (G) 0.4 mg/ml aldolase and (H) expanded view of its near UV region.

2.3.3 CD Thermal Unfolding Measurements.

Using the optimized instrument and sample parameters described above, the physical stabilities of the model proteins were investigated as a function of pH and temperature employing the multimodal spectrometer. These experiments used only 200-250 µg of protein sample and near- and far-UV CD data were collected simultaneously in about 4.5 hours (200-360 nm from 10 to 87.5 ℃). Typical thermal unfolding curves of BSA and three other proteins at pH 7 are shown in Figure 3 and Supplemental Figures 2-4, respectively. Triplicate

measurements produced good reproducibility as indicated by the error bars. As expected, the model proteins lose both secondary and tertiary structure with increasing temperature. Based on the observed effects on the T_m of model proteins, as monitored in both the near and far UV regions of the CD spectra, the order of protein stability was as follows: α-chymotrypsin < aldolase < BSA < lysozyme (Table 1). The estimated T_m values for each model protein were very similar to those obtained in previous work.[14-17] For BSA, lysozyme and α-chymotrypsin, similar T_m values were obtained from both near and far UV regions. For aldolase, the T_m value evaluated from the far UV CD was higher than those obtained in the near UV region, suggesting that a molten globule like state exists between these temperatures. Molten globules generally possess native-like secondary structure but lack significant tertiary structure.

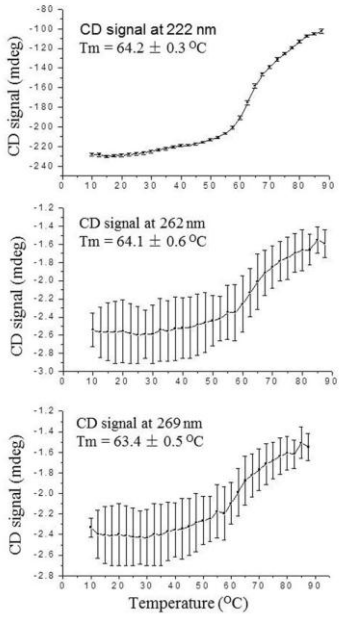

Figure 3. Thermal stability of BSA (0.55 mg/ml at pH 7) as monitored by CD signals at 222, 262 and 269 nm as a function of temperature. Each data point represents the mean of three independent runs with error bars showing the standard deviation. The T_m value was calculated separately then averaged and standard deviation determined.

Protein	T_m (far UV CD) (^OC)	T_m (near UV CD) (^OC)	T_m (literature) (^OC)
BSA	64.2 ±0.3	64.1 ±0.6 (262 nm) 63.4 ±0.5 (269 nm)	61.8[15] a
Lysozyme	75.5 ±0.4	73.6 ±0.4 (261 nm) 75.6 ±0.5 (282 nm) 75.7 ±1.1 (289 nm) 76.3 ±1.3 (295 nm)	74.0[16] a
Chymotrypsin	46.0 ±0.5	46.3 ±0.5 (261 nm) 46.0 ±0.7 (266 nm) 48.6 ±0.5 (288 nm) 47.1 ±1.2 (297 nm)	44.0[17] b
Aldolase	53.9 ±0.3	46.1 ±0.6 (261 nm) 46.4 ±0.6 (282 nm) 47.3 ±0.4 (289 nm) 46.7 ±0.8 (296 nm)	55.7[18] a

a: differential scanning calorimetry.
b: visible/ultraviolet spectrophotometer.

Table 1. Thermal unfolding midpoint temperatures (T_ms) for the model proteins BSA (0.55 mg/ml), lysozyme (0.4 mg/ml), chymotrypsin (0.4 mg/ml), and aldolase (0.5 mg/ml) as determined by simultaneous data collection from near and far UV CD measurements. These experimentally measured T_m values are compared to T_m values obtained from the literature. There are several different T_m values obtained in the near UV CD region by monitoring characteristic CD peaks. Experimental parameters are (1) Sampling time per wavelength, 3 sec. (2) Step size, 1.0 nm.

2.3.4 Simultaneous UV Absorbance Measurements.

Ultraviolet absorption spectroscopy can also be used to provide information concerning protein tertiary structure. By employing second derivative spectra, the overlapping peaks of phenylalanine, tyrosine, and tryptophan residues in the 250-300 nm range can be resolved at high resolution.[18] Typical second derivative UV absorbance results for 0.4 mg/ml α-chymotrypsin are shown in Supplemental Figure 5. The thermal response of all three major derivative peak positions showed good reproducibility. For α-chymotrypsin, the T_m values obtained from UV absorption measurements (47.2 ± 0.6, 46.9 ± 0.8 and 45.6 ± 1.1 ^oC) are very similar to those obtained by near UV CD measurements (46.3 ± 0.5, 46.0 ± 0.7, 47.1 ± 1.2 and 48.6 ± 0.5 ^oC). In contrast to these results, the other three model proteins did not display reproducible results due to low UV absorbance under the experimental conditions employed (data not shown).

Ultraviolet spectroscopy can also be used to monitor the aggregation behavior of a protein by recording the optical density in a non-absorbing region of a protein's UV spectrum (>320 nm). Increased scattering intensity is usually a consequence of protein association behavior. BSA and lysozyme showed aggregation behavior that was pH dependent with increased OD signals appearing at pH 5 and 7-8, respectively. Aldolase manifested aggregation behavior over the entire pH range from pH 5 to 8, while no aggregation was observed for α-chymotrypsin from pH 3 to 8 (data not shown). Typical optical density results as a function of temperature for BSA and other two model proteins at selected solution pH values are shown in Figure 4A and Supplemental Figure 6, respectively.

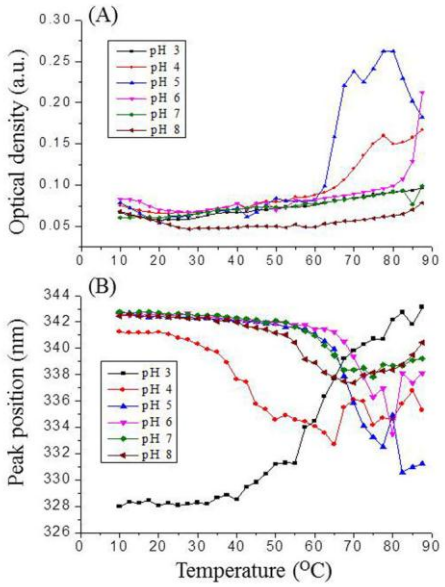

Figure 4. Thermal stability of BSA (0.55 mg/ml) as a function of solution pH. (A) Optical density at 350 nm, and (B) Intrinsic Trp fluorescence emission maximum (peak position). Each data point represents the mean of three independent samples.

2.3.5 Intrinsic Fluorescence Measurements.

Intrinsic fluorescence spectroscopy is another common method employed for examining the tertiary structure of proteins. Proteins containing tryptophan typically produce strong fluorescence emission in the 310-355 nm region with the position of emission maximum very sensitive to the polarity of the indole side chain environment.

Temperature dependent tryptophan fluorescence peak position shifts were observed for BSA and the three other proteins as a function of temperature and pH (Figure 4B and Supplemental Figure 7, respectively). In general, a red shift in the position of a Trp fluorescence maximum indicates increased exposure of Trp residues to a more polar environment, and thus a structural change resulting in partial unfolding of the protein. The fluorescence thermal unfolding results are overall consistent with the observations made from the CD and UV absorption measurements with similar effects of pH and temperature seen on the stabilities of

the proteins observed. From these data, it can be seen that BSA, lysozyme, α-chymotrypsin and aldolase showed the highest thermal stability at solution pH values of 6, 5, 5-6 and 7-8, respectively.

2.3.6 Empirical Phase Diagrams

Empirical phase diagrams of the four proteins were generated from the experiments described above and used to summarize all of the biophysical data collected. Using the Chirascan-plus instrument, the biophysical data were obtained simultaneously in a single scan at the individual temperature and pH values (with the exception of fluorescence which was collected subsequent to the simultaneous collection of near-far CD, UV and light scattering measurements). These results were then compared to EPDs generated from data collected on individual instruments. The EPDs of BSA generated from either a single instrument or by separate instruments are compared in Figure 5. The EPD from near and far UV CD data only (Figure 5A) show very similar defined "apparent" phases when compared with more comprehensive EPDs (Figures 5B-C) including CD, optical density and fluorescence data. EPDs produced from separate instruments (Figures 5D-F) are also very similar to those produced by the simultaneous methodology (Figures 5A-C), and show that data from a single multi-function instrument can provide similar results to those obtained from multiple single function instruments.

There are two clear phases existing at low temperature for BSA, as shown in Figure 5A. In region 1, samples at pH 4-8 manifest a similar color below about 65 ℃, indicating a similar conformation of BSA. Samples at pH 6 show the highest thermal stability, and samples at pH 4 show the lowest stability. In region 2, samples at pH 3 show a distinct color difference from

region 1 indicating the presence of altered structure compared to BSA in region 1. The distinction between region 1 and 2 and those at elevated temperature is evident with an apparent phase boundary around 65 ^{o}C at pH 6 which decreases as pH is increased or decreased from this value. Samples in the high temperature region are highly structurally altered or aggregated.

The EPDs were generated for the other three model proteins using the single instrument (Supplemental Figure 8). The EPDs generated from the near and far UV CD data alone or produced from combined data from CD, fluorescence, optical density and UV absorbance 2nd derivative methods were also compared. Interestingly, all three proteins show similar and clearly defined "apparent" structural phase changes in both CD and comprehensive EPDs. For aldolase, region 4 (green color covering the region from pH 5 to 8) indicates the presence of a molten globule-like conformational state during the protein unfolding process. This observation is in agreement with the different T_m results obtained in CD measurements (Table 1).

2.4 CONCLUSIONS

Using four model proteins, a reproducible, accurate and sensitive method was developed to acquire near and far UV CD spectra simultaneously in a single sample. In addition, turbidity data and in some cases high resolution UV absorption data can also be obtained at the same time. Fluorescence capability was also demonstrated. Thus, different types of spectroscopic data can be obtained in a single set of experiments and used to investigate protein stability as a function of various types of environmental stresses (pH and temperature in this case). This method permits minimal use of protein, and thus saves material, time and resources. A complete, reproduced conformational stability profile of a protein as a function of pH and temperature can

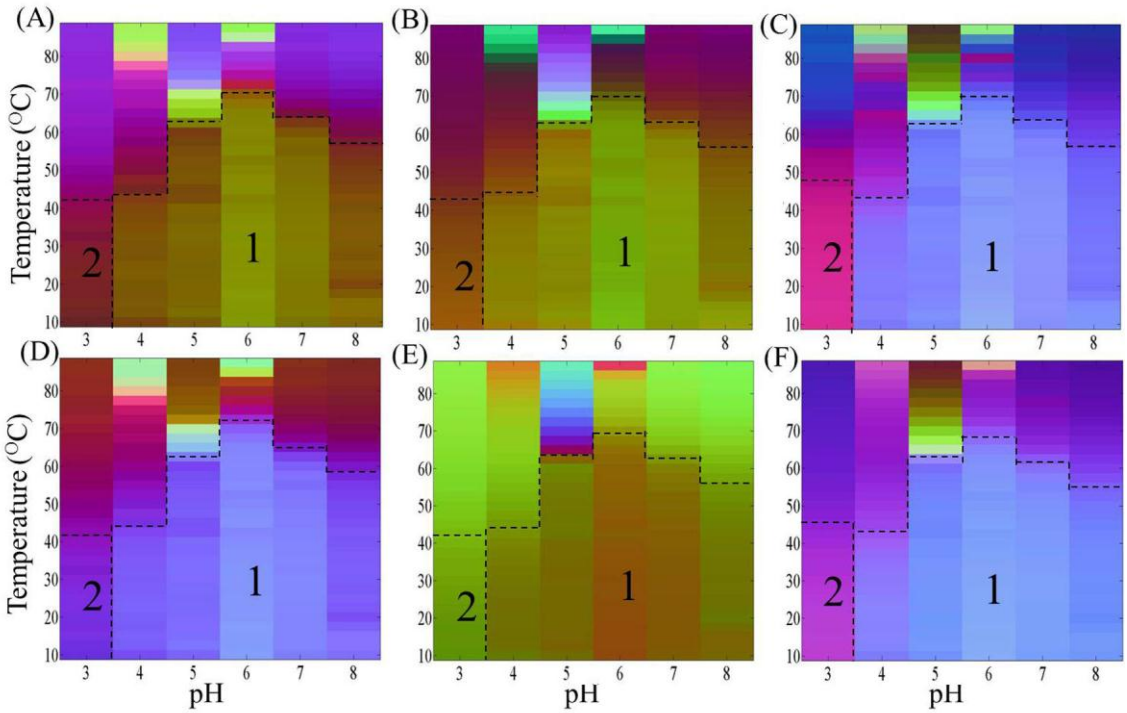

Figure 5. Empirical phase diagrams of BSA. (A, B, C) EPDs were constructed using the data sets obtained from the Chirascan-plus, and (D, E, F) EPDs were generated from data sets obtained from the separate instruments. (A) and (D): EPDs were constructed using near and far UV CD data. (B) and (E): EPDs were constructed using near-far UV CD and optical density data. (C) and (F): EPDs were constructed using near-far UV CD, optical density and intrinsic fluorescence data. The apparent phase boundaries were constructed visually and by reference to the actual data. Region 1, native like state; region 2, structurally altered state.

be obtained within 3 days. We estimate the newly developed method saves at least 40% of protein sample and total data acquisition time compared to the same experiments performed on separate instruments.

Using the optimized instrumental and sample parameters with a 2 mm cell with the Chirascan instrument, empirical phase diagrams can be directly constructed from a single instrument instead of collecting different types of data from multiple single function instruments. This high throughput and robust method can be used to characterize the structural integrity and conformational stability of a wide variety of macromolecular systems such as proteins, plasmid DNA, viruses and virus-like particles.[6] Critical solution parameters (e.g., pH, temperature and stabilizing and destabilizing solutes) which perturb the stability of macromolecules can be rapidly defined. In combination with EPD data analysis, the method can be used to characterize the stability of such biological systems as well as compare them in terms of various levels of macromolecular structure. This approach can also be used as a high throughput analytical strategy to screen for stabilizing agents and thus to design optimally stable formulations for protein therapeutic drug candidates.[19]

2.5. ASSCOCIATED CONTENT

Supporting Information. Supplemental Tables 1-3 and Supplemental Figures 1-8.

2.6 REFERENCES

1. Manning, M. C.; Chou, D. K.; Murphy, B. M.; Payne, R. W.; Katayama, D. S. *Pharm. Res.* **2010**, *27*, 544-575.
2. Frokjaer, S.; Otzen, D. E. *Nat Rev Drug Discov.* **2005**, *4*, 298-306.
3. Kahn, P. *Methods Enzymol.* **1979**, *61*, 339-378.
4. Kelly, S. M.; Price, N. C. *Curr Protein Pept Sci.* **2000**, *1*, 349-384.
5. Strickland, E. H. *CRC Crit. Rev. Biochem.* **1974**, *2*, 113-174.
6. Maddux N. R.; Joshi S. B.; Volkin D. B. ; Ralston J. P.; Middaugh C. R. *J. Pharm. Sci.* **2011**, 100, 4171-4197.

7. Richards, O. C.; Rutter, W. J. *J. Biol. Chem.* **1961**, *236*, 3177-3184.
8. Richards, O. C.; Rutter, W. J. *J. Biol. Chem.* **1961**, *236*, 3185-3192.
9. Sjöholm, I.; Ljungstedt, I. *J. Biol. Chem.* **1973**, *248*, 8434-8441.
10. Dockal, M.; Carter, D. C.; Rüker, F. *J. Biol. Chem.* **2000**, *275*, 3042-3050.
11. Manavalan, P.; Johnson, W. C. *Nature*. **1983**, 305, 831-832.
12. Venyaminov, S. Y.; Vassilenko, K. S. *Anal. Biochem.* **1994**, *222*, 176-184.
13. Wu, J.; Yang, J. T.; Wu, C. S. C. *Anal. Biochem.* **1992**, *200*, 359-364.
14. Murayama, K.; Tomida, M. *Biochemistry.* **2004**, *43*, 11526-11532.
15. Knubovets, T.; Osterhout, J. J.; Connolly, P. J.; Klibanov, A. M. *Proc. Natl. Acad. Sci.U. S. A.* **1999**, *96*, 1262-1267.
16. Lozano, P.; Diego, T.; Iborra, J. L. *Eur. J. Biochem.* **1997**, *248*, 80-85.
17. Beernink, P. T.; Tolan, D. R. *Protein Sci.* **1994**, *3*, 1383-1391.
18. Mach, H.; Middaugh, C. R. *J. Pharm. Sci.* **2011**, *100*, 1214-1217.
19. Kamerzell T. J.; Esfandiary R.; Joshi S. B.; Middaugh C. R.; Volkin D. B. *Adv Drug Deliv Rev*. **2011**,63,1118-1159.

Chapter 2

Supporting Information

Table of Contents

Supplemental Table 1: Basic properties and structural information of four model proteins

Supplemental Table 2: Parameters used in the optimization of near UV CD spectrum of BSA

Supplemental Figure 1: Effect of changing bandwidth on a spectrum's quality

Supplemental Table 3: Effect of changing step size on the thermal unfolding T_m value

Supplemental Figure 2: Thermal unfolding CD measurements of lysozyme

Supplemental Figure 3: Thermal unfolding CD measurements of α-chymotrypsin

Supplemental Figure 4: Thermal unfolding CD measurements of aldolase

Supplemental Figure 5: UV 2nd derivative measurements of α-chymotrypsin

Supplemental Figure 6: Optical density measurements of model proteins

Supplemental Figure 7: Intrinsic fluorescence measurements of model proteins

Supplemental Figure 8: Empirical phase diagrams of model proteins generated by different data sets

Protein	MW (Da)	Extinction coefficient $E^{1\%}_{280nm}$	Alpha - helix %	Beta - structure %	T_m ℃
Bovine serum albumin (BSA)	66,267	6.78	67[1]	10[1]	61.8[1]
Lysozyme	14,390	26.4	45[2]	19[2]	74.0[3]
α-chymotrypsin	25,263	20.4	10[2]	49[2]	44.0[4]
Aldolase	160,000	9.38	46[5]	14[5]	55.7[6]

MW- molecular weight

T_m- thermal unfolding temperature

(1) Murayama, K.; Tomida, M. *Biochemistry.* **2004**, 43, 11526-11532.

(2) Byler, D. M.; Susi, H. *Biopolymers.* **1986**, 25, 469-487.

(3) Liu, Y.; Sturtevant, J. M. *Biochemistry.* **1996**, 35, 3059-3062.

(4) Lozano, P.; Diego, T.; Iborra, J. L. *Eur. J. Biochem.* **1997**, *248*, 80-85.

(5) Sawyer, L.; Fothergill-Gilmore, L. A.; Freemont, P. S. *Biochem J.* **1988**, 249, 789-793.

(6) Beernink, P. T.; Tolan, D. R. *Protein Sci.* **1994**, *3*, 1383-1391.

Supplemental Table 1. Basic biochemical and biophysical properties of four model proteins.

Variable parameters	Values
BSA concentration (mg/ml)	1.0, 0.8, 0.6, 0.4, 0.2
Cell path length (mm)	10, 4, 2
Bandwidth (nm)	0.5, 1.0, 1.5, 2.0, 4.0

Supplemental Table 2. Instrument and sample parameters used in the optimization of experimental settings to measure the near UV circular dichroism (CD) spectrum of BSA.

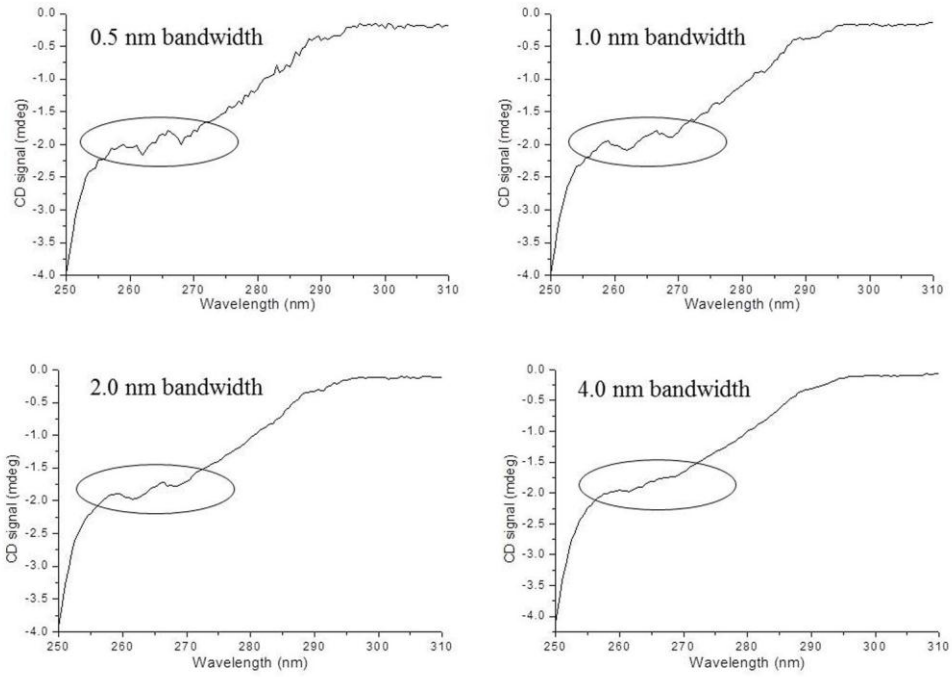

Supplemental Figure 1. Near UV CD spectra of 0.4 mg/ml BSA using different bandwidths (0.5, 1.0, 2.0 and 4.0 nm). The cell path length was 4 mm.

Protein: BSA	T_m (222 nm)	T_m (261.5 or 262 nm)	T_m (268.5 or 269 nm)
1.0 mg/ml BSA (step size 0.5 nm)	—*	64.5±0.6 ℃	63.9±0.7 ℃
0.4 mg/ml BSA (step size 0.5 nm)	64.0±0.6 ℃	63.9±1.0 ℃	63.0±1.0 ℃
0.5 mg/ml BSA (step size 1.0 nm)	64.5±0.4 ℃	64.8±0.6 ℃	64.0±0.8 ℃

*: 1.0 mg/ml BSA could not produce accurate far UV spectra due to high concentration.

Supplemental Table 3. Thermal unfolding midpoint (T_m) values of BSA (0.4, 0.5 and 1.0 mg/ml) as monitored at specific near and far-UV CD signals at different step sizes. The T_m values were obtained from the non-linear curve fit (Boltzmann function). Experimental parameters are (1) Time per wavelength step was 3 sec, and (2) Step size was 0.5 nm for 0.4 and 1.0 mg/ml BSA, and 1.0 nm for 0.5 mg/ml BSA.

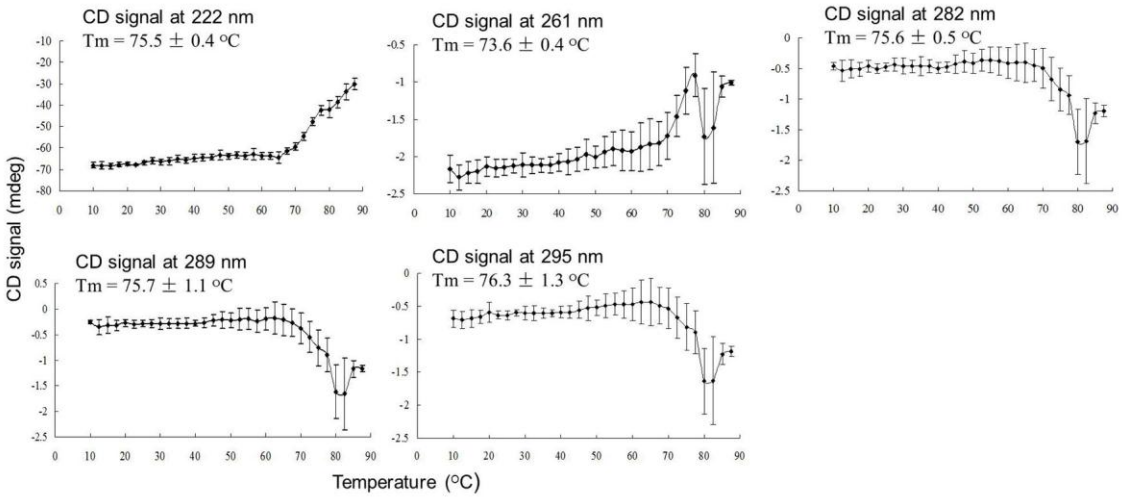

Supplemental Figure 2. Thermal unfolding temperature curves for lysozyme (0.4 mg/ml) as monitored by far- and near-UV CD signals (222, 261, 282, 289 and 295 nm) as a function of temperature. Each data point represents the mean of three independent runs with error bars showing the standard deviation. T_m value was calculated separately, and the three resulting T_m values were averaged and the standard deviation determined as shown in figure.

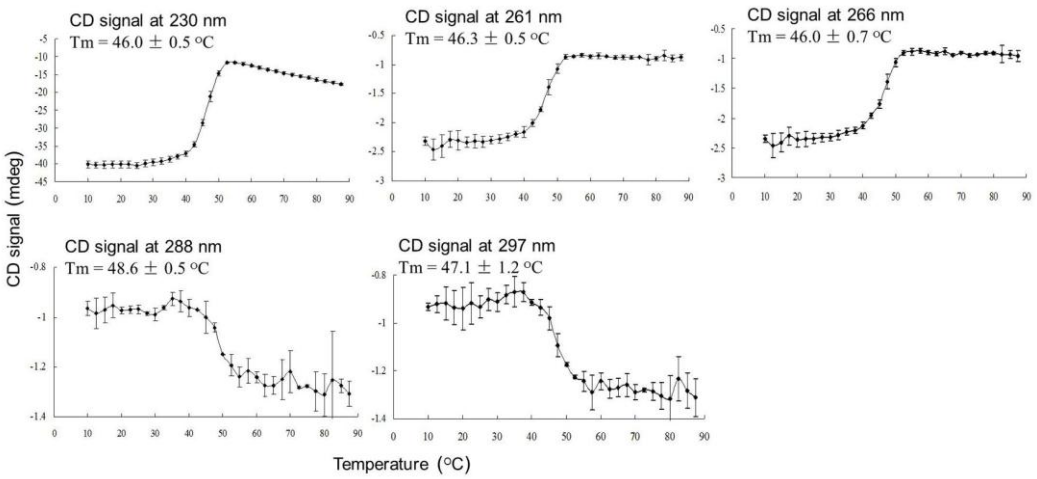

Supplemental Figure 3. Thermal unfolding temperature curves for α-chymotrypsin (0.4 mg/ml) as monitored by far- and near-UV CD signals (230, 261, 266, 288 and 297 nm) as a function of temperature. Each data point represents the mean of three independent runs with error bars showing the standard deviation. T_m value was calculated separately, and the three resulting T_m values were averaged and the standard deviation determined as shown in figure.

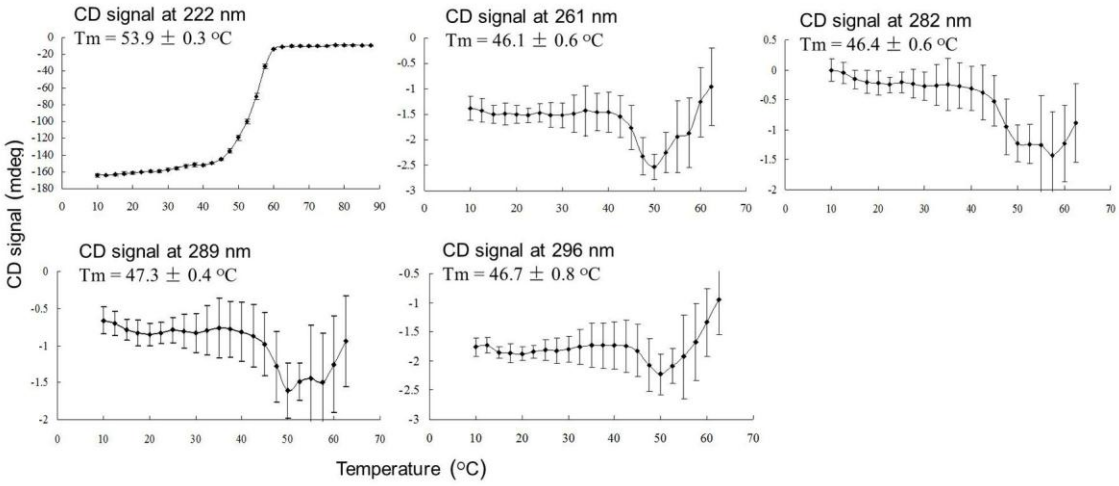

Supplemental Figure 4. Thermal unfolding temperature curves for aldolase (0.4 mg/ml) as monitored by far- and near-UV CD signals (222, 261, 282, 289 and 296 nm) as a function of temperature. Each data point represents the mean of three independent runs with error bars showing the standard deviation. T_m value was calculated separately, and the three resulting T_m values were averaged and the standard deviation determined as shown in figure.

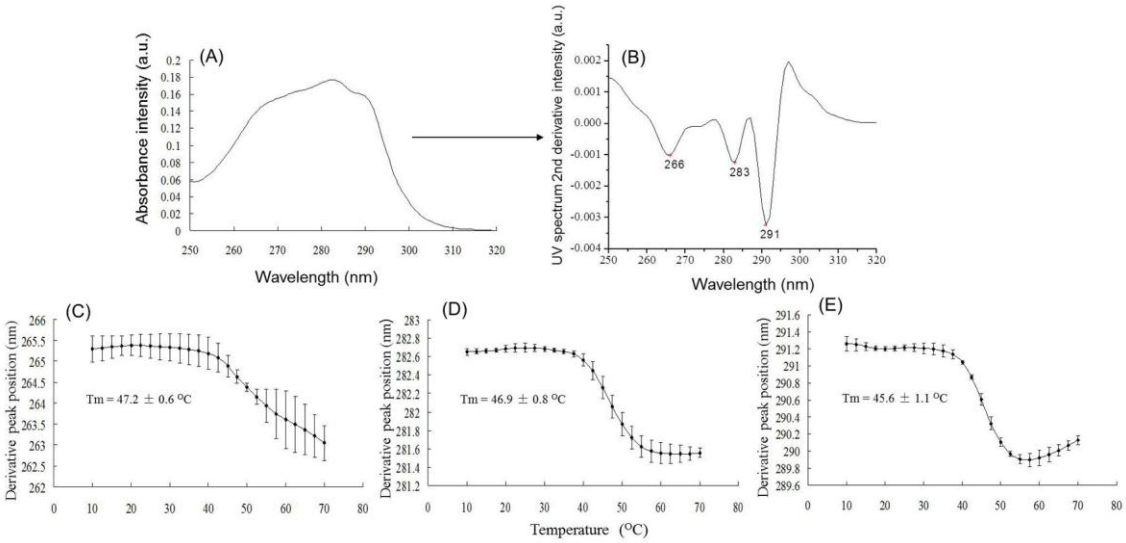

Supplemental Figure 5. (A) UV absorption spectra of α-chymotrypsin, and (B) Second derivative UV absorption curve of α-chymotrypsin. (C), (D) and (E): The changes in second derivative peak position were plotted as a function of temperature at pH 7. Each data point represents the mean of three independent samples. T_m value was calculated separately, and three resulting T_m values were averaged and the standard deviation was determined. Protein concentration was 0.4 mg/ml.

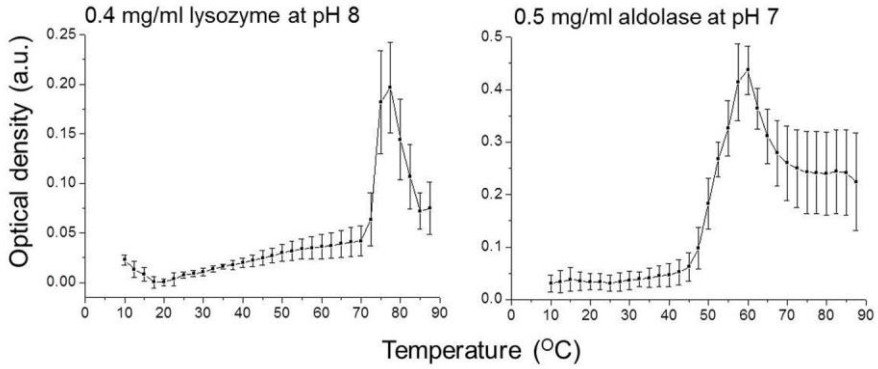

Supplemental Figure 6. The change in optical density at 350 nm for lysozyme and aldolase were plotted as a function of temperature at a specific protein concentration and solution pH. Each data point represents the mean of three independent samples with error bars showing the standard deviation.

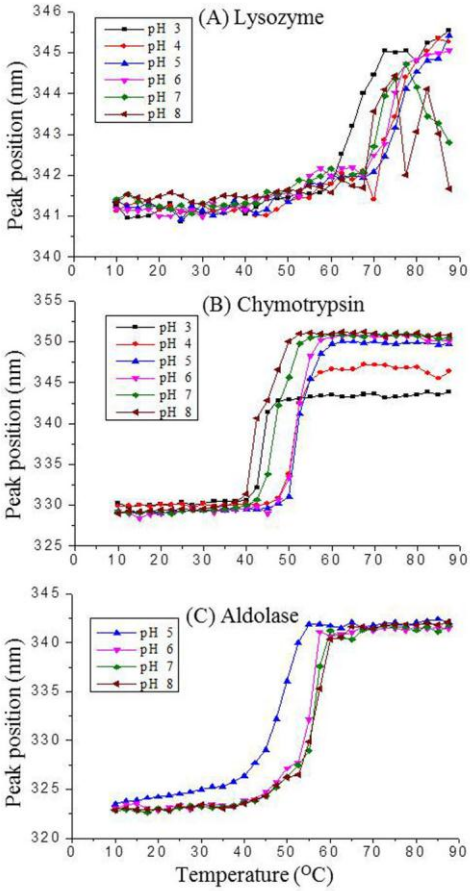

Supplemental Figure 7. Thermal stability of model proteins as monitored by change in intrinsic Trp fluorescence emission maximum (peak position) as a function of temperature and solution pH for (A) lysozyme, (B) chymotrypsin, and (C) aldolase. Each data point represents the mean of three independent samples.

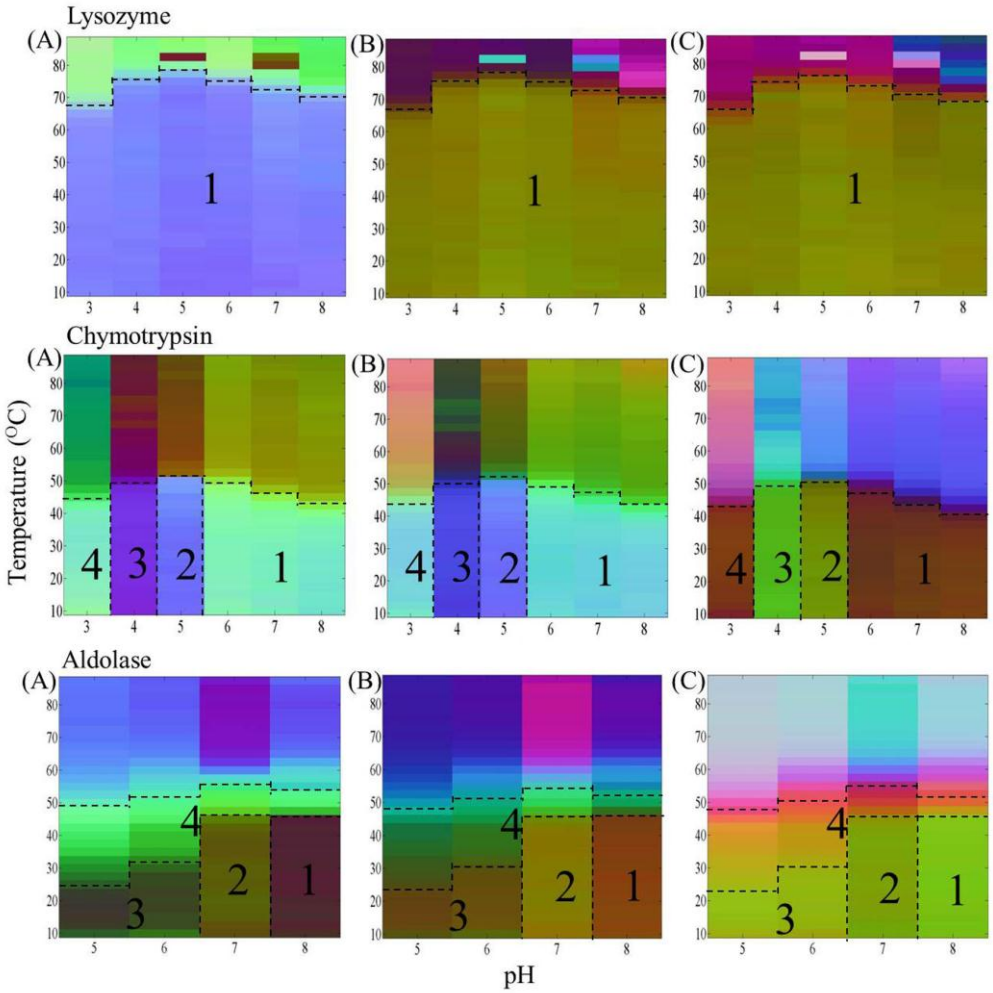

Supplemental Figure 8. Empirical phase diagrams of model proteins were generated by different data sets obtained from Chirascan-plus. For lysozyme and aldolase, (A): EPD was constructed by using far and near UV CD data, (B): EPD was constructed by using near-far UV CD and optical density data, and (C): EPD was constructed by using near-far UV CD, optical density and fluorescence peak position data. For α-chymotrypsin, (A): EPD was constructed by using far and near UV CD data, (B): EPD was constructed by using near-far UV CD and UV 2nd derivative data, and (C): EPD was constructed by using near-far UV CD, UV 2nd derivative and fluorescence peak position data. The apparent phase boundaries were constructed visually and by reference to the actual data.

Chapter 3 Application of the high throughput method for the biophysical characterization of protein stability

3.1 INTRODUCTION

Anthrax, a lethal disease caused by spores of the Gram-positive bacterium *Bacillus anthracis*, attacks mammalian hosts by cutaneous, inhalation and gastrointestinal routes. Mortality from anthrax disease is high in untreated cases and varies by infective routes. The inhaled form of the disease is the most severe and results from the inhalation of airborne spores. The mortality in untreated inhalational anthrax cases is almost 100%.[1] There are recent serious concerns about the inhaled form due to its potential use as a biological weapon.[2] Therefore, major efforts have involved the development of effective anthrax countermeasures such as vaccines.

Protective antigen (PA) is nontoxic by itself but essential for the toxic activity of *Bacillus anthracis*, the causative agent of anthrax. PA is an 83 kDa, four domain multifunctional protein, which is recognized by anthrax toxin receptors 1 and 2 on host cells.[3,4] Following receptor binding, PA is cleaved by a furin-like protease to yield a 63 kDa fragment (PA_{63}) and an N-terminal 20 kDa fragment (PA_{20}).[5] Cleaved PA_{63} assembles on the surface of cells into a heptameric[6] or octameric[7] donut-shaped structure called a prepore. The prepore subsequently combines with edema factor (EF) and lethal factor (LF) to create a number of different, but functionally similar, complex toxins such as edema toxin (EdTx) and lethal toxin (LeTx). After receptor-mediated endocytosis, and a subsequent conformational change in PA from a prepore to a pore in acidified endosomes (pH 5~6), actively toxic proteins EF and LF can be translocated through the pore into the cytoplasm of target cells, which results in cellular toxicity causing cell killing and host death.[5,8,9,10] Since PA plays an important role

in the pathology of anthrax, yet is a non-toxic and a strongly immunogenic molecule, it is used as a primary antigen in anthrax vaccines.

PA is the protein antigen component in the currently used vaccine and provides a certain level of protective immunity against anthrax infection. The licensed U.S. anthrax vaccine (AVA, BioThrax) contains predominantly protective antigen adsorbed to aluminum hydroxide. It is an effective vaccine for the protection of humans anthrax[5], however, there are limitations of the current AVA vaccine. The AVA vaccine has limited duration of protection, and 6 doses are required over 18 months followed by annual boosters.[11] The AVA is composed of PA and an incompletely defined culture supernatant adsorbed to the adjuvant, so the vaccine purity is not easily determined. Therefore, there is a need to develop newer versions of vaccines such as those based on recombinant PA, which have more defined composition and can produce the long-lasting immunity.

A novel recombinant protein analogue of PA, designated 2-fluorohisidine recombinant protective antigen (2-FHis rPA), was recently found to have the capability to block the key step of pore formation.[12,13] The preparation of the 2-FHis rPA analogue was achieved by incorporation of the unnatural amino acid 2-fluorohisidine, an isosteric analogue of histidine with a significantly reduced pKa (~1)[14], during fermentation resulting in ten histidine residues in rPA being biosynthetically replaced by 2-fluorohistidines. The protein was structurally similar to the WT protein as determined by X-ray crystallography[13], but this replacement was found to block low pH-induced pore formation with cells and thus protected

from the lethal effects of the toxin.[12,13] These results suggested that 2-FHis rPA might potentially be used as an antitoxin or a vaccine to treat anthrax infections.

We have therefore examined the effect of 2-fluorohistidine labeling of rPA on its stability and dynamics to further explore its potential use as a therapeutic entity. The conformational stability and dynamic properties of rPA and 2-FHis rPA were evaluated and compared as a function of solution pH and temperature. The physical stability of the two proteins was investigated as a function of pH (4-8) and temperature (10-85 ℃) using the developed method in Chapter 2. Near and far UV circular dichroism, intrinsic and extrinsic fluorescence as well as light-scattering optical density data were collected and empirical phase diagrams were constructed to summarize the large volume of the data collected. The physical stability profiles were then compared to distinguish stability differences between the two proteins. Based on the biophysical characterization results, the dynamic properties of the two proteins at pH 5 were then studied to better understand the difference in thermal stability observed between the two proteins at pH 5. The dynamic properties of proteins were investigated by red-edge excitation shifts and high-resolution ultrasonic spectroscopy.

3.2 MATERIALS AND METHODS

3.2.1 Materials

Recombinant protective antigen (rPA) and its 2-fluorohistidine labeled analogue (2-FHis rPA) were produced by the Laboratory of Bioorganic Chemistry at Wichita State University (Wichita, KS) as liquid solutions (~20 mg/ml) in 20 mM Tris buffer containing 150 mM NaCl at pH 8. Expression, production, and purification of rPA and 2-FHis rPA were carried out as described previously.[14] All other reagents including buffers and salts were purchased from

Sigma-Aldrich (St. Louis, MO).

For the physical characterization studies, high concentrations of stock protein samples (~ 20 mg/ml) were freshly prepared by dilution into 20 mM citrate phosphate buffer with an ionic strength of 0.15 (adjusted with sodium chloride) ranging from pH 4 to 8, at one pH unit intervals. The final experimental protein concentration was 0.5 mg/ml.

For dynamic studies, high concentrations of stock protein samples were freshly diluted to approximately 1.5 mg/ml using 20 mM Tris buffer containing 150 mM NaCl at pH 8. Diluted samples were then dialyzed in 20 mM citrate phosphate buffer at pH 5 at 4 ℃ using Slide-A-Lyzer dialysis cassettes (Thermo Scientific, Rockford, IL) with a 3.5 kDa MW cutoff. The pH value of 5 for the working buffer was determined from the biophysical characterization results. Protein concentration was 0.5 mg/ml for red-edge excitation shifts experiments, and was 0.9 mg/ml for both density and high resolution ultrasonic spectroscopy measurements.

3.2.2 Biophysical Characterization

3.2.2.1 Far and Near UV Circular Dichroism Spectroscopy

Circular dichroism analysis was performed with a Chirascan-plus Circular Dichroism Spectrometer (Applied Photophysics Ltd, Leatherhead UK) equipped with a Peltier temperature controller and a 4-position cuvette holder. Far and near UV spectra of samples (0.5 mg/ml) were collected simultaneously in the range of 200-360 nm using a 0.2 cm path length cuvette (method described in Chapter 2).[15] The step size of spectra scanning was 1 nm. A sampling time per point of 3 s and a bandwidth of 1 nm were used. The characteristic CD signals of proteins (pH 4-8) at 220, 262, 269, 284 and 291 nm observed in the near and far

UV CD regions were monitored as a function of temperature from 10 to 85 ℃ at 2.5 ℃ intervals. Triplicate measurements were made, and the equilibration time at each temperature was 1 minute.

3.2.2.2 Optical Density Measurements

Ultraviolet absorbance measurements were made simultaneously during the near and far UV CD experiments using the same experimental parameters.[15] The aggregation behavior of rPA and 2-FHis rPA (0.5 mg/ml) was monitored by recording the optical density at 350 nm as a function of temperature (10-85 ℃) and pH (4-8).

3.2.2.3 Intrinsic Fluorescence Spectroscopy

In a series of separate experiments, fluorescence emission scan data were also collected on the Chirascan-plus instrument by using an attached fluorescence detector. A 2 x 10 mm quartz cuvette was used in all experiments, and excitation of the proteins was carried out along the shorter path length (2 mm). Fluorescence emission spectra of the two proteins (0.5 mg/ml) were recorded using the same temperature program as used previously. Triplicate samples were measured using an excitation wavelength of 295 nm (> 95% tryptophan emission). Emission spectra were collected from 305 to 395 nm with a step size of 1 nm and 2 s sampling time per point. The excitation and emission slits were set at 4 and 9 nm, respectively. The position of the emission wavelength maximum was determined using a polynomial derivative fitting method executed in Origin 7.0 software.

3.2.2.4 Extrinsic Fluorescence Spectroscopy

8-Anilino-1-naphthalene sulfonate (ANS) was used as an extrinsic probe to study conformational changes of the two proteins that result in changes in its surface polarity. The

interaction of ANS with the apolar surfaces of rPA and 2-FHis rPA were monitored as a function of temperature (10-85 ℃) and pH (4-8) using a QuantaMaster Spectrophotometer (Photon Technology International (PTI), Inc., Birmingham, NJ). Each sample solution (0.5 mg/ml) containing 89 μM diluted ANS (a molar ratio of the ANS to the protein of 15:1) was incubated at 10 ℃ in the dark for 20 minutes before measurement. Samples were excited at 375 nm and spectra were collected from 400 to 600 nm at 2.5 ℃ intervals, with a 3 min equilibration time at each temperature. Duplicate measurements were made using a 2 mm path length quartz cuvette to check for inner filter effects (none were seen). Buffer baselines containing ANS were subtracted from each sample spectrum prior to analysis. Peak positions and intensities of the emission spectra were obtained using a polynomial derivative fitting method as described above (Section: Intrinsic Fluorescence Spectroscopy).

3.2.2.5 Empirical Phase Diagram (EPD)

The empirical phase diagram (EPD) was constructed as described previously[16,17] to summarize and facilitate the analysis of the complex biophysical data sets obtained. The EPD is used to identify coherent parameter regions that define protein structural states as a function of solution variables (temperature and pH in this case). CD signals at 220, 262, 269, 284 and 291 nm, optical density, intrinsic Trp fluorescence peak positions, and extrinsic fluorescence intensities data were used for construction of the EPDs of rPA and 2-FHis rPA. All calculations were performed using Matlab software (MathWorks, Natick, MA).

3.2.3 Dynamic Properties Measurements

3.2.3.1 High Resolution Ultrasonic Spectroscopy

Ultrasonic spectroscopy measurements were performed using an HR-US 102

Spectrometer (Ultrasonic Scientific, Dublin, Ireland) with a frequency range of 2–18 MHz and a resolution of 0.2 mm/s for velocity and 0.2% for attenuation measurements. The differential velocity and attenuation between sample and reference cells were monitored at 12 MHz from 10 to 85^{o}C and pH 5. The sample and reference solutions (0.9 mg/ml) were thoroughly degassed before each measurement. The sample and reference cells contained 1 ml of protein and buffer solution, respectively. The temperature of the cells was controlled by a Phoenix P2 water circulator (Thermo Haake, Newington, NH). Data were analyzed using HRUS v4.50.27.25 software. The coefficient of adiabatic compressibility (β_s) was determined using the equations described previously.[18] The adiabatic compressibility of the sample and buffer are related to the density (ρ) and ultrasonic velocity (u) by the Laplace equation, $\beta=1/\rho u^2$.

3.2.3.2 Density

The densities of the two protein solutions (0.9 mg/ml) and corresponding buffer solutions were measured using a DMA-5000 high precision densitometer (Anton Paar, Graz, Austria) at a precision of 1 x10^{-6} g/cm^3 and ±0.001^{o}C. The densities of degassed solutions were measured from 5–22^{o}C and 5–32^{o}C for rPA and 2-FHis rPA in their unfolding pre-transition ranges, respectively. The increment of the temperature was 1^{o}C. The instrument was calibrated with dry air and degassed water before analysis.

3.2.3.3 Red-Edge Excitation Shifts

Fluorescence measurements used in the determination of red-edge excitation shifts were performed with the PTI QuantaMaster Spectrophotometer. Protein concentration was 0.5 mg/ml. Excitation wavelengths of 292, 296, 300 and 304 nm were used, and the emission

spectra were collected from 300 to 400 nm. The excitation and emission slit widths were set to 2 nm. The data were collected from 10 to 50 ℃ in 2 ℃ increments with a 3 minutes equilibration time. Triplicate measurements were made using a 2 mm path length quartz cuvette. The relative change in peak position was determined using a mean spectral center of mass (MSM) method spanning the emission spectra range of 310 to 400 nm. This range of data analysis and the lower pathlength employed for fluorescence measurements (2 mm) should minimize the contribution of Rayleigh scattering even when the data is collected at 304 nm (the highest excitation wavelength employed) as well as the lower excitation wavelengths used in these studies. The mean spectral center of mass method is a peak picking algorithm to determine the peak maximum. The maximum peak position is based on the center-of mass position of the area in a selected peak integration region (from 310- 400 nm in this case). The peak position maxima obtained by the MSM method are generally ~8-10 nm higher than the actual peak position obtained by derivative analysis but result in a better signal to noise ratio.

3.3 RESULTS

3.3.1 Biophysical Characterization

3.3.1.1 Near and Far UV Circular Dichroism Spectroscopy

Near and far UV CD spectra of 0.5 mg/ml rPA and 2-FHis rPA at pH 7 and 10 ℃ are shown in Figure 1. In the far- UV region (200-250 nm), both proteins display a broad peak with a minimum at around 210 nm and a shoulder at 220 nm, suggesting that proteins contain a mixture of α-helix and β-sheet structures. In the near-UV region (250-320 nm), four characteristic peaks at 262, 269, 284 and 291 nm were observed, presumably due to the

aromatic amino acid side chains.[19,20]

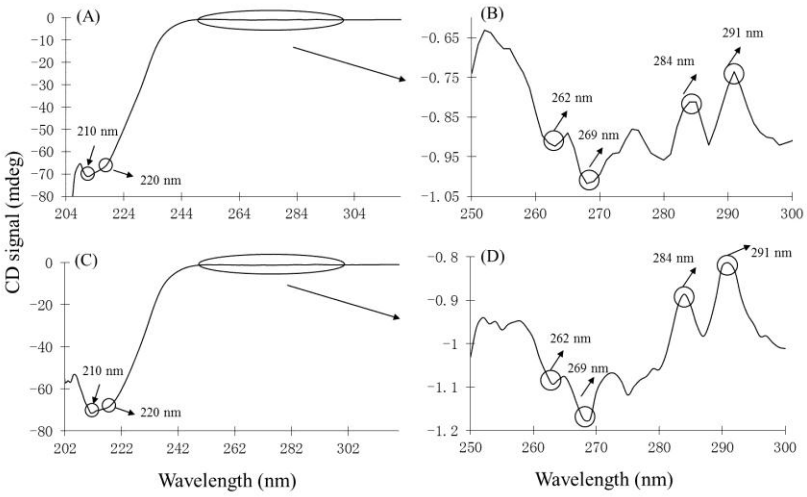

Figure 1: Near- and far-UV CD spectra for rPA and 2-FHis rPA at pH 7 and 10°C. Near and far UV CD (A, C) and Near-UV CD (B, D) spectra are shown for (A) 0.5 mg/ml rPA at pH 7 and (B) expanded view of its near-UV region. (C) 0.5 mg/ml 2-FHis rPA at pH 7 and (D) expanded view of its near-UV region.

The effect of temperature on the two protein's secondary and tertiary structures was further investigated by using thermal melt analysis. CD signals at five characteristic peaks (220, 262, 269, 284 and 291 nm) were monitored across the pH range of 4-8. Typical thermal unfolding curves of 2-FHis rPA and rPA at pH 7 are shown in Figure 2 and Supplemental Figure S1, respectively, with triplicate measurements resulting in good reproducibility. The rPA and 2-FHis rPA proteins show similar pattern in their CD thermal unfolding curves across the entire pH range examined. Although an overall loss in secondary and tertiary structures is observed as a function of increasing temperature for both proteins, the thermal transition midpoint (T_m) values vary greatly between the two proteins as the pH value decreases. For example, the two proteins show a significantly lower thermal stability at pH 5 (Supplemental Figures S2 and S3). The T_m values from CD thermal melt curves were calculated for both proteins and results are summarized in Table 1. The two proteins show similar conformational

stability at pH 7 and 8. Differences in thermal stability between the two proteins are, however, observed at pH 5 and 6 (see Table 1), especially at pH 5. Interestingly, the T_m value for 2-FHis rPA at pH 5 evaluated from the Far-UV CD data was greater than that obtained from the near-UV CD data, suggesting that a molten globule like state exists in the temperature range from 35 – 41 ^oC. Molten globules generally possess native-like secondary structure but lack significant tertiary structure. While the T_m values for both proteins decrease as a function of pH, the 2-FHis rPA exhibits a slightly higher thermal stability than rPA at pH 6, and the analogue rPA has significantly higher stability than rPA at pH 5 with an increased T_m value of approximately 10 ℃.

3.3.1.2 Intrinsic Fluorescence Spectroscopy

Alternations in tertiary structure as a function of temperature and solution pH of the two rPA proteins were also investigated by intrinsic fluorescence spectroscopy. Figures 3A and B show the changes in the position of the emission peak maximum and structural changes occurred in both proteins but at different temperatures depending on pH. rPA and 2-FHis rPA show their highest thermal stability at pH 7-8 and 6-8, respectively. The stability of rPA decreases much more dramatically compared to 2-FHis rPA between pH 4 and 6 (see Table 1 for the calculated T_m values). At pH 7 and 8, both proteins show comparable structural integrity with initial peak positions of about 329 nm at low temperatures. With increasing temperature, the emission peak maximum shifts to about 342 nm, indicating the proteins were conformationally altered but not completely unfolded at elevated temperatures. In summary, both proteins show their highest thermal stability at pH 7 and 8, and manifest lower thermal stability with decreasing pH.

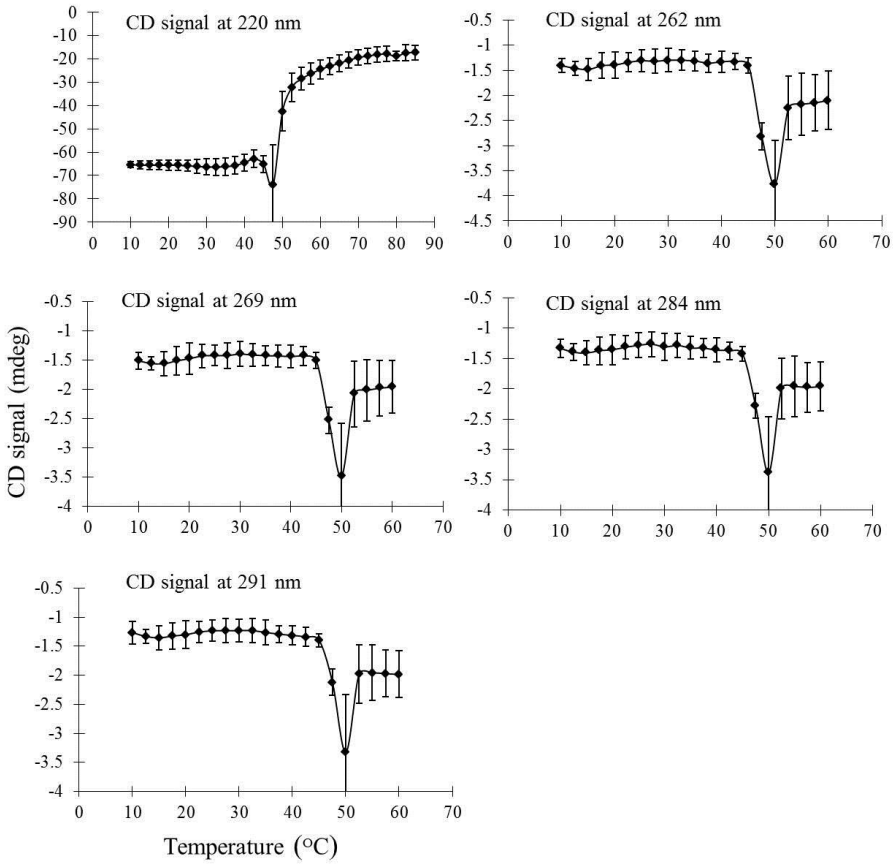

Figure 2. Thermal stability of 2-FHis rPA (0.5 mg/ml at pH 7) as monitored by CD signals at indicated values (220, 262, 269, 284 and 291 nm) as a function of temperature. Each data point represents the mean of three independent runs, with error bars showing the standard deviation.

Sample	pH	Circular Dichroism					Optical Density	Intrinsic Fluorescence	ANS Fluorescence
		220 nm	262 nm	269 nm	284 nm	291 nm			
rPA	8	49.0	50.0	50.5	50.5	50.5	51.0	46.5	46.5
2-FHis rPA	8	47.0	49.0	49.0	49.0	49.0	48.5	45.0	46.5
rPA	7	49.0	48.5	48.5	48.5	48.5	48.5	46.5	48.5
2-FHis rPA	7	49.0	47.0	47.0	48.5	48.5	46.5	46.5	50.5
rPA	6	43.5	41.0	41.0	41.0	41.0	43.5	39.0	41.0
2-FHis rPA	6	44.0	43.5	43.5	43.5	43.5	43.5	43.5	44.0
rPA	5	28.5	26.0	26.0	26.0	26.0	28.5	33.5	29.0
2-FHis rPA	5	41.0	34.5	36.5	36.5	36.5	39.0	43.0	41.0
rPA	4	36.0	36.0	36.0	36.0	36.0	34.0	29.0	31.0
2-FHis rPA	4	36.0	34.0	34.0	33.5	34.0	34.0	34.0	29.5

Table 1: Thermal unfolding temperature values ($T_{m,}$ ℃) calculated from the thermal unfolding curves using different biophysical techniques. Indicated T_m values were calculated from the first derivative of the thermal unfolding curves from each technique. Values are ± 0.5 ℃.

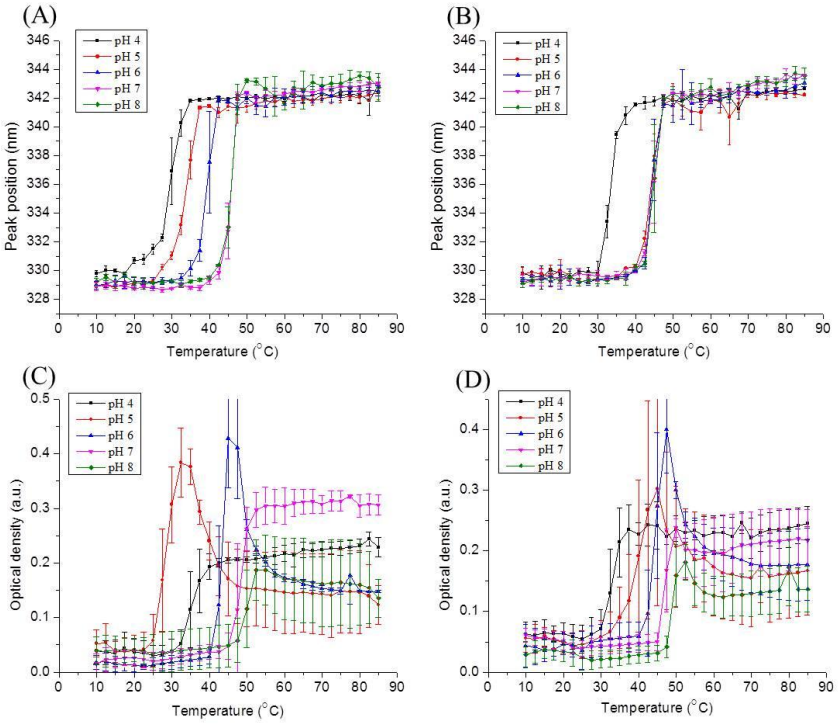

Figure 3. Thermal stability of rPA (Figures A and C) and 2-FHis rPA (Figures B and D) at 0.5 mg/ml as a function of solution pH: (A) and (B) intrinsic Trp fluorescence emission maximum (peak position) was monitored; (C) and (D) optical density at 350 nm was monitored. Each data point represents the mean of three independent samples, with error bars showing the standard deviation.

3.3.1.3 Optical Density Measurements

Optical density (OD) data at 350 nm were collected simultaneously during CD measurements. rPA and 2-FHis rPA both manifested aggregation as measured by increases in OD values with increasing temperature (Figures 3C and D). The temperature dependent OD changes (i.e., protein aggregation) are overall consistent with the observations made from the CD and intrinsic fluorescence measurements, with similar trends of pH and temperature. Again, 2-FHis rPA was significantly more stable than rPA at pH 5, where the midpoint of the aggregation values for rPA and 2-FHis rPA were 39.0^{o}C and 28.5^{o}C, respectively. Interestingly, the 2-FHis rPA analogue is actually more stable at pH 5 than at pH 4, in contrast to the recombinant rPA protein.

3.3.1.4 Extrinsic Fluorescence Spectroscopy

ANS is a fluorescent dye that binds to apolar regions in proteins, resulting in large increases in fluorescence quantum yield and a blue shift in peak position.[21] This observation must always be qualified, however, by the possibility of electrostatic interactions of the negatively charged dye with a protein. Figure 4 shows the thermal melting curves of the two proteins at various pH values. These curves were obtained by monitoring the ANS emission peak intensity as a function of temperature. At pH 4, ANS data for rPA show significant fluorescence intensity even at low temperatures (Figure 4A). This increased fluorescence intensity is presumably induced by the binding of ANS to the structurally altered rPA protein under acidic conditions. Increased ANS fluorescence intensity with increases in temperature is observed over the pH range of 4 to 8. The T_m values for these transitions are summarized in Table 1. In agreement with results obtained from other biophysical techniques,

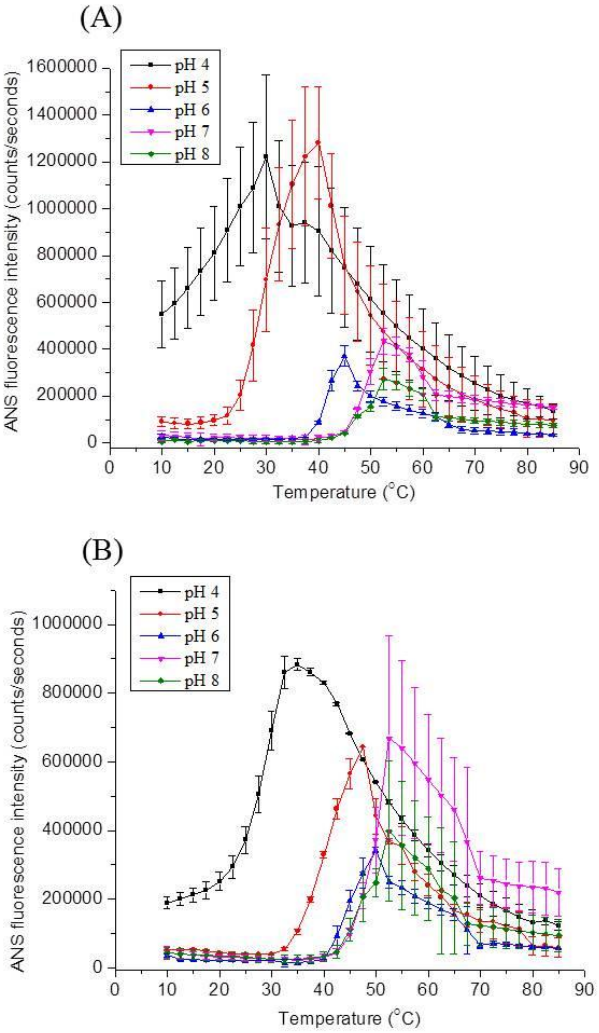

Figure 4. ANS fluorescence intensity values in the presence (A) rPA and (B) 2-FHis rPA as a function of temperature and solution pH. Both samples were at 0.5 mg/ml. Each data point represents the mean of two independent samples, with error bars showing the standard deviation.

both proteins show their greatest structural stability at pH 7-8. At pH 6, 2-FHis rPA is slightly more stable than rPA. Again, at pH 5, the maximum difference in the stability of two proteins is observed.

3.3.1.5 Empirical Phase Diagrams

Empirical phase diagrams are used to summarize large amounts of data to provide a more comprehensive view of the stability profiles of proteins. Such diagrams should not be confused with thermodynamic phase diagrams, however, since no equilibrium between phases is implied. The EPDs of rPA and 2-FHis rPA generated from all of the collected data are shown in Figures 5A and B, respectively. Overall, the EPD of the rPA protein (Figure 5A) shows similar defined "apparent" phases compared to those in the EPD of 2-FHis rPA (Figure 5B). There are two major phases seen for both proteins. In region 1, both proteins at pH 5-8 show a similar color below about 48^{o}C, suggesting that they exist in similar structural states. By examining the data obtained from the specific techniques, region 1 at low temperatures from pH 5-8 is presumably the native state of protein. rPA and 2-FHis rPA show similar apparent phase boundaries across the pH range 6 to 8. In contrast, rPA shows lower stability than 2-FHis rPA at pH 6 as evidenced by a decreased T_m value of about 2.5^{o}C (Table 1). At pH 5, there is a much more significant thermal stability difference between the two proteins. Both the EPDs and the individual experimental methods all show that 2-FHis rPA has much greater thermal stability (T_m value difference of 10-12^{o}C). Unlike the EPD of 2-FHis rPA, the EPD of rPA displays an additional region (Region 2 in Figure 5A) based on phase color changes. In region 2, rPA samples at pH 4 show a distinct color (green) difference from region 1. This observation clearly arises from results obtained from extrinsic (ANS)

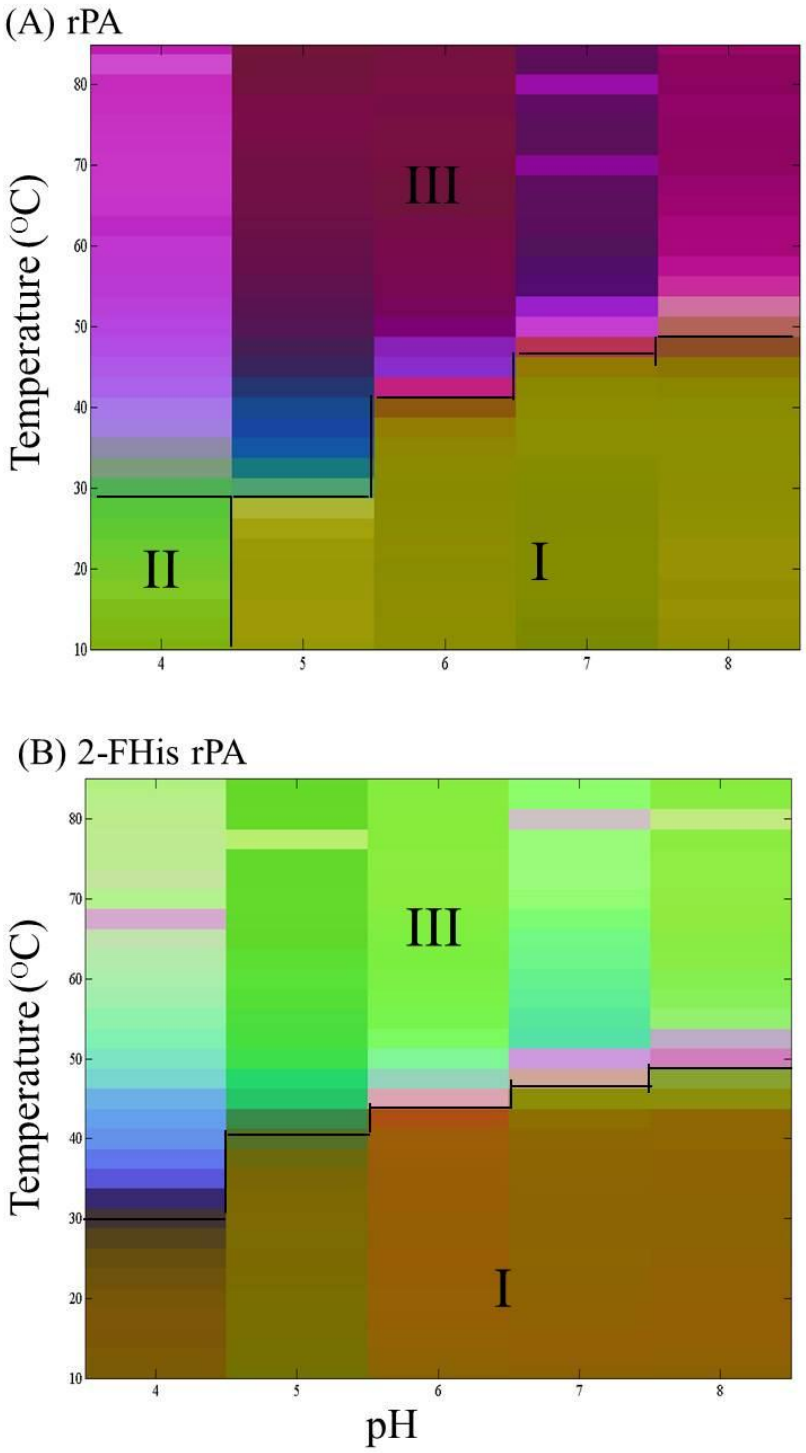

Figure 5. Empirical phase diagrams (EPDs) of (A) rPA and (B) 2-FHis rPA. The EPD was prepared from near/far-UV CD, optical density, intrinsic fluorescence (peak position), and extrinsic (ANS) fluorescence data collected across a pH range from 4 to 8 and a temperature range from 10 ℃ to 85 ℃.

fluorescence data. As discussed previously, at pH 4, rPA with ANS shows significant fluorescence intensity even at low temperature (Figure 4A), suggesting the binding of ANS to a partially unfolded protein at this acidic condition. At high temperatures, both proteins are structurally altered and aggregate as indicated by the presence of region 3. From the EPDs, we can see that the most stable region of two proteins is in the pH range of 7 to 8.

3.3.2 Dynamic Properties Measurements

3.3.2.1 High Resolution Ultrasonic Spectroscopy (HR-US)

HR-US spectroscopy employs high-frequency sound waves to probe intramolecular forces in materials such as proteins.[22,23] Oscillating compression (and decompression) of the ultrasonic wave causes oscillations in internal molecular rearrangement. A protein will respond by corresponding compression and expansion of its volume. In HR-US measurements, attenuation and velocity of ultrasonic waves were determined. Combined with high precision density measurements, the adiabatic compressibility of each protein sample was calculated.

Protein compressibility is influenced by both a protein's internal fluctuations in volume and its hydration. Because 2-FHis rPA showed greater stability than rPA at pH 5, based on the EPD characterization results discussed above, measurements of the dynamic properties of the two proteins were made under this condition. The magnitude of a protein's apparent adiabatic compressibility has positive contributions from a protein's intrinsic volume fluctuations and negative contributions from the hydration water.[24] In Figure 6A, the apparent adiabatic compressibility values were found to increase with increases in temperature for both rPA and 2-FHis rPA . 2-FHis rPA displays higher values of adiabatic compressibility than those of rPA

at low temperatures where both proteins exist in their native states. The negative compressibility, however, suggests a dominant contribution of hydration water to the experimentally determined compressibility values. The increase in compressibility with temperature for rPA and 2-FHis rPA therefore could either represent increases in their intrinsic fluctuations and/or reflect alterations in hydration dynamics around the protein's surface due to temperature. Figure 6B shows Trp peak position shifts as a function of temperature for rPA and 2-FHis rPA when excited at 304 nm (obtained from red-edge shifts measurements). Excitation of Trp by 304 nm radiation should probe residues with greater degrees of solvent exposure which are presumably located on the surface of the protein. The Trp peak position at 10^{o}C was red-shifted for rPA compared to 2-FHis rPA. This red-shift in peak position could be due to the differences in protein's tertiary structure and/or hydration of the surface. The magnitude of the red-shift, however, was greater when probed with 304 nm compared to 292 nm light (data not shown), suggesting that hydration contributions to the red-shift are possible. This result along with the compressibility data (Figure 6A) suggests that the native structure of rPA and 2-FHis rPA may have differences in their hydration state. Generally, increased dynamic motions, flexibility, void volume changes and elasticity of proteins will result in higher values of adiabatic compressibility. In contrast, hydration of proteins, which reduces many of the above processes, will decrease values of compressibility.

3.3.2.2 Red-Edge Excitation

Red edge excitation spectroscopy is a fluorescence based technique used for studying the dynamic properties of proteins. For fluorophores under conditions where solvent relaxation is not complete (such as the viscous environment surrounding the buried protein fluorophore),

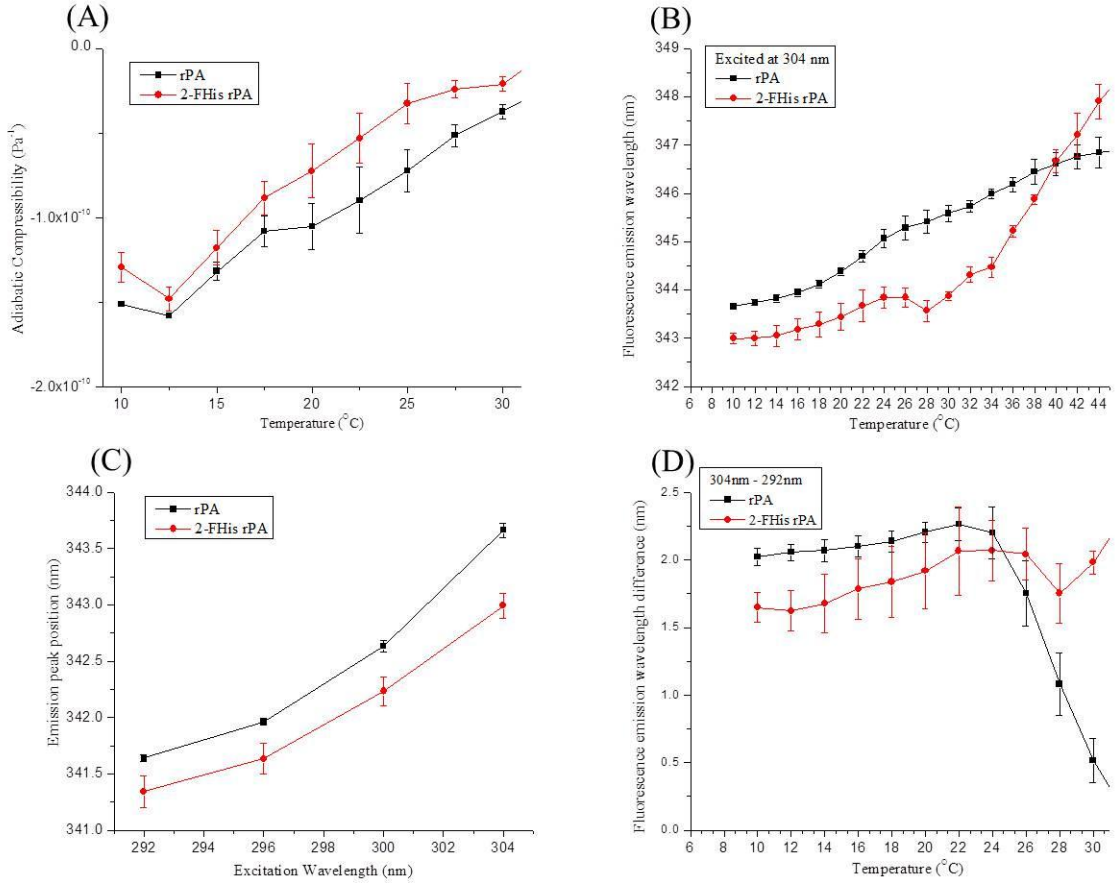

Figure 6. Measurements of dynamic properties of rPA and 2-FHis rPA collected at pH 5. (A) Ultrasonic measurements of the adiabatic compressibility of the two proteins. (B) Emission peak positions' comparison between rPA and 2-FHis rPA at an excitation wavelength of 304 nm. Tryptophanyl dynamics were examined by red-edge excitation shifts of (C) rPA and 2-FHis rPA based on excitation at 292, 296, 300 and 304 nm. (D) red-edge excitation shifts compared between excitation at 292 and 304 nm for both proteins. Each data point represents the mean of three independent runs, with error bars showing the standard deviation.

emission spectra shift to longer wavelengths when excitation wavelengths move to longer wavelengths.[25,26] In less viscous environments, where solvent relaxation is more complete, the magnitude of the red-edge effect decreases with shifts disappearing in fluid solvents.

The effect of red-edge excitation on tryptophan fluorescence is quantified here as the shift in the emission peak when excited at 296, 300, and 304 nm relative to 292 nm. In Figure 6C, both proteins show clear red shifts at 10^{o}C when the excitation wavelength increases. These results show that the magnitude of the red-shifts increase as excitation is moved to longer wavelengths. Similar results were obtained throughout the pre-transition temperature range (10-20^{o}C for rPA, and 10-30^{o}C for 2-FHis rPA) of their thermal unfolding curves. This observation suggests that Trp residues located in restricted environments can be sampled and probed to study the differences in dynamics of such environments in both rPA and 2-FHis rPA. In Figure 6D, the red-edge excitation shifts, representing the difference in emission maxima upon red-edge excitation from 292 to 304 nm, are compared for both rPA and 2-FHis rPA. The magnitude of the shift of rPA is always larger than 2-FHis rPA at low temperatures prior to thermal structural perturbation. This observation suggests that 2-FHis rPA displays more dynamic behavior compared to rPA at pH 5. Above the unfolding temperature, rPA and 2-FHis rPA are prone to aggregate and eventually precipitate out of solution.

3.4 DISCUSSION

In the present study, the physical stability of rPA and 2-FHis rPA was investigated using the analytical method developed in Chapter 2. Temperature/pH stability profiles of the two proteins were created and compared. The proteins exhibited similar CD and fluorescence spectra at low temperatures. The estimated secondary structure contents of the two proteins

are very similar to each other, although 2-FHis rPA displays an increased (about 6.5 %) α-helix content and a corresponding decrease in β-structure compared to rPA[12], as estimated by the spectral deconvolution software CDNN. Similar thermal unfolding profiles of the two proteins were also obtained by different techniques at pH 6-8. We conclude that the overall structural integrity and conformational stability of the protein was not affected by incorporation of 2-FHis around neural pH values. These results are in agreement with a previous study of the equilibrium stability of rPA and 2-FHis rPA using urea in which both proteins showed similar urea denaturation profiles.[12]

At lower pH values, however, differences in the conformational stability of 2-FHis rPA and rPA were noted. At pH 5, and to a lesser extent at pH 6, 2-FHis rPA exhibited higher stability than rPA. This result suggests that 2-FHis incorporation into rPA inhibits pH dependent unfolding under these mildly acidic pH conditions. Thus, the 2-FHis rPA is much more thermally stable at lower pH compared to rPA (Table 1).

To better understand why the two rPA proteins demonstrate a stability difference at pH 5, the dynamic properties of the proteins were compared by red-edge excitation shifts and HR-US measurements. HR-US measurements suggest that both rPA and 2-FHis rPA may have differences in their hydration and/or intrinsic fluctuations in which rPA may be more hydrated than 2-FHis rPA. It is well known that fluorinated compounds exhibit increased hydrophobicity compared to their hydrogenated counterparts.[27] Such increased apolar character in 2-FHis rPA may cause increased water mobility and less residence times near such regions.[28,29] It is therefore possible that 2-FHis rPA has different hydration characteristics than rPA but this hypothesis needs further investigation. In addition, red-edge

excitation shift results indicate that 2-FHis rPA has greater dynamic character than rPA at pH 5. It is often assumed that more dynamic proteins possess less stability.[30,31,32] Many thermostable proteins are, however, quite dynamic, so an increase in thermostability does not necessarily correlate with a decrease in dynamic behavior.[33,34,35,36,37] The relationship between protein dynamics and stability is not fully understood. The lower extent of hydration and/or higher dynamic character may increase the stability of the 2-FHis rPA at lower pH. Solution pH can potentially alter the microenvironmental pH around proteins, especially in their hydration layer. If such a phenomenon occurs at lower pH in these studies, a greater extent of hydration (with higher residence time) may explain the inverse relationship between the extent of hydration and stability for rPA and 2-FHis rPA. rPA was earlier determined to be potentially more hydrated than 2-FHis rPA using HR-US studies. The two methods used in this study both reflect the global dynamic properties of the two proteins at a specific pH condition. More detailed information about the dynamic properties of proteins can be obtained by methods such as NMR and H-D exchange mass spectrometry, which provide information about the local dynamic properties in specific regions of proteins.

This study provides important biophysical information about the effect of 2-FHis on the conformational stability of rPA in response to environmental stress factors such as pH and temperature. Our results show that the two proteins have similar stability at pH 7 to 8. The 2-FHis rPA analogue is slightly more stable at pH 6 and shows dramatically increased stability at pH 4-5. The 2-FHis rPA protein is also more dynamic than rPA at pH 5. These data provide useful information to better understand the similarities and differences in physical properties of the two proteins in solution. PA is a primary component in the currently licensed

anthrax vaccine. In comparison, 2-FHis rPA possesses higher thermal stability under acidic conditions and has the capability to block key steps in its cellular cytotoxicity. These data suggest that 2-FHis rPA has the potential to for use as an alternative, more stable antigen in newer, recombinant versions of the anthrax vaccine. Given the potential need for long term storage of anthrax vaccines as a counter-terrorism measure, the increased stability of the 2-FHis analogue is an attractive property of this form of the rPA protein. The pH/temperature stability profile of 2-FHis rPA was generated through a comprehensive biophysical characterization of the secondary and tertiary structural integrity, as well aggregation behavior, of the protein. These data can be used as a starting point for further formulation development of the 2-FHis rPA as a potential anthrax vaccine or as a potential antitoxin to treat anthrax during the infection.

3.5 ASSCOCIATED CONTENT

Supplemental Figures 1-3.

3.6 REFERENCES

1. Donegan S, Bellamy R, Gamble CL. 2009. Vaccines for preventing anthrax. Cochrane Database Syst Rev 2: CD006403.
2. Inglesby TV, O'Toole T, Henderson DA, Bartlett JG, Ascher MS, Eitzen E, Friedlander AM, Gerberding J, Hauer J, Hughes J. 2002. Anthrax as a biological weapon, 2002. JAMA: the journal of the American Medical Association 287(17):2236-2252.
3. Bradley KA, Mogridge J, Mourez M, Collier RJ, Young JAT. 2001. Identification of the cellular receptor for anthrax toxin. Nature 414(6860):225-229.
4. Scobie HM, Rainey GJA, Bradley KA, Young JAT. 2003. Human capillary morphogenesis protein 2 functions as an anthrax toxin receptor. Proceedings of the National Academy of Sciences 100(9):5170.
5. Brey RN. 2005. Molecular basis for improved anthrax vaccines. Advanced drug delivery reviews 57(9):1266-1292.
6. Petosa C, Collier RJ, Klimpel KR, Leppla SH, Liddington RC. 1997. Crystal structure of the anthrax toxin protective antigen. Nature 85: 833 - 838.
7. Mogridge J, Cunningham K, Lacy DB, Mourez M, Collier RJ. 2002. The lethal and edema factors of anthrax toxin bind only to oligomeric forms of the protective antigen.

Proceedings of the National Academy of Sciences. 99(10):7045-7048.
8. Collier RJ, Young JAT. 2003. Anthrax toxin. Annual review of cell and developmental biology 19(1):45-70.
9. Bann JG. 2012. Anthrax toxin protective antigen—Insights into molecular switching from prepore to pore. Protein Science 21(1):1-12.
10. Gao-Sheridan S, Zhang S, John Collier R. 2003. Exchange characteristics of calcium ions bound to anthrax protective antigen. Biochemical and biophysical research communications 300(1):61-64.
11. Wright JG, Quinn CP, Shadomy S, Messonnier N. 2010. Use of anthrax vaccine in the United States. Morbid Mortal Wkly Rep 59 (rr06): 1-30.
12. Wimalasena DS, Cramer JC, Janowiak BE, Juris SJ, Melnyk RA, Anderson DE, Kirk KL, Collier RJ, Bann JG. 2007. Effect of 2-fluorohistidine labeling of the anthrax protective antigen on stability, pore formation, and translocation. Biochemistry 46(51):14928-14936.
13. Wimalasena DS, Janowiak BE, Lovell S, Miyagi M, Sun J, Zhou H, Hajduch J, Pooput C, Kirk KL, Battaile KP. 2010. Evidence that histidine protonation of receptor-bound anthrax protective antigen is a trigger for pore formation. Biochemistry 49:6973-6983.
14. Eichler JF, Cramer JC, Kirk KL, Bann JG. 2005. Biosynthetic incorporation of fluorohistidine into proteins in E. coli: a new probe of macromolecular structure. ChemBioChem 6(12):2170-2173.
15. Hu L, Olsen CM, Maddux NR, Joshi SB, Volkin DB, Middaugh CR. 2011. Investigation of Protein Conformational Stability Employing a Multimodal Spectrometer. Analytical chemistry 83: 9399-9405.
16. Kueltzo LA, Ersoy B, Ralston JP, Middaugh CR. 2003. Derivative absorbance spectroscopy and protein phase diagrams as tools for comprehensive protein characterization: A bGCSF case study. Journal of pharmaceutical sciences 92(9):1805-1820.
17. Maddux NR, Joshi SB, Volkin DB, Ralston JP, Middaugh CR. 2011. Multidimensional methods for the formulation of biopharmaceuticals and vaccines. Journal of pharmaceutical sciences 100*:* 4171-4197.
18. Ramsey JD, Gill ML, Kamerzell TJ, Price ES, Joshi SB, Bishop SM, Oliver CN, Middaugh CR. 2009. Using empirical phase diagrams to understand the role of intramolecular dynamics in immunoglobulin G stability. Journal of pharmaceutical sciences 98(7):2432-2447.
19. Strickland EH, Beychok S. 1974. Aromatic contributions to circular dichroism spectra of protein. Critical Reviews in Biochemistry and Molecular Biology 2(1):113-175.
20. Kelly SM, Price NC. 2000. The use of circular dichroism in the investigation of protein structure and function. Current protein and peptide science 1(4):349-384.
21. Hawe A, Sutter M, Jiskoot W. 2008. Extrinsic fluorescent dyes as tools for protein characterization. Pharmaceutical research 25(7):1487-1499.
22. Sarvazyan AP. 1991. Ultrasonic velocimetry of biological compounds. Annual review of biophysics and biophysical chemistry 20(1):321-342.
23. Buckin V, O'Driscoll B, Smyth C, Alting A, Visschers R. 2003. Ultrasonic spectroscopy for materials analysis: Recent advances. Spectroscopy Europe 15(1):20-25.
24. Gavish B, Gratton E, Hardy CJ. 1983. Adiabatic compressibility of globular proteins. Proc Natl Acad Sci U S A 80(3):750-754.

25. Lakowicz JR, Keating-Nakamoto S. 1984. Red-edge excitation of fluorescence and dynamic properties of proteins and membranes. Biochemistry 23(13):3013-3021.
26. Demchenko AP. 2002 The red-edge effects: 30 years of exploration. Luminescence 17(1); 19-42.
27. Neil E, Marsh G. 2000. Towards the nonstick egg: designing fluorous proteins. Chem Biol 7(7):R153-157.
28. Russo D, Hura G, Head-Gordon T. 2004. Hydration dynamics near a model protein surface. Biophys J 86(3):1852-1862.
29. Russo D, Murarka RK, Copley JR, Head-Gordon T. 2005. Molecular view of water dynamics near model peptides. J Phys Chem B 109(26):12966-12975.
30. Vihinen M. 1987. Relationship of protein flexibility to thermostability. Protein engineering 1(6):477-480.
31. Tang K, Dill KA. 1998. Native protein fluctuations: the conformational-motion temperature and the inverse correlation of protein flexibility with protein stability. Journal of biomolecular structure & dynamics 16(2):397-411.
32. ZAvodszky PE, Kardos J, Svingor Á, Petsko GA. 1998. Adjustment of conformational flexibility is a key event in the thermal adaptation of proteins. Proceedings of the National Academy of Sciences 95(13):7406-7411.
33. Hernández G, Jenney FE, Adams MWW, LeMaster DM. 2000. Millisecond time scale conformational flexibility in a hyperthermophile protein at ambient temperature. Proceedings of the National Academy of Sciences 97(7):3166-3170.
34. Ferreon JC, Volk DE, Luxon BA, Gorenstein DG, Hilser VJ. 2003. Solution structure, dynamics, and thermodynamics of the native state ensemble of the Sem-5 C-terminal SH3 domain. Biochemistry 42(19):5582-5591.
35. Durney MA, Wechselberger RW, Kalodimos CG, Kaptein R, Vorgias CE, Boelens R. 2004. An alternate conformation of the hyperthermostable HU protein fromThermotoga maritima has unexpectedly high flexibility. FEBS letters 563(1):49-54.
36. LeMaster DM, Tang J, Paredes DI, Hernández G. 2005. Enhanced thermal stability achieved without increased conformational rigidity at physiological temperatures: Spatial propagation of differential flexibility in rubredoxin hybrids. Proteins: Structure, Function, and Bioinformatics 61(3):608-616.
37. Kamerzell TJ, Middaugh CR. 2008. The complex inter-relationships between protein flexibility and stability. *Journal of pharmaceutical sciences* 97(9): 3494-3517.

Chapter 3

Supporting Information

Table of Contents

Supplemental Figure 1: Thermal unfolding CD measurements of rPA at pH 7

Supplemental Figure 2: Thermal unfolding CD measurements of 2-FHis rPA at pH 7

Supplemental Figure 3: Thermal unfolding CD measurements of rPA at pH 5

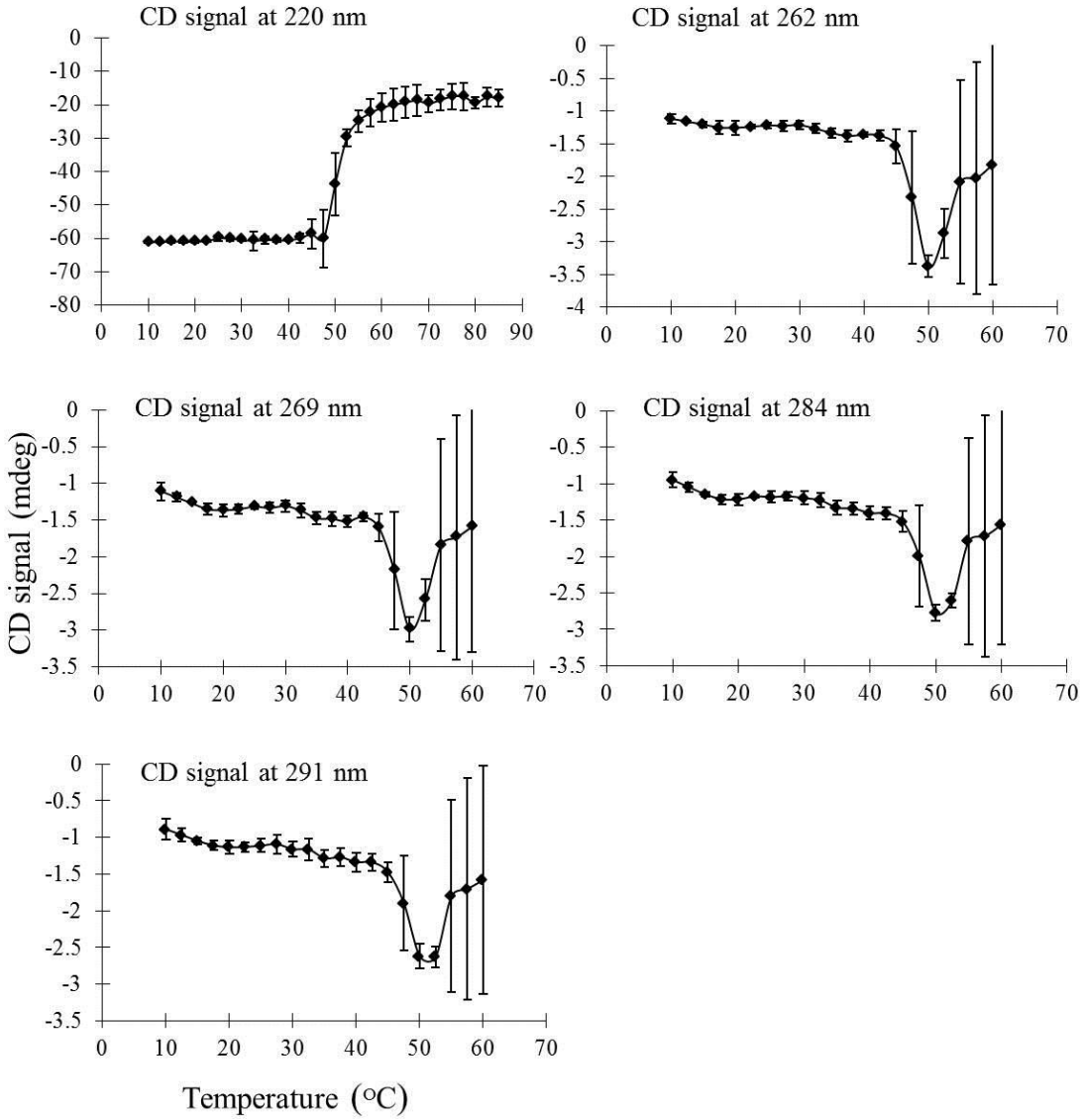

Supplemental Figure S1. Thermal stability of rPA (0.5 mg/ml at pH 7) as monitored by CD signals at indicated values (220, 262, 269, 284 and 291 nm) as a function of temperature. Each data point represents the mean of three independent runs, with error bars showing the standard deviation.

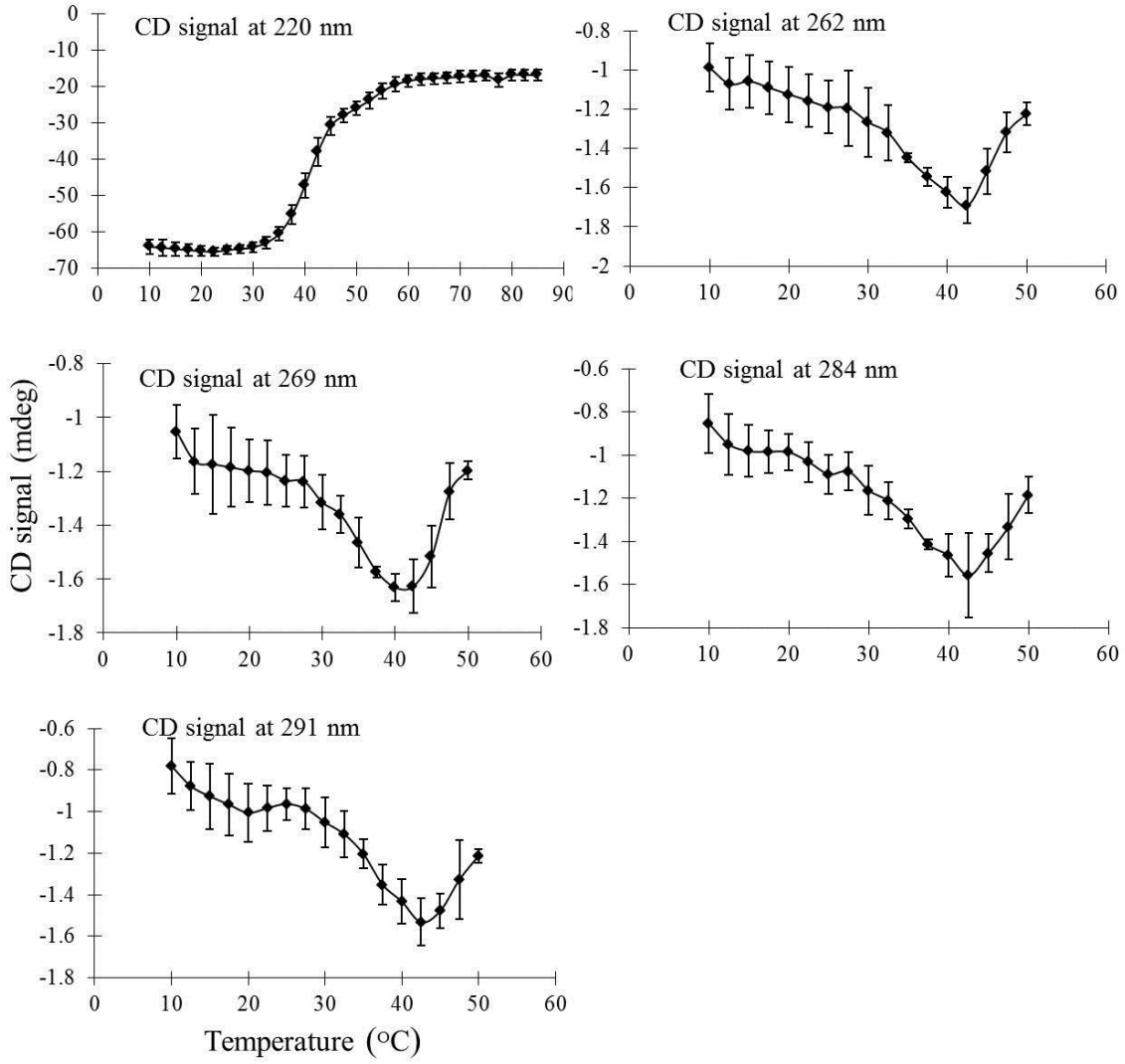

Supplemental Figure S2. Thermal stability of 2-FHis rPA (0.5 mg/ml at pH 5) as monitored by CD signals at indicated values (220, 262, 269, 284 and 291 nm) as a function of temperature. Each data point represents the mean of three independent runs, with error bars showing the standard deviation.

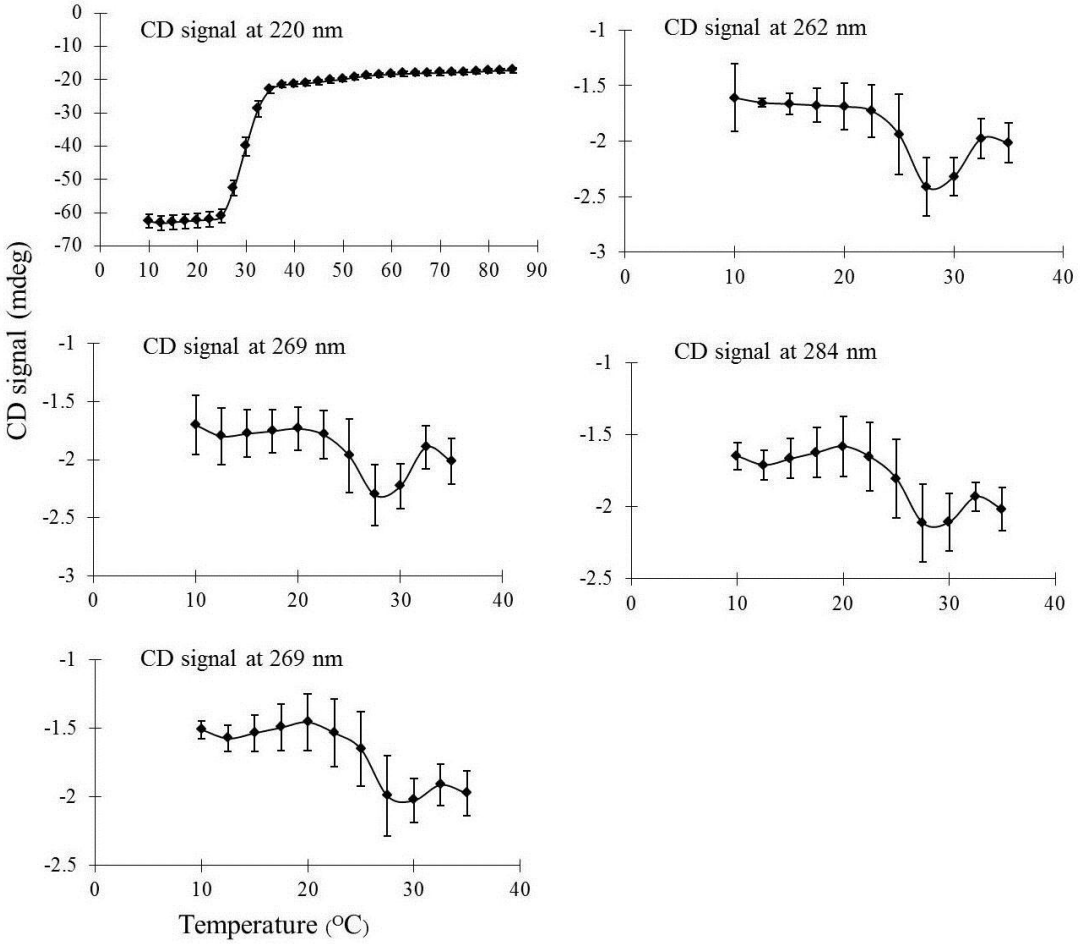

Supplemental Figure S3. Thermal stability of rPA (0.5 mg/ml at pH 5) as monitored by CD signals at indicated values (220, 262, 269, 284 and 291 nm) as a function of temperature. Each data point represents the mean of three independent runs, with error bars showing the standard deviation.

Chapter 4 Analytical Characterization and Adjuvant Studies of Dominant Negative Inhibitor as an Anthrax Vaccine

4.1. INTRODUCTION

In Chapter 3, I introduced the background concerning anthrax disease caused by *Bacillus anthracis*. The anthrax toxin, a tripartite toxin, plays a key role in the pathogenesis of anthrax.[1] It is formed by three nontoxic proteins secreted by *B. anthracis*, namely protective antigen (PA), lethal factor (LF), and edema factor (EF).[2] The combination of PA with LF and EF results in complex toxins such as edema (EdTx) and lethal toxin (LeTx).[2,3] Because PA plays an important role in the pathology of anthrax and its highly immunogenic, it is used as the major antigen in most anthrax vaccine formulations. As described in Chapter 3, the current licensed US anthrax vaccine (AVA, BioThrax) has a very limited duration of protection and requires multiple immunizations and yearly boosts.[4] In addition, it may not be optimal and/or safe to administer a PA-based vaccine for post-exposure vaccination, because the administration of native PA may aid in anthrax toxin formation with disasterous consequesnces.[5,6,7] Therefore, there is a need to develop improved versions of anthrax vaccines. Specific mutations of PA in domains 2 and 3 have been constructed to block the translocation and/or self-assembly of the toxin.[5-8] These mutants have shown both potential improvements in safety (diminished toxicity) and immunogenicity.

A dominant-negative inhibitor (DNI) of the anthrax toxin has been demonstrated to be a potential antitoxin and a potent imunnogen as an anthrax vaccine. DNI is a translocation-deficient mutant of anthrax protective antigen with the double mutation of K397D and D425K. This mutant co-oligomerizes with the wild-type PA protein and blocks its ability to translocate LF or EF into the cell cytosol. Thus inhibiting cellular toxicity caused by LF/EF.[8] DNI strongly inhibits toxin action in cell culture and in animal intoxication

models[5,8]. This suggests that it has the therapeutic potential to be used as an antitoxin. Aside from the therapeutic potential of DNI, previous studies have shown that DNI is more immunogenic than PA in a mice study in which DNI elicited a higher antibody titer than PA.[5,6] Because of the enhanced immunogenicity of DNI, the use of DNI as a replacement for PA in anthrax vaccines has significant potential. In summary, DNI is a promising candidate for use in the treatment of anthrax, which can potentially provide both improved immunogenicity in vaccines and therapeutic activity in antitoxic therapy.

In the present study, to evaluate the physical stability of the lyophilized DNI protein that had been stored at 4 ℃ for about eight years, the stability of the reconstituted proteins under unstressed and stressed conditions (at elevated temperatures of 40 and 70 ℃ for one, two and four weeks) was characterized by various techniques at pH 7 from 10 to 80 ℃. SDS-PAGE, near and far circular dichroism (CD), intrinsic fluorescence, and optical density measurements were used, as well as a static light scattering technique. The size of the proteins was characterized by dynamic light scattering and micro-flow imaging methods. The soluble aggregates of the samples were characterized by size-exclusion liquid chromatography. In addition, the chemical stability (deamidation) was also evaluated using capillary isoelectric focusing (cIEF). The Studies of DNI with aluminum adjuvants were further performed to study antigen/adjuvant interactions and the stability of DNI on the surface of the adjuvant. Because purified recombinant proteins are usually not highly immunogenic, an adjuvant is usually needed to boost their immunogenicity. In addition, the biophysical characterization results of DNI were compared to those obtained from the unmodified recombinant protective antigen, and the physicochemical properties of rPA and

its mutant (DNI) were compared. Through these characterization studies, the conformational stability of lyophilized DNI was comprehensively evaluated. These results provide important information about the conformational integrity of DNI that had been stored for eight years. Key parameters such as pH, temperature, and buffers were also defined to facilitate for further formulation development.

4.2 MATERIALS AND METHODS

4.2.1 Materials

The dominant negative inhibitor antigen was produced by Pharmaceutical Solutions LLC (Bloomington, IN) as a lyophilized powder in sealed glass vials. The vials of the DNI protein contained 25 mg of protein, 113 mg mannitol, 33 mg sucrose, and 2.4 mg dibasic sodium phosphate. They were reconstituted with 3.3 ml of water for injection (WFI), the reconstituted protein concentration was 91 μM. 10 mg of recombinant protective antigen was also purchased from List Biological Laboratories Inc (Campbell, CA).

For the physical characterization of unstressed samples, individual protein solutions at pH 6-8 were prepared by reconstituting 2.0 ml of water and then diluting with 20 mM citrate phosphate buffer with a total ionic strength of 0.15 (adjusted with NaCl). Before making measurements, the samples of DNI were dialyzed at 4 ℃ using Slide-A-Lyzer® Dialysis Cassettes (Thermo Scientific, Rockford, IL) with a 3.5 kDa MW cutoff. For adjuvant studies, 10 mM histidine buffer containing 150 mM NaCl at pH 7 was used. DNI protein was reconstituted with 2.0 ml water then dialyzed into 10 mM histinde buffer containing 150 mM NaCl overnight at 4 ℃. The adjuvants aluminum hydroxide (Alhydrogel®) and aluminum phosphate (Adju-Phos®) were purchased from Brenntag Biosector (Frederikssund, Denmark).

For the stressed study at elevated temperatures, vials were placed at 40 and 70 ℃. Vials were withdrawn at three time points; one week, two weeks and four weeks. Then the vial was reconstituted with 2.0 ml of water. The stressed sample was then diluted to 0.5 mg/ml with 20 mM citrate phosphate buffer containing NaCl (I=0.15) at pH 7. The same biophysical analysis was conducted as performed with the unstressed DNI samples.

4.2.2 Analytical Characterization

4.2.2.1 SDS-PAGE

Unstressed and stressed DNI samples were characterized by reducing SDS-PAGE. The amount of protein loaded was 20 μg. For the experiments, DNI protein was mixed with 50 mM reducing agent dithiothreitol (DTT). All samples including the molecular standards were heated at 80 ℃ for five minutes before loading.

4.2.2.2 Far and Near UV Circular Dichroism Spectroscopy

Circular dichroism analysis was performed with a Chirascan-plus circular dichroism spectrometer (Applied Photophysics Ltd, Leatherhead UK) equipped with a Peltier temperature controller and a 4-position cuvette holder. Far and near UV spectra of samples (0.5 mg/ml) were collected in the range of 200-360 nm using a 0.2 cm path length cuvette sealed with a Teflon stopper. A sampling time per point of 3 s and a bandwidth of 1 nm were used. The characteristic CD signals of the samples at 220, 262, 269, 284 and 291 nm were monitored as a function of temperature from 10 to 80 ℃ at 2.5 ℃ intervals. Triplicate measurements were made with a heating rate of 1 ℃/min, and an equilibration time at each temperature of 1 minute.

For the 70 ℃, one week stressed samples, because low signal to noise ratios were

observed in the far UV CD region, the CD signal was monitored at 229 nm instead of 220 nm. Measurements of far UV CD were also performed separately from near UV CD measurements using lower protein concentration and cell path length. Far UV spectra of samples (0.2 mg/ml) were collected in the range of 200-260 nm using a 0.1 cm path length cuvette. A sampling time per point of 1 s and a bandwidth of 1 nm were used. The CD signals of the samples at 220 nm were monitored as a function of temperature from 10 to 80 ℃ at 2.5 ℃ intervals. Triplicate measurements were made.

4.2.2.3 Intrinsic Fluorescence Spectroscopy

The intrinsic fluorescence of DNI (0.5 mg/ml) was measured using a QuantaMaster Spectrofluorometer (Photon Technology International, Inc., Birmingham, NJ) equipped with a 4-position cell holder and Peltier temperature control device. Fluorescence emission spectra of samples were recorded as a function of temperature (10-82.5 ℃). Duplicate samples were measured using an excitation wavelength of 295 nm (> 95% tryptophan emission). Emission spectra were collected from 300 to 400 nm with a step size of 1 nm and an integration time of 1 s. The excitation and emission slits were set at 2 and 3 nm, respectively. The spectra were collected at 2.5 ℃ intervals with a 3 min equilibration time at each temperature. A 2 x 10 mm quartz cuvette was used in all experiments. Data analysis was performed using FelixTM (Photon Technology International, Inc.) software. The position of the emission wavelength maximum was determined using a polynomial derivative fitting method executed in *Origin 7.0* software.

4.2.2.4 Optical Density Measurements

The aggregation behavior of DNI was determined simultaneously during the near and far

UV CD experiments. The optical density at 350 nm was obtained as a function of temperature (10-80 ℃).

4.2.2.5 Static Light Scattering

The aggregation behavior of DNI was also determined simultaneously during the intrinsic fluorescence experiments employing a second photomultiplier located 180 ° to the fluorescence detector and using a 0.25 nm slit width. The scattering intensities at 295 nm were obtained as a function of temperature (10-82.5 ℃).

4.2.2.6 Dynamic Light Scattering

The mean effective hydrodynamic diameters of the DNI (0.5 mg/ml) were monitored by dynamic light scattering at 25 ℃, and five measurements were taken at this temperature. Data was collected on a ZetaPALS Zeta Potential Analyzer (Brookhaven Instrument Corp., Holtzille, NY). A digital autocorrelator (BI-9000 AT) was used to create the autocorrelation function. The diffusion coefficients of the particles were extracted by cumulant analysis of the auto correlation functions. The effective hydrodynamic diameter was calculated from the diffusion coefficient by the Stokes-Einstein equation. Viscosity and refractive index corrections were applied to each measurement using NanoDLS Particle Sizing software (Brookhaven Instrument).

4.2.2.6 Deamidation studies using capillary isoelectric focusing (cIEF)

The cIEF experiments were performed on an iCE280 instrument from Convergent Biosciences (Toronto, Canada) to characterize the charge variants of the protein. All experiments were performed at 10 ℃ using a temperature controlled auto-sampler.

Unstressed and stressed DNI samples in 10 mM histidine buffer at pH 7 were mixed with

12 M urea stock solution, 1% methyl cellulose solution (Convergent Bioscience, Toronto, Canada), Pharmalyte 3-10 (GE Healthcare, Uppsala, Sweden) and two PI markers. The pH values of the pI markers were 4.65 and 8.18. The final protein concentration used was 0.4 mg/ml and the urea concentration was 6 M. Duplicate measurements were run. Qualification and quantification of charge variants were performed using Chrom Perfect® software.

4.2.2.7 Size-Exclusion Liquid Chromatography

The size-exclusion liquid chromatography experiments were performed on a Shimadzu HPLC system (Columbia, MD) to characterize the soluble aggregates of samples under unstressed and stressed conditions. A protein concentration of 1.0 mg/ml in 10 mM histidine buffer (pH 7) containing 150 mM NaCl was used. A TSKgel G2000SW_{xL} analytical column (7.8mm x 30cm, 5µm) was used and the column temperature was 30 ^{o}C. The mobile phase was 50 mM sodium phosphate buffer at pH 6.8 containing 200 mM NaCl. The injection volume was 50µl and the flow rate was 0.65 mg/ml. Triplicate measurements were made. Two observed peaks corresponding two major species were quantified by their peak areas using LCsolution software (Shimadzu Corporation).

4.2.2.8 Micro flow imaging

A micro-flow imaging (MFI) instrument from Brightwell Technologies® was used for subvisible particle characterization from 2 micron and up, using the set point 3 mode (low magnification and open aperture settings). One ml of the unstressed or stressed samples (0.5 mg/ml) were pipetted in barrier tips and used in the MFI experiments. Optimization of illumination was done using the respective buffer solutions of a given sample. The particle size and count distribution was subjected to a 0.85 aspect ratio cut off to remove any

interference by air bubbles.

4.2.2 Adjuvant-Antigen study

The experiments in the presence of the adjuvants were conducted by adding Alhydrogel® or Adjuphos® to the protein. The binding of DNI to the two adjuvants was tested in the presence of three different buffers: histidine, imidazole and citrate-phosphate at pH 7. After finding maximum adsorption to Alhydrogel in the histidine buffer, this buffer was retained as the buffer of choice in further experiments in the presence of adjuvant. The protein antigens were first tested to determine whether DNI adsorbs preferentially to Alhydrogel® or Adjuphos®. This was done by adding 100 µg of protein to 250 µg of adjuvant. The amount of unadsorbed protein was determined by measuring the amount of protein in the supernatant using UV absorbance spectroscopy after centrifugation. An adsorption isotherm was constructed for each protein in the presence of 0.25 mg/ml Alhydrogel® using various protein concentrations (0.05 – 1.0 mg/ml).

4.3. Results

4.3.1 Anlytical Characterization

4.3.1.1 SDS-PAGE

The DNI protein was analyzed using SDS-PAGE electrophoresis. Figure 1 shows a gel of the non-stressed and stressed DNI samples at various time points. The samples in the various lanes are described below in the Table 1. All samples were analyzed in the presence of a reducing agent.

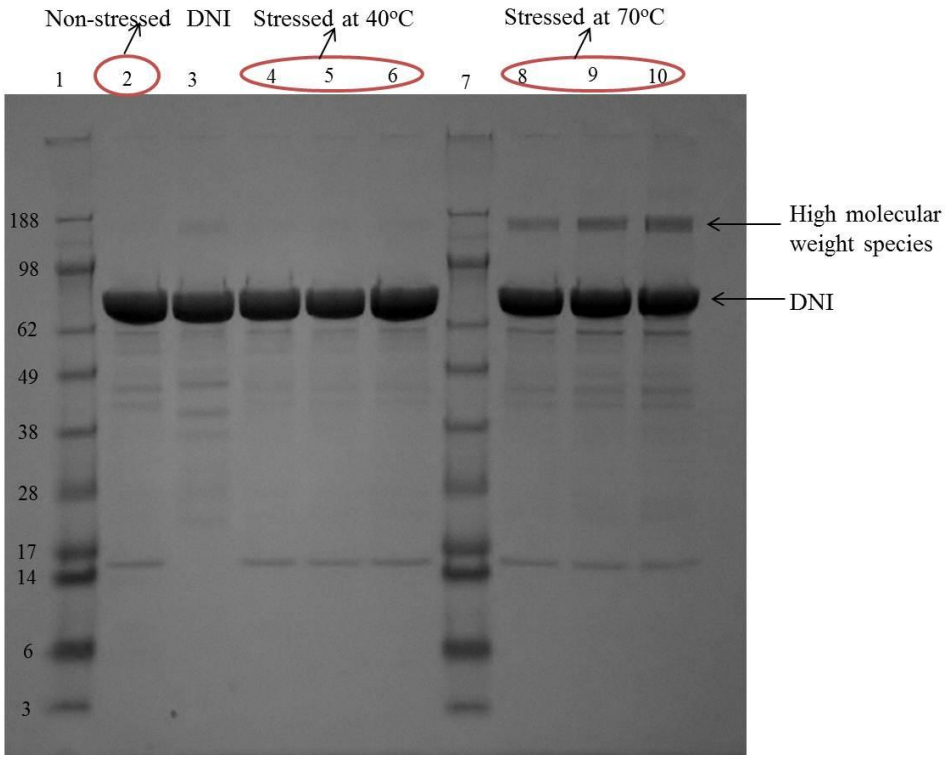

Figure 1: Reducing SDS-PAGE analysis of DNI under various stressed and non-stressed conditions, along with the molecular weights of the markers (in kDa) in the left. Lanes 1 and 7, molecular weight markers; lanes 2 and 3, unstressed DNI and rPA; lanes 4, 5, and 6, DNI protein stressed at 40 ℃ for one week, two weeks and four weeks; lanes 8, 9, and 10, DNI protein stressed at 70 ℃ for one week, two weeks and four weeks.

Lane	Sample
1	Marker
2	DNI Protein at time 0
3	rPA
4	DNI protein Stressed at 40 ℃ for 1 Week
5	DNI protein Stressed at 40 ℃ for 2 Week
6	DNI protein Stressed at 40 ℃ for 4 Week
7	Marker
8	DNI protein Stressed at 70 ℃ for 1 Week
9	DNI protein Stressed at 70 ℃ for 2 Week
10	DNI protein Stressed at 70 ℃ for 4 Week

Table 1: The different samples used in the SDS-Page gel.

The DNI protein and the control rPA are shown in lanes 2 and 3 in Figure 1. No significant differences were seen in the two proteins, except for the band between 17 kDa and 14 kDa. No significant differences were seen when DNI were exposed to 40 ℃ for up to four weeks (lanes 4, 5, and 6). The marker is again shown in lane 7. The DNI protein stressed at 70 ℃ is shown in lanes 8, 9 and 10 (stressed for one, two and four weeks respectively). The only significant difference noticed when DNI was stressed at 70 ℃ is the appearance of a high molecular weight species between the 188 kDa and the 98 kDa bands. This appears after one week at 70 ℃ and increases in intensity when stressed for longer times.

The multiple bands seen for the DNI protein at time 0 and other conditions may indicate impurities or products of degradation. These bands are very light compared to the monomer that shows up between the 98 kDa and 62 kDa bands.

4.3.1.2 Near and Far UV Circular Dichroism Spectroscopy

Non-Stressed Samples of DNI and rPA

Typical near- and far-UV CD spectra of 0.5 mg/ml DNI at pH 6 at 10 ℃ are shown in Figure 2. In the far-UV region (200-250 nm), DNI displays a broad peak with a minimum CD signal near 215 nm. In the near-UV region (250-320 nm), four characteristic peaks at 262, 269, 284 and 291 nm were observed, which arise from the aromatic amino acid residues.

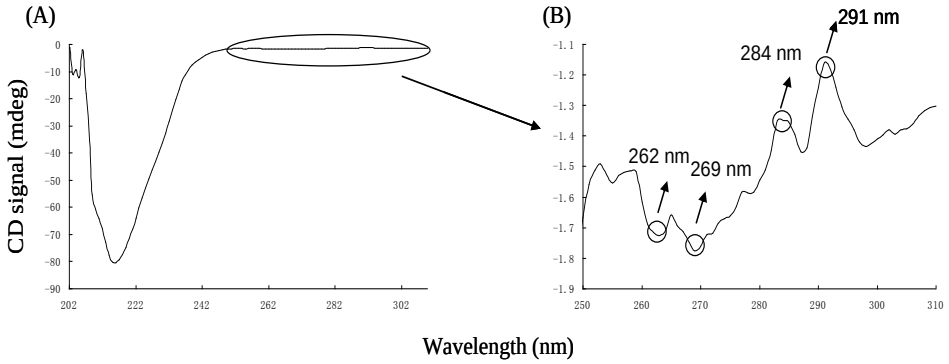

Figure 2: Near- and far-UV CD spectra for DNI protein collected simultaneously. Near/far-UV CD spectra are shown for (A) 0.5 mg/ml DNI at pH 6 and (B) expanded view of the near-UV region.

The effect of temperature and pH on the DNI's secondary and tertiary structures was further investigated by using thermal melt analysis. CD signals at five characteristic peaks (220, 262, 269, 284 and 291 nm) were monitored across the pH range of 6-8 (Figure 3-5). An overall loss in secondary and tertiary structures is observed as a function of increasing temperature. In the near- or far- UV CD regions, the onset temperature (T_{on}) of thermal transitions occurs at about 32.5 ℃ at pH 6, 45 ℃ at pH 7, and 47.5 ℃ at pH 8, suggesting that proteins at pH 8 are the most stable.

For the rPA standard protein at pH 7, similar near- and far- UV CD spectra at 10 ℃ were obtained compared to the spectrum produced by DNI (Figure 2). The CD thermal melt curves monitored at different wavelengths are shown in Figure 6. The T_{on} temperature occurs at about 42.5 ℃, which is 2.5 ℃ lower than that observed for the DNI protein at pH 7.

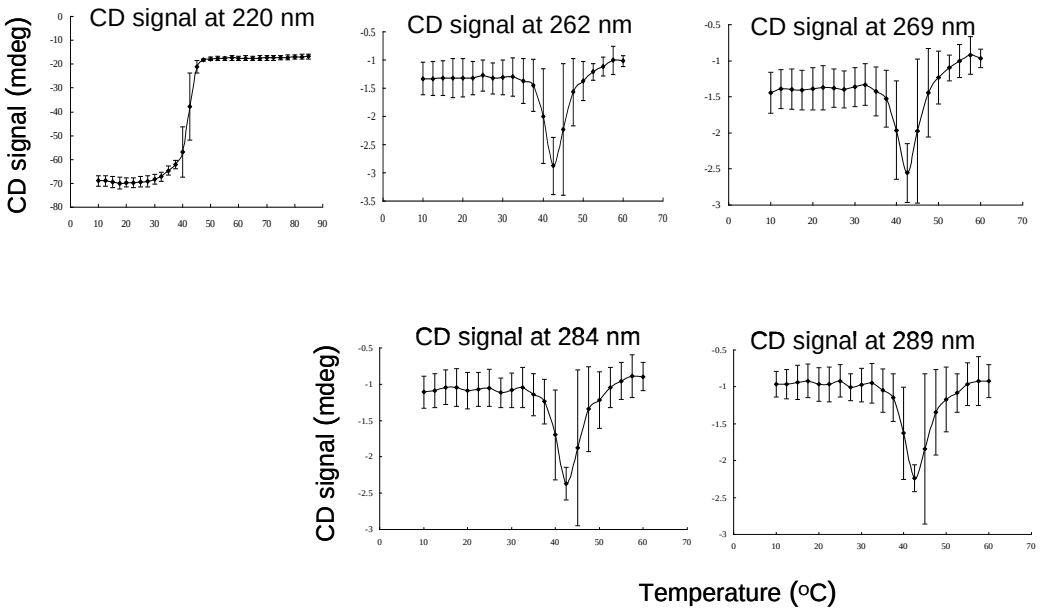

Figure 3. Thermal stability of DNI (0.5 mg/ml at pH 6) as monitored by CD signals at 220, 262, 269, 284 and 291 nm as a function of temperature. Each data point represents the mean of three independent runs, with error bars showing the standard deviation.

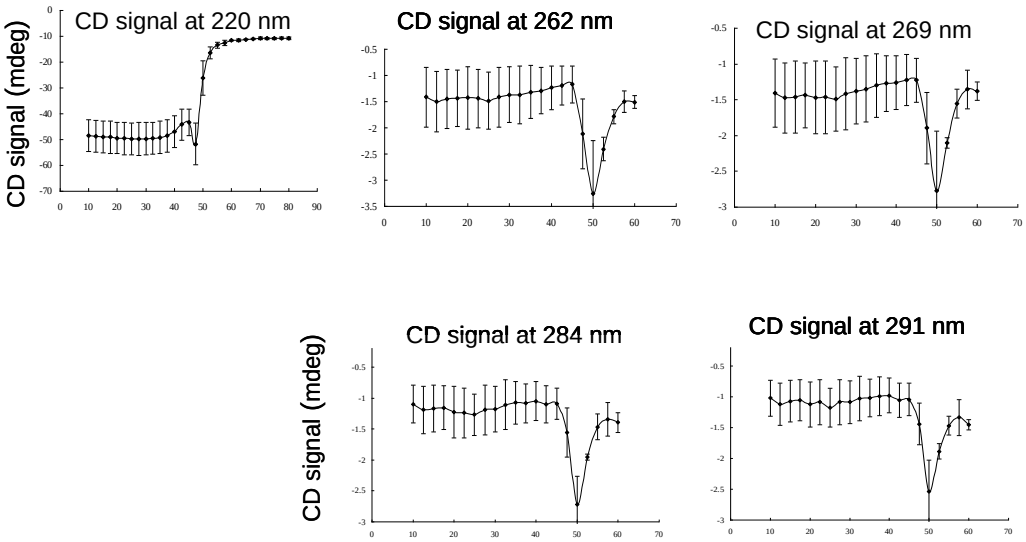

Figure 4. Thermal stability of DNI (0.5 mg/ml at pH 7) as monitored by CD signals at 220, 262, 269, 284 and 291 nm as a function of temperature. Each data point represents the mean of three independent runs, with error bars showing the standard deviation.

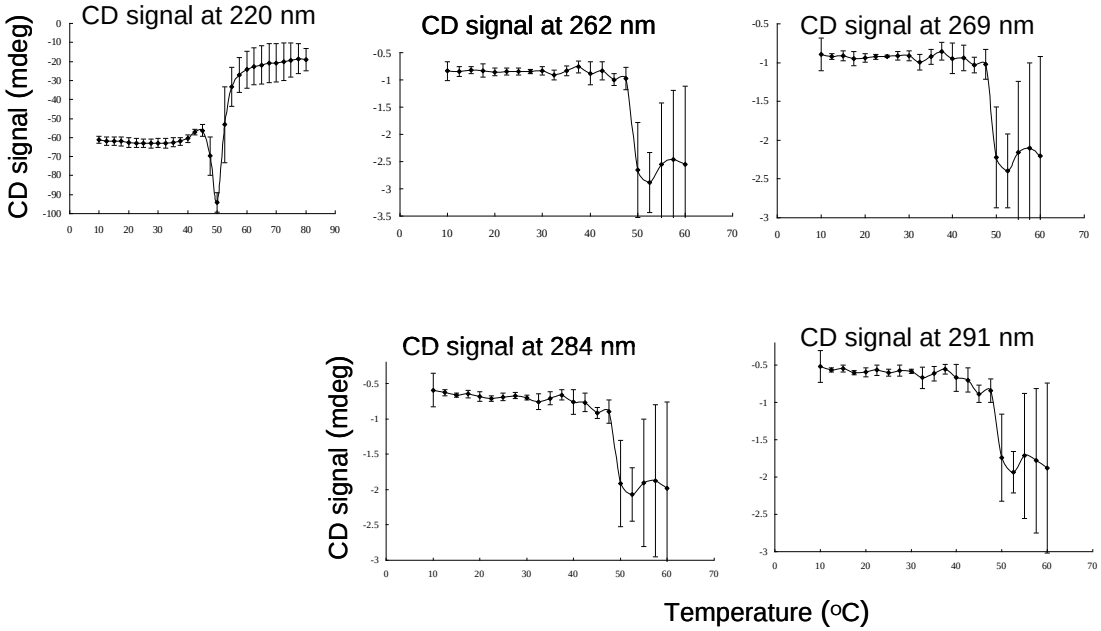

Figure 5. Thermal stability of DNI (0.5 mg/ml at pH 8) as monitored by CD signals at 220, 262, 269, 284 and 291 nm as a function of temperature. Each data point represents the mean of three independent runs, with error bars showing the standard deviation.

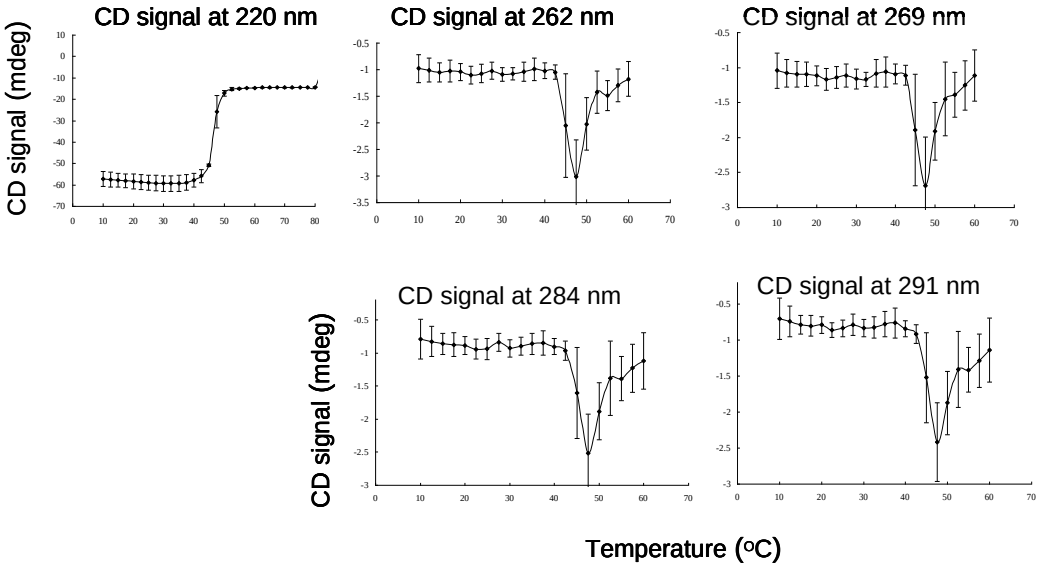

Figure 6. Thermal stability of rPA (0.5 mg/ml at pH 7) as monitored by CD signals at 220, 262, 269, 284 and 291 nm as a function of temperature. Each data point represents the mean of three independent runs, with error bars showing the standard deviation.

Stressed Samples of DNI

The near- and far-UV CD spectra of stressed samples (40 and 70 ℃ for one and two weeks) at pH 7 display similar spectra to those at 10 ℃ (data not shown). For the samples at pH 7 (DNI at 40 ℃ for one, two and four weeks, DNI at 70 ℃ for one, two and four weeks), the thermal melts at 220, 264, 269, 284, and 291 nm all initiate at about 45 ^{o}C monitored in both the near and far UV CD regions (Figures 7A-E and Figures 8A-E for samples stressed at 40 and 70 ℃, respectively); the same results are seen in the non-stressed DNI samples. This suggests that lyophilized DNI manifests high resistance to physical degradation even after a month of exposure to 70 ℃. The thermal melts do not change significantly when exposed to temperatures of 40 ℃ or 70 ℃ for four weeks. In addition, non-stressed and stressed DNI proteins show a 2.5 ℃ higher T_{on} value than rPA.

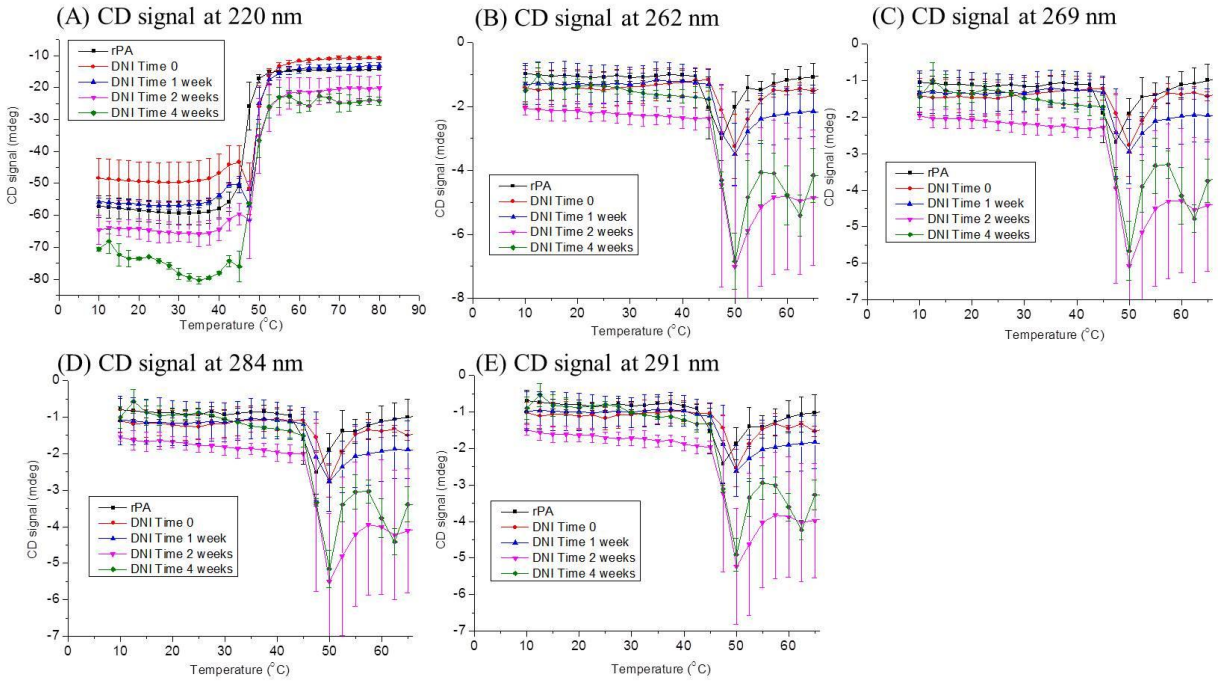

Figure 7. Thermal stability of DNI stressed at 40 ℃ for one to four weeks (0.5 mg/ml at pH 7) as monitored by CD signals at 220, 262, 269, 284 and 291 nm as a function of temperature. Non-stressed DNI and rPA were added for comparison. Each data point represents the mean of three independent runs, with error bars showing the standard deviation.

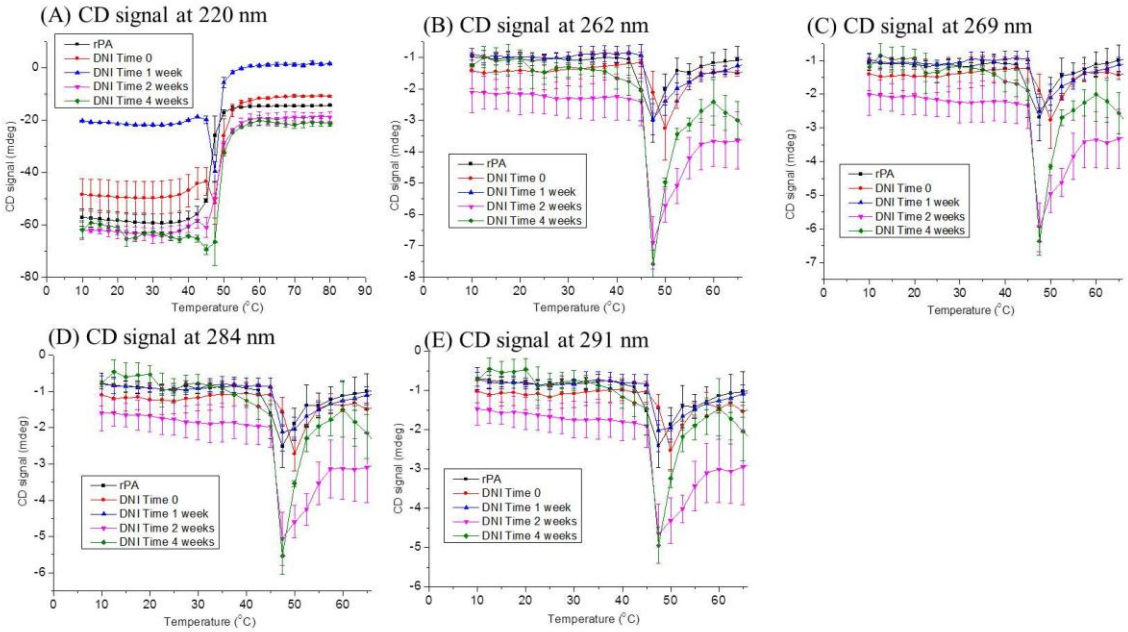

Figure 8. Thermal stability of DNI stressed at 70 ℃ for one to four weeks (0.5 mg/ml at pH 7) as monitored by CD signals at 220, 262, 269, 284 and 291 nm as a function of temperature. Non-stressed DNI and rPA were added for comparison. Each data point represents the mean of three independent runs, with error bars showing the standard deviation. Because of the noise in the far UV region, the CD signal of DNI one week stressed samples was monitored at 229 nm instead of 220 nm.

4.3.1.3 Intrinsic Fluorescence Spectroscopy

Non-Stressed Samples of DNI and rPA

Figure 9A shows the changes in the peak maximum position of the fluorescence emission as a function of temperature for rPA and DNI. Both proteins show a peak position of about 328 nm at low temperatures. With increasing temperature, the proteins begin to unfold, shifting the emission peak maximum by about 10 nm to 338 nm. This suggests less than complete unfolding where a $\lambda_{max} > 350$ nm would be expected. This change in conformation occurs at about 40 ^{o}C, which is typically the T_{on} temperature for anthrax protective antigen. DNI was found to be least stable at pH 6, a condition which showed changes in peak position as early as 30 ^{o}C. High standard deviations were noted at high temperatures, presumably due to differences in aggregation pathways and final states.

Stressed Samples of DNI

When lyophilized DNI was exposed to temperatures of 40 and 70 ℃, no significant changes in thermal profiles were seen. Figure 9B details the changes in fluorescence peak position maxima when exposed to 40 ℃ for up to four weeks. Reference rPA was also added for comparison. No changes in T_{on} values (40 ℃) were observed for DNI when the proteins were maintained at 40 ℃ for four weeks. High standard deviations were observed at high temperatures, presumably due to aggregation. Figure 9C illustrates the changes in fluorescence peak position maxima when exposed to 70 ℃ for four weeks. Minor decrease in T_m was noticed for DNI when exposed to 70 ℃ for one week, although these small changes were within the standard errors of the measurements. A slight drop in T_m was also observed for DNI when exposed to 70 ℃ for four weeks. Overall, very similar thermal transition

curves were observed from both the non-stressed and stressed samples, suggesting that formulated DNI proteins have high thermal stability and are able to resist surprisingly elevated temperature stress at long incubation times.

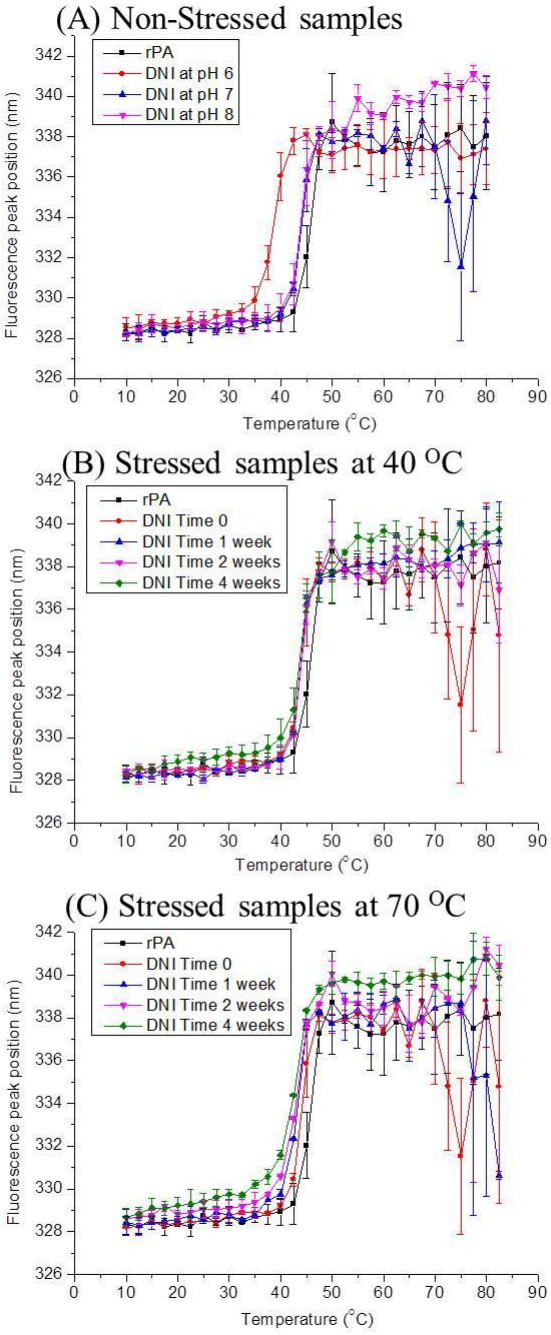

Figure 9 Intrinsic fluorescence peak position shifts as a function of temperature for (A) Non-stressed DNI and rPA samples, (B) DNI samples stressed at 40 ^{o}C, and (C) DNI samples stressed at 70 ^{o}C. Non-stressed DNI and rPA were added for comparison. Error bars reflect standard deviations from two separate runs.

4.3.1.4 Optical density measurements

Non-Stressed Samples of DNI and rPA

Optical density (OD) data at 350 nm were collected simultaneously during CD measurements. DNI showed aggregation a reflected by increased OD intensity with increasing temperature (Figure 10). The OD thermal unfolding results are overall consistent with the observations made from the CD measurements, with similar effects of pH and temperature seen on the aggregation stabilities of the proteins. Again, DNI at pH 6 shows a lower stability than samples at pH 7 and 8.

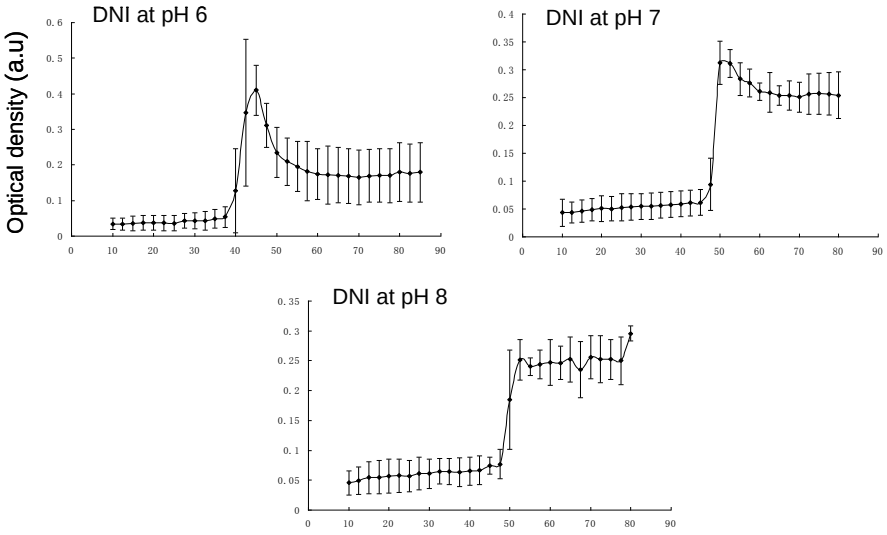

Figure 10. Thermal stability of DNI (0.5 mg/ml at pH 6, 7 and 8) as monitored by optical density at 350 nm. Each data point represents the mean of three independent runs, with error bars showing the standard deviation.

Stressed Samples of DNI

For the stressed DNI protein (at 40 ℃ for one, two and four weeks, DNI protein at 70 ℃ for one, two and four weeks), the T_{on} of thermal transitions occurs at about 45 ℃ at pH 7 (Figure 11A-B). Again, the same T_{on} values of the unstressed and stressed values were observed, indicating that the stressed samples manifest the same structural integrity as native DNI.

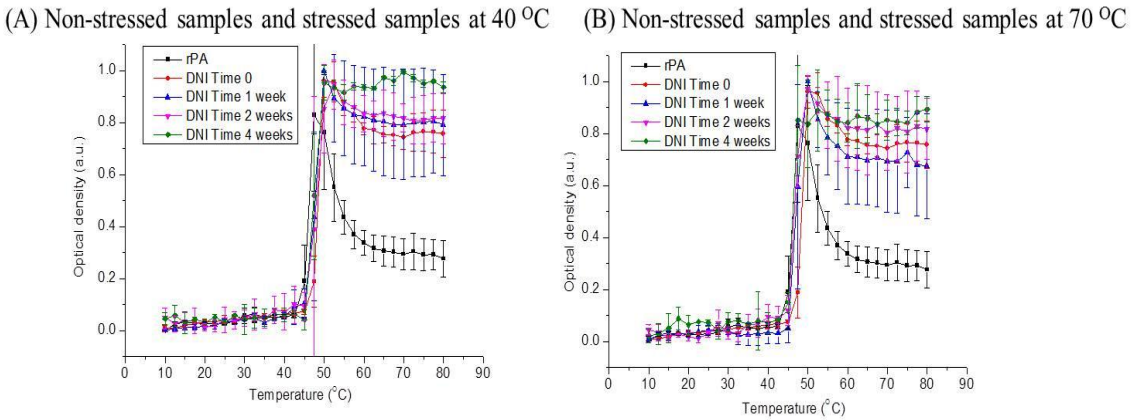

Figure 11. Thermal stability of stressed DNI (0.5 mg/ml at pH 7) as monitored by optical density at 350 nm. (A) DNI at 40 ℃ for one to four weeks. (B) DNI at 70 ℃ for one to four weeks. Non-stressed DNI and rPA were added for comparison. Each data point represents the mean of three independent runs, with error bars showing the standard deviation.

4.3.1.4 Static Light Scattering

Non-Stressed Samples of DNI and rPA

Light scattering was also monitored while acquiring intrinsic fluorescence data using a secondary detector placed 180^{o} to the primary fluorescence detector. Increases in light scattering are observed due to the formation of aggregates. Figure 12A shows the changes in light scattering intensity as a function of temperature. Increases in light scattering were observed at about 45 ℃ for rPA and DNI at pH 7. This increase in scattering was delayed slightly for DNI at pH 8. DNI was found to be least stable at pH 6. Increases in light scattering were observed as early as 40 ^{o}C for DNI at pH 6.

Stressed Samples of DNI

Similar to the results observed by intrinsic fluorescence spectroscopy and other techniques, no significant differences in the transition onset temperatures were observed when DNI was stressed at 40 ^{o}C for up to four weeks. The changes in light scattering intensity as a function of temperature are shown in Figure 12B for DNI samples exposed to 40 ^{o}C. When DNI was stressed for two weeks at 70 ^{o}C, a slight reduction in the transition T_{on} was observed. This is shown in Figure 12C. Very high standard deviations were observed in most samples, however, presumably due to variations in the settling of the protein aggregates in the cuvette.

4.3.1.5 Dynamic Light Scattering

The hydrodynamic properties of the DNI proteins were measured by dynamic light scattering. Results show that native unstressed proteins at pH 7 have a diameter of 6.7±0.4 nm based on analysis of particle number distribution. All of the stressed samples have a

similar diameter around 6.7 nm. These results suggest that stressed and unstressed samples have similar hydrodynamic properties.

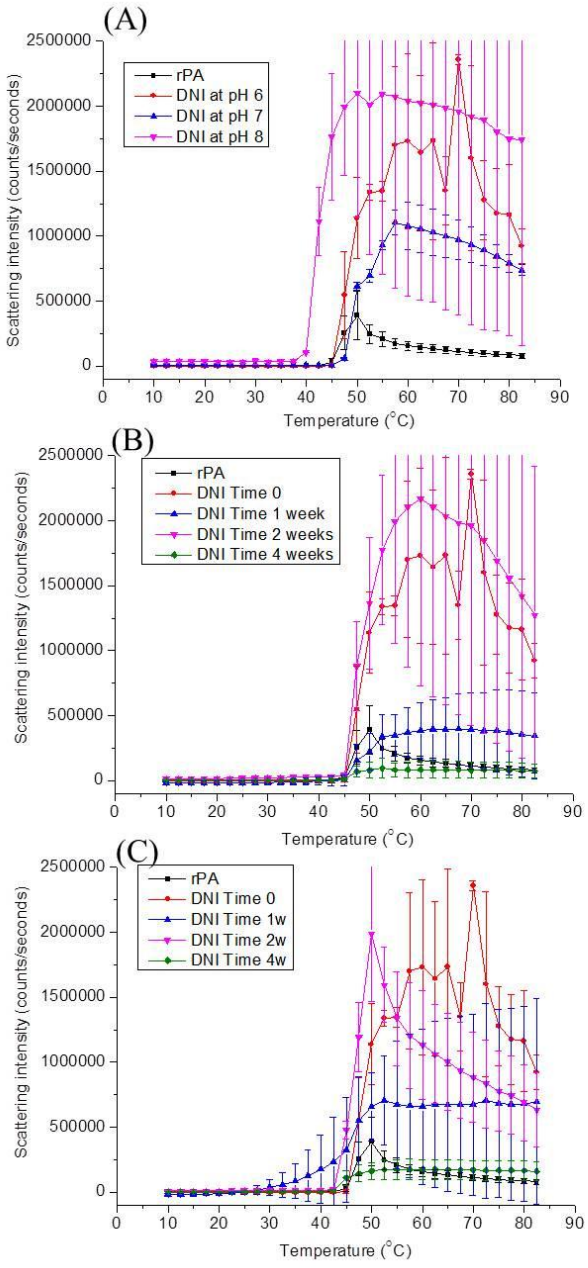

Figure 12. Thermal stability of stressed DNI (0.5 mg/ml at pH 7) as monitored by static light scattering. (A) Non-stressed DNI and rPA samples, (B) DNI at 40 ℃ for one to four weeks. (C) DNI at 70 ℃ for one to four weeks. Non-stressed DNI and rPA were added for comparison. Each data point represents the mean of three independent runs, with error bars showing the standard deviation.

4.3.1.6 Deamidation studies using capillary isoelectric focusing (cIEF)

In the absence of urea, DNI only shows poorly separated peaks (data not shown). In the presence of urea (6 M), however, DNI shows five major peaks with moderate resolution. Figure 13 shows the cIEF results of day 0's DNI. Five major peaks could be easily identified at day 0, which suggests that this material was a heterogeneous mixture of charge isoforms. However, the peak at pI value around 6.00 is very small compared to the other four peaks. Figure 13 also shows the cIEF profiles of DNI protein at elevated temperature (40 and 70 ℃) with increased incubation time (four weeks). For the four weeks stressed sample at 40 ℃(Figure13B), the cIEF profile is similar to that of the unstressed sample. For the four weeks stressed sample at 70 ℃ (Figure13C), the largest peak (pI=6.19) decreases while other four smaller peaks increase. The amount of three acidic isoforms (pIs around 6.00, 6.05 and 6.12) increase, and one basic isoform with pI value of 6.27 also increases. By quantification of the peak areas of five isoforms (Table 2 and Table 3), for the samples stressed at 40 ℃, we see that the major isoform with pI value of 6.19 decreases slightly from 59.6% to 56.0%, while other isoforms increase their area percentages slightly (Table 2). In contrast, for the samples stressed at 70 ℃, the major isoform (pI=6.19) decreases dramatically from 59.6% to 40.2%, and other four isoforms increase their area percentages (Table 3). These observations suggest that the DNI samples maintain their chemical stability under the condition of the 40 ℃ for up to 4 weeks. And DNI samples are prone to deamidate at higher temperature such as 70 ℃ with increased incubation time.

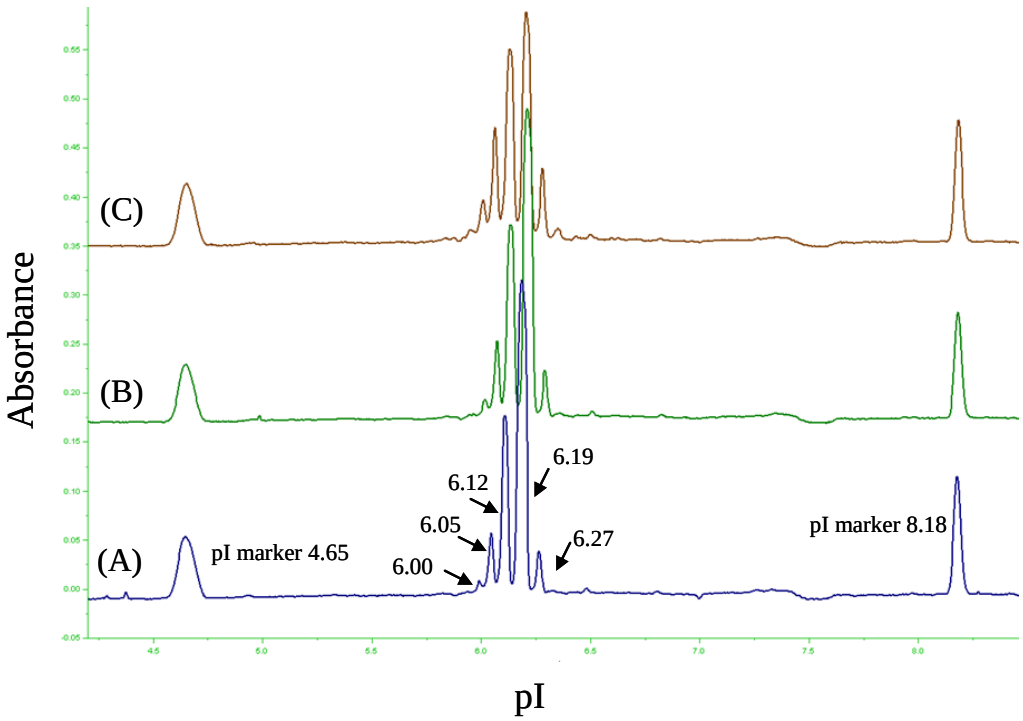

Figure 13. cIEF electropherograms of 0.4 mg/ml stressed DNI at pH 7. (A) DNI at Time 0. (B) DNI at 40 ℃ for four weeks. (C) DNI at 70 ℃ for four weeks.

	Time 0	Time 1 week 40 ℃	Time 2 weeks 40 ℃	Time 4 weeks 40 ℃
Peak 1	1.42 ± 0.16%	1.48 ±0.13%	1.55 ±0.32%	1.85 ±0.15%
Peak 2	7.22 ±0.16%	7.46 ±0.10%	7.79 ±0.20%	8.24 ±0.27%
Peak 3	27.10 ±0.21%	27.83 ±0.38%	28.38 ±0.05%	29.15 ±0.29%
Peak 4	59.62 ±0.18%	58.62 ±0.73%	57.35 ±0.52%	55.93 ±0.60%
Peak 5	4.64 ± 0.03%	4.61 ± 0.11%	4.93 ± 0.05%	4.81 ± 0.11%

Table 2: Quantification of the isoform's peak area of the unstressed and stressed samples at 40 ℃ for four weeks.

	Time 0	Time 1 week 70 ℃	Time 2 weeks 70 ℃	Time 4 weeks 70 ℃
Peak 1	1.42 ± 0.16%	2.69 ±0.01%	3.47 ±0.15%	4.15 ±0.31%
Peak 2	7.22 ±0.16%	10.75 ±0.21%	12.63 ±0.02%	14.79 ±0.32%
Peak 3	27.10 ±0.21%	31.00 ±0.29%	32.13 ±0.30%	32.67 ±0.18%
Peak 4	59.62 ±0.18%	48.90 ±0.37%	44.33 ±0.42%	40.24 ±0.58%
Peak 5	4.64 ± 0.03%	6.66 ± 0.14%	7.43 ± 0.04%	8.15 ± 0.58%

Table 3: Quantification of the isoform's peak area of the unstressed and stressed samples at 70 ℃ for four weeks.

4.3.1.7 Size-Exclusion Liquid Chromatography

The typical chromatographs of 1.0 mg/ml DNI at pH 7 at time 0, time four weeks 40 ^{o}C and time four weeks 70 ^{o}C are shown in Figure 14. Two SEC peaks are observed at retention times of 10.4 and 11.7 mins, respectively. The molecular weights of the species were estimated by using standard proteins' calibration plot. The bigger peak (peak 2) corresponds to the monomer of the protein, and the smaller peak (peak 1) corresponds to the dimmer of the protein. There seems to be no differences between the samples at time 0 and the samples at time four weeks 40 ^{o}C. For the sample stressed for four weeks at 70 ^{o}C, the dimmer peak area increases from 4.9 % to 9.1% while the monomer peak area decreases from 95.1% to 90.9%. By quantification of the peak area (Table 4), no significant differences of the peak 1 area (about 5%) and peak 2 area (about 95%) were observed when DNI was stressed at 40 ^{o}C for up to four weeks. Only about 0.5% slight changes of the peak areas of peak 1 and peak 2 were observed with increased incubation time up to four weeks. These observations suggest that formulated DNI proteins have high thermal stability to resist elevated temperature up to 40 ^{o}C with increased incubation time. However, for the stressed samples at 70 ^{o}C, we see bigger changes of the two peak areas. The peak 1 area increases progressively from 4.9% to 9.1% and the peak 2 area decreases from 95.1% to 90.9% with increasing the incubation time. These results suggest that the samples stressed at 70 ^{o}C are easy to form small amount of the aggregates at high temperature. However, majority of samples (about 90.9%) still maintain in the monomer state.

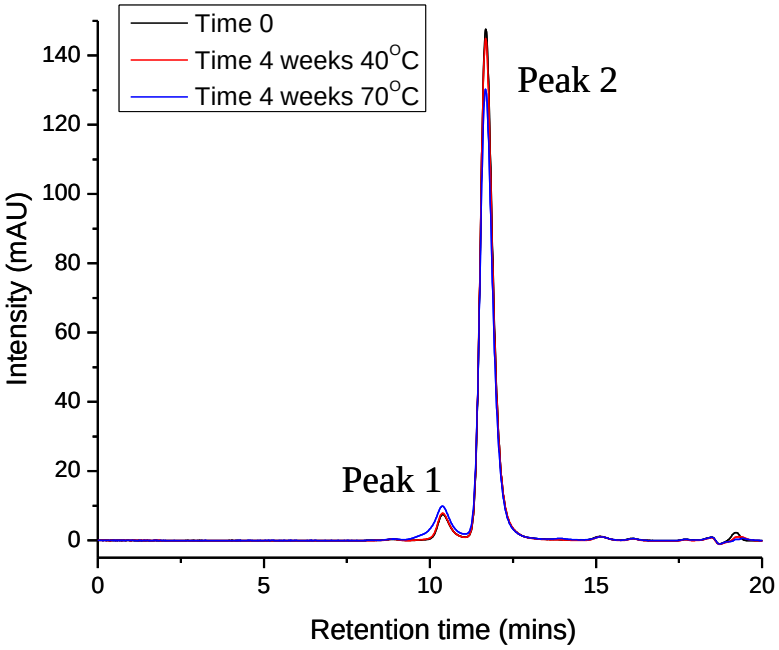

Figure 14: Size exclusion HPLC chromatograms of 1.0 mg/ml stressed DNI at pH 7. Black curve: DNI at Time 0. Red curve: DNI at 40 ℃ for four weeks. Blue curve: DNI at 70 ℃ for four weeks.

	Time 0	Time 1 week 40 ℃	Time 2 weeks 40 ℃	Time 4 weeks 40 ℃
Peak 1	4.9 ± 0.13%	5.0 ±0.03%	5.2 ±0.06%	5.4 ±0.05%
Peak 2	95.1 ±0.13%	95.0 ±0.03%	94.8 ±0.06%	94.6 ±0.05%
	Time 0	Time 1 week 70 ℃	Time 2 weeks 70 ℃	Time 4 weeks 70 ℃
Peak 1	4.9 ± 0.13%	6.8 ±0.06%	7.5 ±0.03%	9.1 ±0.04%
Peak 2	95.1 ±0.13%	93.2 ± 0.06%	92.5 ± 0.03%	90.9 ± 0.04%

Table 4. Quantification of the SEC peak 1 and peak 2 areas for DNI samples stressed at 40 ^{o}C and 70 ^{o}C from one to four weeks. Triplicate measurements were made.

4.3.1.8 Micro flow imaging

The unstressed and stressed samples of DNI at pH 7 were analyzed for sub-visible particles or aggregates in the 2-100 μm range using micro-flow imaging. The particle count and size distribution for DNI stressed at 40 ^{o}C are shown in Figure 15A. At time 0, very few particles are seen at all size ranges. The number of protein particles progressively increase with time when the samples are stressed at 40 ^{o}C. Very similar trends were seen when DNI was exposed to 70 ^{o}C, as shown in Figure 15B, although a more significant increase in particle count was observed after two weeks. It must be noted that even after weeks of exposure at high temperatures, the particle count remained below the USP guidelines for the number of sub-visible particles for injectables, which is about 6000 per 10 μm particles and 600 per 25 μm particles.

4.3.2 Adjuvant-Antigen study

4.3.2.1 Adsorption studies

Initial adsorption studies were conducted to determine whether DNI preferentially binds to Alhydrogel or Adjuphos. These experiments were done separately in three different buffers: 20 mM phosphate, 10 mM histidine or 10 mM imidazole. Figure 16A shows the percent adsorption of DNI to Alhydrogel and Adjuphos in the different buffer systems tested. Near 100% adsorption of DNI to Alhydrogel was observed in histidine and imidazole buffers. Phosphate presumably lowered adsorption of DNI to Alhydrogel by modifying the surface charge by converting aluminum hydroxide to aluminum phosphate. Histidine was therefore chosen as the buffer of choice in which to perform adjuvant studies. Extremely low levels of adsorption to Adjuphos were observed. Adsorption isotherms were constructed for both DNI

and rPA in the histidine buffer. In Figure 16B, Alhydrogel demonstrated a high adsorption capacity for DNI. 125 µg of Alhydrogel was able to adsorb over 240 µg of DNI and rPA.

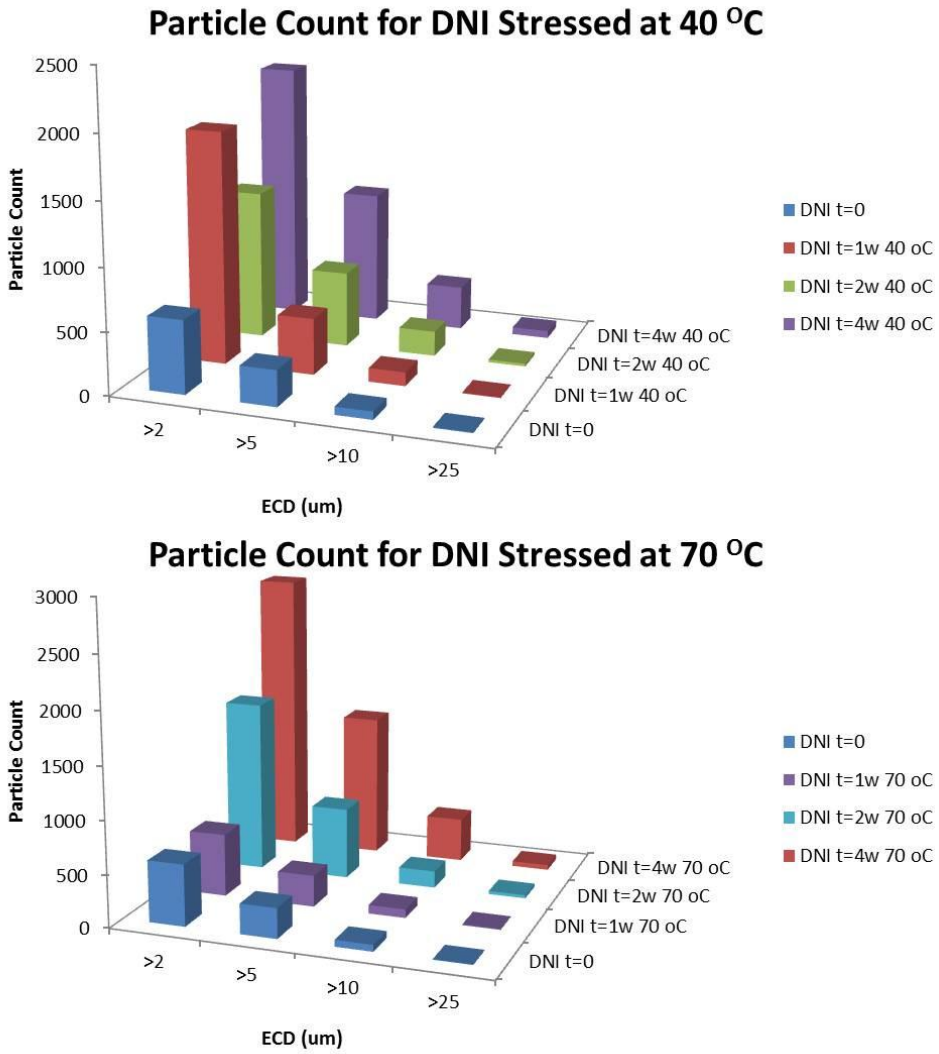

Figure 15: Particle count and size distribution for DNI samples stressed at 40 °C (top) and 70 °C (bottom). 1 ml of DNI sample was analyzed for each run.

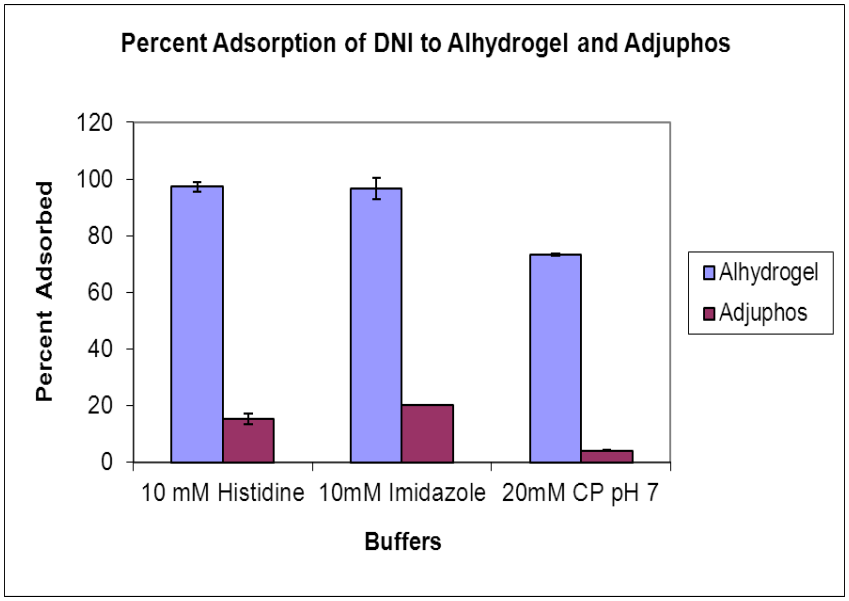

Figure 16 (A) Initial adsorption studies of DNI to Alhydrogel and Adjuphos in three different buffers. 0.2 mg/ml of antigen was adsorbed to 0.5 mg/ml adjuvant in 0.5 ml dose.

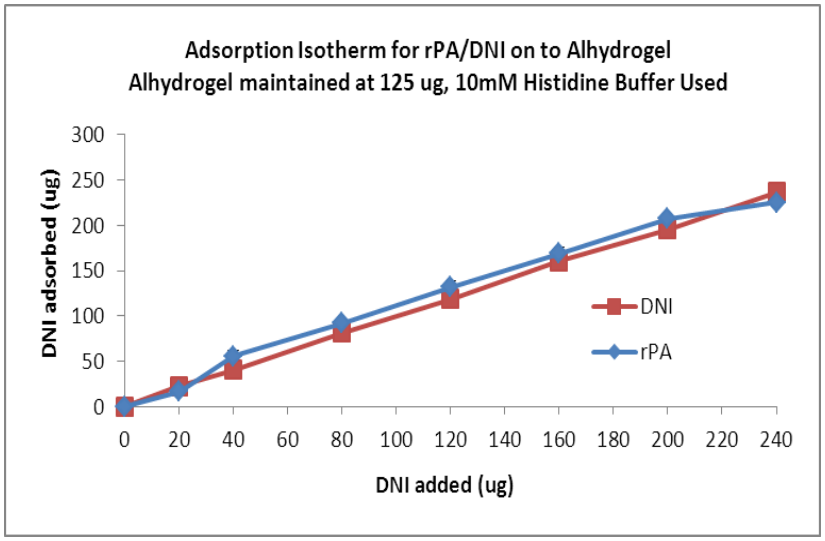

Figure 16 (B) Adsorption isotherms for DNI and rPA in presence of 0.5 mg/ml Alhydrogel.

4.3.2.2 Stability of DNI on the surface of Alhydrogel

The stability of DNI on the surface of Alhydrogel was assessed using intrinsic fluorescence. The protein was adsorbed onto Alhydrogel as described in section 2.2. The resulting suspension was then transferred to a 1 mm cuvette and allowed to settle overnight. The resulting pellet was then analyzed with intrinsic fluorescence spectroscopy. Figure 17 shows the melting curves for DNI and rPA on the surface of the Alhydrogel. The melting curves of protein alone are included as well. The buffer used in these experiments was again 10 mM histidine. A significant decrease in thermal stability is seen in the case of both DNI and rPA when adsorbed onto the surface of Alhydrogel. The steep transition is replaced by a gradual transition that initiates at around room temperature. DNI appears to be slightly more stable than the rPA control while adsorbed onto the surface, as evidenced by the small blue shifts in the peak positions between the two melting curves, but additional studies need to be undertaken to verify this.

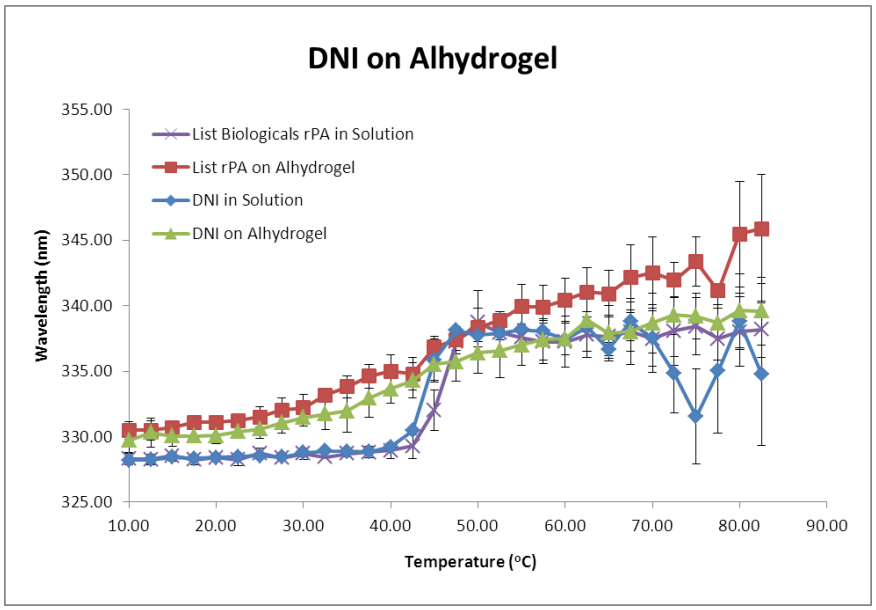

Figure 17: Intrinsic fluorescence peak position shifts as a function of temperature for DNI and rPA control when adsorbed on the surface of Alhydrogel. Melting curves of protein alone are added for comparison as well.

4.4 CONCLUSIONS

By using a variety of spectroscopic, hydrodynamic and particle-sizing techniques, the conformational stability of the DNI was characterized comprehensively under unstressed and stressed conditions. These techniques provide insight into different levels of protein structure (secondary and tertiary) and aggregation behavior of DNI and rPA. Comparing the stability profiles of DNI and rPA at pH 7 with various technqiues, both proteins show overall similar conformational stability. Comparing the stability profiles of non-stressed and stressed DNI showed that the thermally stressed molecule appears to retain its native structure up to temperatures as high as 70 ^{o}C for a month. Lyophilized DNI was formulated with common excipients that permit preservation of protein structure in the dried state. The long-term stability of DNI was also demonstrated after refrigerated storage for about eight years. Adjuvant adsorption studies showed that DNI had much more efficient binding to aluminum hydroxide than aluminum phosphate. Both adsorbed DNI and rPA showed a significant decrease in thermal stability through monitoring with intrinsic fluorescence. More importantly, our collaborator's work (Soligenix Inc.) showed that animals vaccinated with an aluminum salt adjuvanted DNI-based vaccine developed high titer neutralizing antibodies that confer protection against anthrax (results not illustrated).

This study provides important stability information for the development of an anthrax vaccine to protect against anthrax disease either as a pre-exposure prophylactic vaccine or post-exposure vaccine. DNI demonstrates significant improvements in safety and immunogenicity compared to PA in mice studies.[5] This suggests that DNI has significant potential to be used as an alternative antigen in anthrax vaccines. Since the primary use of an

anthrax vaccine is for bioterrorism defense, the remarkable thermostability of DNI should permit it to be stored for long periods of time for use when necessary. In addition, DNI can potentially provide therapeutic activity in antitoxic therapy, which provides immediate protection against anthrax toxins in vivo.[8,5] The data described here define critical parameters (such as solution pH, temperature and buffers) affecting the stability of the DNI protein. It should thus be useful to aid in the development of stable DNI-based anthrax vaccines.

4.5 REFERENCES

1. Moayeri, M.; Leppla, S. H., The roles of anthrax toxin in pathogenesis. *Current opinion in microbiology* **2004,** *7* (1), 19-24.
2. Collier, R. J.; Young, J. A. T., Anthrax toxin. *Annual review of cell and developmental biology* **2003,** *19* (1), 45-70.
3. Bann, J. G., Anthrax toxin protective antigen—Insights into molecular switching from prepore to pore. *Protein Science* **2012,** *21* (1), 1-12.
4. Wright, J. G.; Quinn, C. P.; Shadomy, S.; Messonnier, N., Use of anthrax vaccine in the United States. *Morbid Mortal Wkly Rep* **2010,** *59*.
5. Aulinger, B. A.; Roehrl, M. H.; Mekalanos, J. J.; Collier, R. J.; Wang, J. Y., Combining anthrax vaccine and therapy: a dominant-negative inhibitor of anthrax toxin is also a potent and safe immunogen for vaccines. *Infection and immunity* **2005,** *73* (6), 3408-3414.
6. Yan, M.; Roehrl, M. H.; Basar, E.; Wang, J. Y., Selection and evaluation of the immunogenicity of protective antigen mutants as anthrax vaccine candidates. *Vaccine* **2008,** *26* (7), 947-955.
7. Cao, S.; Guo, A.; Liu, Z.; Tan, Y.; Wu, G.; Zhang, C.; Zhao, Y.; Chen, H., Investigation of new dominant-negative inhibitors of anthrax protective antigen mutants for use in therapy and vaccination. *Infection and immunity* **2009,** *77* (10), 4679-4687.
8. Sellman, B. R.; Mourez, M.; Collier, R. J., Dominant-negative mutants of a toxin subunit: an approach to therapy of anthrax. *Science* **2001,** *292* (5517), 695-697.

Chapter 5 Physical Characterization and Formulation Development of a Recombinant Pneumolysoid Protein based Pneumococcal Vaccine

5.1 Introduction

Streptococcus pneumoniae (pneumococcus) is one of the leading causes of death affecting high-risk populations such as infants, the elderly and patients with immunodeficiency. Pneumococcal disease is responsible for more than half a million deaths annually for children under five years of age.[1,2,3] *S. pneumoniae* has 40 serogroups comprising more than 90 serotypes worldwide, and presents in various populations based on geographical location and age. The major clinical effects of pneumococcal disease are pneumonia, bacteremia and meningitis, which can lead to high morbidity and mortality, particularly in the young and elderly.[4] In the United States, up to 175,000 hospitalizations from pneumococcal pneumonia occur per year, with approximately 50,000 cases of pneumococcal bacteremia and 3000-6000 cases of pneumococcal meningitis annually.[4] The pneumococcal disease can be treated with antibiotics or prevented by vaccines, although their efficacy is limited due to the wide variety of bacterium serotypes, the diversity of geographical regions and populations affected, and the resistance of pneumococci to antibiotics. Therefore, major efforts have been undertaken to develop effective vaccines against pneumococcal infections using common protein antigens to effectively cover as many serotypes as possible for both regional and global use.

Currently, polysaccharide and polysaccharide-conjugate based vaccines are commercially available in the US. Although these vaccines are effective against the most-prevalent serotypes causing invasive pneumococcal disease, their efficacy is limited worldwide due to the restricted number of serotypes recognized by these prophylactic agents.[4,5] Non-vaccine serotypes have the potential to become the main disease causing

agents, thereby accentuating the disease (known as "replacement disease") in the future.[4] Thus, the long-run efficacy of currently marketed vaccines could be threatened by serotype replacement. In addition, worldwide use of current vaccines is potentially restricted due to serotype differences in different geographic locations.

Alternatives to current serotype-specific vaccinations are being investigated. The development of recombinant protein-based vaccines, which target common pneumococcal protein antigens across different serotypes, is attractive for several reasons.[4,6] Protein-based vaccines are T-cell dependent in nature, and are expected to be immunogenic in infants and the elderly. More importantly, coverage of protein-based vaccines is expected to be broader since they contain protein antigens common to all or most pneumococcal serotypes. In addition, protein-based vaccines are also expected to be less expensive because of their relative simplicity in production since they contain fewer components than multivalent conjugate vaccines currently on the market. Protein–based vaccines are thus an attractive and promising approach to the prevention and treatment of invasive pneumococcal disease.

Multiple putative pneumococcal virulence proteins have been investigated and pneumolysin has emerged as a promising vaccine protein antigen candidate. Pneumolysin, a sulfhydryl-activated cytolytic toxin (53 kDa), is produced by virtually all invasive strains of *S. pneumoniae* and is considered an important virulence factor.[7,8,9,10] It is involved in the pathogenesis of invasive pneumococcal disease and has been shown to be immunogenic in numerous animal models[11,12,13] and humans[14,15], and thus has become a promising vaccine target. Due to its cytolytic effects, however, pneumolysin cannot be used directly in a vaccine.

Non-toxic, genetically altered pneumolysin toxoid mutants have been generated and shown to be immunogenic.[16,17] We have used a recombinant pneumolysin mutant (L460D) where the L460D mutation removes toxic cytolytic activity.[18,19] The pneumolysoid antigen (L460D) has been shown to be effective against *Streptococcus pneumoniae* colonization in the lungs of mice[20,21] and thus is a promising vaccine candidate for pneumococcal disease.

To develop a stable pneumolysoid (L460D) based vaccine formulation, the structural stability of the pneumolysin mutant protein was characterized and assays were developed to screen potential stabilizers. The physical stability of the L460D pneumolysoid was characterized by various techniques over the pH range of 3 to 8 from 10 to 87.5 ℃. Purified recombinant proteins are generally not highly immunogenic and thus an adjuvant is usually used to boost their immunogenicity.[22,23] Studies of L460D pneumolysoid with an aluminum hydroxide adjuvant (Alhydrogel) were thus performed to characterize antigen/adjuvant interactions and to better understand the stability of protein antigen on the surface of Alhydrogel.

5.2 MATERIALS AND METHODS

5.2.1 Materials

The pneumolysoid (L460D) antigen was supplied by St. Jude Children's Research Hospital (Memphis, TN) as a solution in 10% glycerol in phosphate buffered saline (PBS). For the physical characterization, individual protein solutions at pH 3-8 were prepared by dissolving L460D pneumolysoid in 20 mM citrate phosphate buffers with a total ionic strength of 0.15 (adjusted with NaCl). Before making measurements, the samples of L460D pneumolysoid were dialyzed twice at 4 °C using Slide-A-Lyzer® Dialysis Cassettes (Thermo

Scientific, Rockford, IL) with a 3.5 kDa MW cutoff. For excipient screening and adjuvant studies, 10 mM histidine buffer at pH 6 was used. The adjuvant alhydrogel was purchased from Brenntag Biosector (Frederikssund, Denmark).

5.2.2 Physical Characterization

5.2.2.1 Far-UV Circular Dichroism Spectroscopy

Circular dichroism analysis was performed with a Chirascan-plus circular dichroism spectrometer (Applied Photophysics Ltd, Leatherhead UK) equipped with a Peltier temperature controller and a 4-position cuvette holder. Far UV spectra of samples (0.1 mg/ml) were collected in the range of 200-260 nm using a 0.1 cm path length cuvette. A sampling time per point of 1 s and a bandwidth of 1 nm were used. The CD signals of the samples at 217 nm were monitored as a function of temperature from 10 to 87.5 ℃ at 2.5 ℃ intervals. Duplicate measurements were made with an equilibration time at each temperature of 1 minute.

5.2.2.2 Intrinsic Fluorescence Spectroscopy

The intrinsic fluorescence of L460D pneumolysoid (0.1 mg/ml) was measured using a QuantaMaster Spectrofluorometer (Photon Technology International (PTI), Inc., Birmingham, NJ) equipped with a 4-position cell holder. Fluorescence emission spectra were recorded as a function of temperature (10-87.5 ℃) and pH (3-8). Duplicate samples were measured using an excitation wavelength of 295 nm (> 95% tryptophan emission). Emission spectra were collected from 300 to 400 nm with a step size of 1 nm. The spectra were collected at 2.5 ℃ intervals with a 3 min equilibration time at each temperature. A 1 cm path length quartz cuvette was used in all experiments. Data analysis was performed using FelixTM (Photon

Technology International, Inc.) software. The position of the protein's emission wavelength maximum was determined using a mean spectral center of mass method (msm) executed in *Origin 7.0* software. This results in a value that is shifted to a 8-12 nm higher wavelength than the actual peak position.

5.2.2.3 Extrinsic Fluorescence Spectroscopy

8-Anilino-1-naphthalene sulfonate (ANS) was used as an extrinsic probe to study the appearance of apolar binding sites in the protein under the various forms of stress employed. The interaction of ANS with the hydrophobic surfaces of the L460D pneumolysoid was monitored as a function of temperature (10-87.5 ℃) and pH (3-8) using the PTI spectrophotometer. Each sample solution (0.1 mg/ml) contained 25 μM diluted ANS (an optimized molar ratio of the ANS to the protein of 15:1). Samples were excited at 375 nm and spectra were collected from 400 to 600 nm at 2.5 ℃ intervals. Duplicate measurements were made using a 1 cm path length quartz cuvette. Buffer baselines containing ANS were subtracted from each sample spectrum prior to analysis. Peak intensities of the emission spectra were obtained using the msm method as described above.

5.2.2.4 Static Light Scattering

The aggregation behavior of L460D pneumolysoid was determined simultaneously during the intrinsic fluorescence experiments employing a second photomultiplier located 180 ° to the fluorescence detector. The scattering intensities at 295 nm were obtained using the same temperature program described above. Buffer baselines were subtracted from each sample spectrum before data analysis.

5.2.2.5 Data Visualization Techniques

Three-index empirical phase diagrams, radar charts and Chernoff face diagrams are used to summarize the large amounts of biophysical data generated from multiple techniques and to visualize macromolecular stability of L460D pneumolysoid as a function of various environmental stress variables. These techniques visualize data using (1) a red, green and blue (RGB) color system, (2) equiangular polygons, and (3) human facial features, respectively. The diagrams are used to identify coherent parameter regions that define protein structural states as a function of temperature and pH, in this case.

In brief, the secondary structure index (SI), tertiary structure index (TI), and aggregation index (AI) are calculated from the collected data sets. These indices represent the difference amounts of structure (secondary, tertiary and quaternary) of a macromolecule under a given set of environmental conditions. In this study, the secondary, tertiary, and aggregation indices are calculated from far UV CD signals at 217 nm, intrinsic fluorescence peak positions, and static light scattering data, respectively. A structural index is defined as the degree of corresponding structural change within a given range of environmental stress conditions. The structure index varies from a value of zero to one, indicating the lowest to highest amount of the corresponding structure seen over the entire range of solution variables. For example, native secondary or tertiary structure is represented by a value of 1, while the most significantly structurally altered state is represented by 0. Similarly, the AI is also defined a value from 0 to 1. The number 0 of AI implies no protein aggregation while a value of 1 reflects the maximum level of aggregation.

The three-index EPD is constructed by mapping each structural index to an RGB

color component. We have assigned SI to red, TI to green, and AI to blue. Thus, a color produced by the summation of these three color components can be mapped to a specific structural state of the macromolecule. For example, yellow or shades of yellow typically represent the native state of a protein, while the blue color indicates an aggregated state. The three-index EPD provides a meaningful relationship between color itself and molecular features. It cannot, however, include data from more than three experimental methods.

The radar chart and the Chernoff face diagram can display more than three experimental data sets. ANS data are also used in both cases in this study. All data are adjusted to represent the native state either as a dot or a smiling face (along with a short nose combined with no hair or ears). Because both original diagrams require more space to represent molecular features (see supplemental Figure S1) compared to the three-index EPD, the clustered versions of diagrams are used to symbolize characteristics of macromolecules in selected regions. The apparent phase boundaries are first calculated using a k-Means clustering algorithm then manually corrected based on interpretation of the raw data. The objective of the clustering analysis is to find groups of solution variables where the macromolecule is observed to have a similar conformational state. For each solution variable, it is possible to construct a vector of measurements that detect the structural behavior of the macromolecule. This vector can be represented as a single point in the multidimensional measurement space. The *k*-Means clustering algorithm tries to partition these points into *k* clusters (groups) in which each point belongs to the cluster with the nearest distance. The assumption is that if a group of points that is close in Euclidean distance, the macromolecule with the associated solution variables can be considered to be in a similar conformational

state.[24,25,26,27,28] Each cluster is represented by a single radar chart and Chernoff face. These single iconic plots are then generated by an average value of the data inside a cluster. A more complete description of the construction and interpretation of these three phase diagrams are described elsewhere.[28]

5.2.3 Excipient Screening

Based on the initial characterization studies, L460D pneumolysoid was found to be most stable at pH 6-7. Based on this, a common buffer consisting of 10 mM histidine at pH 6 was employed for the excipient screening and adjuvant work. NaCl was not used in these studies to decrease the osmolarity of the formulations. Intrinsic tryptophan fluorescence spectroscopy and static light scattering as a function of temperature were used to screen for stabilizing excipients for the L460D pneumolysoid antigen.

In the initial round of screening, higher concentrations of the excipients were tested to facilitate the selection of the more promising stabilizers under accelerated stress conditions. These stabilizers were then evaluated in the second round over a wider range of concentration. The effect of the selected stabilizers (sucrose and trehalose at 10 or 15% weight percent) on the stability of L460D pneumolysoid (at 0.1, 0.5, 1.0 and 4.0 mg/ml) was then examined (see results). Because a high concentration (4.0 mg/ml) of protein was used in the fluorescence and static light scattering studies, a short pathlength cell (2 mm x 10 mm) was used. Excitation of the proteins was carried out along the short path length axis (2 mm). For other protein concentrations, the 10 mm x 10 mm pathlength cells were used.

The extent of stabilization of L460D pneumolysoid by the excipients was measured by their ability to shift the melting temperature (T_m) of the protein to higher temperatures.

The melting temperature is defined as the temperature at which the transition from folded to unfolded states is half complete. T_m values were calculated using a Boltzmann function to produce a sigmoidal curve using Origin 8.1 software.

The stabilizing effects of sucrose and trehalose (at 10 or 15% weight percent) were examined by differential scanning calorimetry (DSC) at 1.0 mg/ml. A capillary differential scanning calorimeter (MicroCal LLC, Northampton, MA) was used for these measurements. A scan rate of 60 ℃/hour was used from 6 to 82 ℃. DSC data were analyzed using Origin version 7.0 software. The thermogram for buffer alone was subtracted from the thermograms of the proteins in solution prior to data analysis.

5.2.4 Adjuvant-Antigen Studies

5.2.4.1 Adsorption Study

Experiments to study L460D pneumolysoid in the presence of adjuvant were conducted by adding Alhydrogel to the protein solution. An adsorption isotherm was constructed for L460D pneumolysoid at nine protein concentrations from 0.05 to 3.25 mg/ml (concentrations are listed in Supplemental Figure S3) in the presence of 0.6 mg/ml Alhydrogel. Protein solutions containing Alhydrogel were prepared and tumbled in an end-over-end rotator for 30 minutes at 4 ℃. The resultant suspension was centrifuged at 5,000xg for 4 minutes to pellet the adjuvant using an IEC MicroMax microcentrifuge (International Equipment Company, Needham Heights, MA). The amount of protein in solution (non-bound) was determined by measuring the protein concentration in the supernatant using UV absorbance spectroscopy and an extinction coefficient of 69960 $M^{-1}cm^{-1}$.

5.2.4.2 Stability of L460D Pneumolysoid on the Surface of the Aluminum Hydrogel

The thermal stability of the adsorbed protein was assessed by front-face fluorescence spectroscopy and DSC. Front face fluorescence was used to probe changes in the tertiary structure of the protein, both in solution and when adsorbed to adjuvant. Front face sampling geometry was necessary because of the opacity of the adjuvant suspensions. Samples of protein adsorbed onto the adjuvant were prepared as described previously for the binding isotherms. For all front face fluorescence studies, protein concentration was 1.0 mg/ml. For samples containing adjuvant, the alhydrogel concentration was 1.2 mg/ml. Samples containing adjuvant were allowed to settle in the cuvettes for about 14 hours at 4℃ to minimize variability due to settling of the adjuvant during the course of the experiment. An excitation wavelength of 295 nm was employed, and emission spectra were recorded from 305 to 390 nm using a PTI spectrophotometer.

For DSC studies, the thermal transition temperatures were determined separately for protein in solution and protein adsorbed onto the adjuvant. Samples containing protein (1.0 mg/ml) completely adsorbed onto the surface of the adjuvant (0.6 mg/ml) were prepared as described for the binding isotherms. Both the protein samples and buffers containing adjuvant were settled in the DSC cells for about 10 hours at 4℃ to minimize variability. A scan rate of 60 ℃/hour was used to scan from 6 to 82℃. Buffers containing adjuvant and samples containing adjuvant were analyzed separately.

5.3 Results

5.3.1 Physical Characterization

5.3.1.1 Far-UV Circular Dichroism Spectroscopy

Representative CD spectra of L460D pneumolysoid at 10 ℃ are shown in Figure 1A. Samples at pH range of 3 to 8 have CD spectrum displaying a broad minimum at near 217 nm and a shoulder at 208 nm. At pH 7, the secondary structure components were estimated by CDNN CD spectra deconvolution software[29] to be as follows: α-helix (~35%), β-structure (~33%) and random coil (~31%). The CD spectra at pH 6 and 7 show the two strongest CD signals compared to those at other pH values. The spectrum at pH 4 shows the weakest CD signals in the far UV CD region, suggesting a loss of secondary structure at low pH.

The effect of temperature on L460D pneumolysoid secondary structure was investigated using CD thermal melt analysis at 217 nm (Figure 1B). An overall loss in the secondary structure is observed as a function of increasing temperature across the pH range 4 to 8, excluding the sample at pH 3. At pH 3, a very small CD signal change is seen, suggesting that the protein exists in a conformationally altered state. The onset temperature (T_{onset}) of thermal transitions occurs at about 43 ℃ at pH 5, 50 ℃ at pH 6 and 7, and 45 ℃ at pH 8, suggesting that protein at pH 6 and 7 is most stable. At pH 4, the protein is much less stable and the transition onset is near 33 ℃. Based on these CD studies, the most conformationally stable form of the protein in terms of overall secondary structure exists between pH 6 and 7.

5.3.1.2 Intrinsic Fluorescence Spectroscopy

Alterations in the tertiary structure of L460D pneumolysoid were studied by monitoring the changes in its tryptophan emission peak position as a function of pH and temperature

(Figure 1C). At pH 4 to 8, a trend of decreasing peak position followed by a sharp blue shift in the Trp emission maximum is observed with increasing temperature, suggesting that the L460D pneumolysoid aggregates with increasing temperature (i.e., the blue shift indicating burial of indole side chains rather than to red shifts expected for exposure). In contrast, at

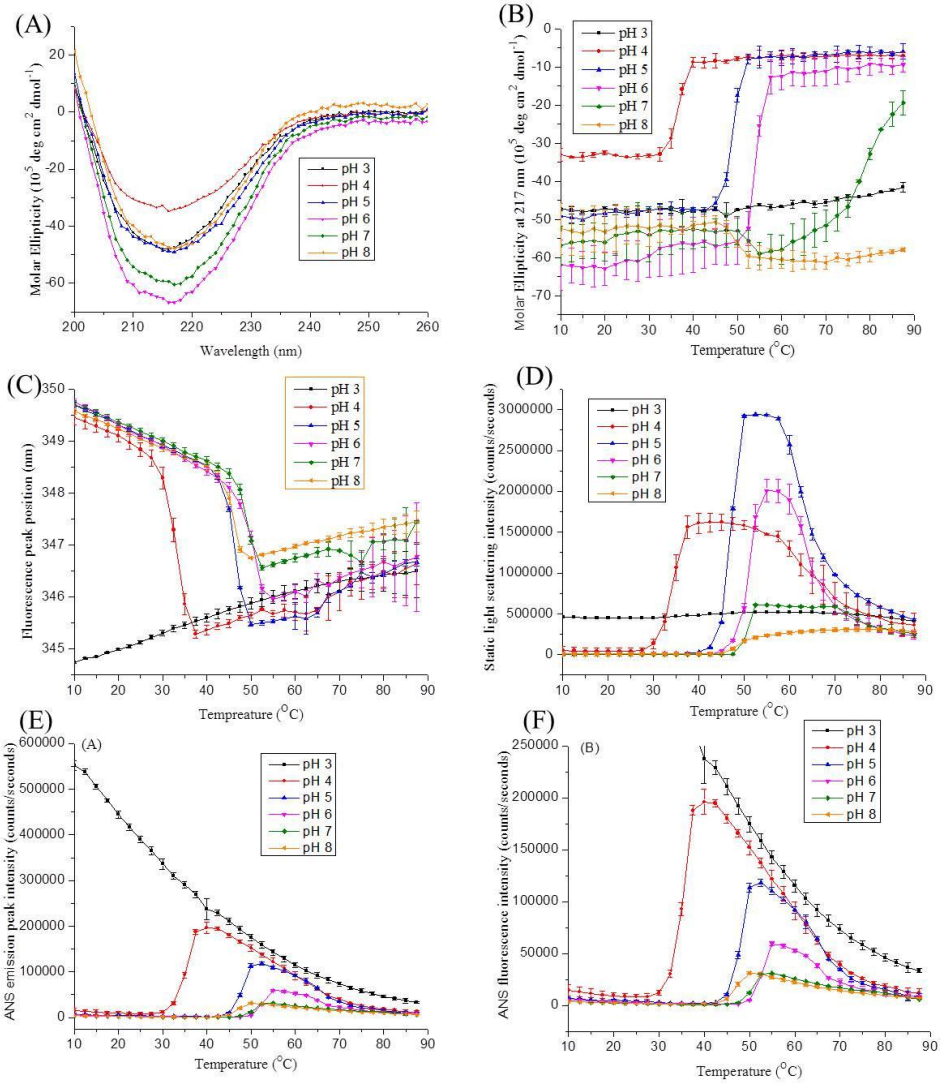

Figure 1. Biophysical characterization of recombinant L460D pneumolysoid. (A) Far-UV circular dichroism (CD) at 10 ℃. Thermal stability of protein as a function of temperature and solution pH: (B) CD signal at 217 nm, (C) intrinsic Trp fluorescence emission maximum (peak position), (D) static light scattering intensities, (E) ANS fluorescence intensities, (F) an enlargement of Y axis of Figure 1E. Each data point represents the mean of two independent samples, and error bars show the standard deviation. Protein concentration was 0.1 mg/ml in a citrate-phosphate buffer with NaCl at indicated pH values.

pH 3 a gradual linear increase in the emission peak position is observed and no shift to lower wavelength is seen. This difference again suggests that the protein exists in a conformationally altered state at low pH. The T_{onset} temperatures occur at about 28 ℃ at pH 4, 43 ℃ at pH 5 and 8, and 45 ℃ at pH 6 and 7. These T_{onset} values suggest that the protein is most stable at pH 6-7. The T_{onset} values were approximately 5 ℃ lower than that seen with CD, suggesting molten-globular state formation under these conditions. Other than this, the temperature-dependent Trp fluorescence data show results generally similar to those obtained in the CD studies (Figure 1B).

5.3.1.3 Static Light Scattering

The aggregation behavior of the L460D pneumolysoid was examined by monitoring the scattered light at the fluorescence excitation wavelength of 295 nm. The protein manifests aggregation behavior over the pH range 4 to 8, while no aggregation is observed at pH 3, presumably due to its altered structure (Figure 1D). At pH 4, an increase in scattering intensity is observed at about 28 ℃, whereas at pH 5, 6, 7, and 8, the increases in light scattering occur near 40, 45, 48 and 43 ℃, respectively. The overall effects of pH and temperature on the structural stability observed by static light scattering are similar to the results obtained from CD (Figure 1B) and intrinsic fluorescence (Figure 1C).

5.3.1.4 Extrinsic Fluorescence Spectroscopy

ANS is a fluorescent dye that binds to nonpolar regions in proteins, resulting in large increases in its fluorescence quantum yield and a blue shift in peak position. It should be noted, however, that there may be an electrostatic component to this interaction. Figure 1E and 1F shows the thermal melting curves of L460D pneumolysoid at various pH values.

These curves were obtained by monitoring the ANS emission peak intensity as a function of temperature. At pH 3, ANS fluorescence shows significant fluorescence intensity even at low temperatures (Figure 1E). This increased fluorescence intensity is presumably induced by the binding of ANS to the structurally altered protein at low pH. This observation is in agreement with results obtained from Figures 1B-1D. Increased ANS fluorescence intensity is observed over the pH range of 4 to 8 (Figure 1F). The T_{onset} values for these transitions occur at about 28℃ at pH 4, 43℃ at pH 5 and 8, 48℃ at pH 6 and 45℃ at pH 7. As observed with other techniques, the L460D pneumolysoid shows its greatest structural stability in the pH range of 6-7.

5.3.1.5 Data Visualization Techniques

The various types of data generated were integrated into three visual diagrams to provide a more global picture of L460D pneumolysoid behavior under the stressed conditions of temperature and pH (Figures 2A to C). The non-clustered plots of Figures 2B and C are shown in the Supporting Figure S1. Five similar apparent structural phases for the protein can be recognized in all three diagrams (Figure 2A, B, C and S1). In the three-index EPD (Figure 2A), regions of continuous color define uniform structural states, while abrupt changes in color identify alterations in the physical state of the protein over the conditions examined. In Region 1, samples at pH 5 to 8 manifest a similar color (yellow or shades of yellow) below 47.5℃, suggesting a similar conformation for native L460D pneumolysoid across this pH range. Samples at pH 6 and 7 show the highest stability. Samples at pH 5 and 8 show similar stability, but lower compared to samples at pH 6 and 7. In Regions 2 and 3, samples at pH 3 and 4 show distinct colors from those in Region 1. The sample at pH 4 probably

contains protein in a partially unfolded state, while the sample at pH 3 contains protein in a more structurally altered state, even at low temperatures. Region 4 (blue color) indicates that the protein in the high-temperature region are highly structurally aggregated. Region 5 defines a structurally altered state with a lower degree of aggregation compared to that in Region 4. Similar results were observed in the radar chart (Figure 2B) and Chernoff face diagrams (Figure 2C). From the three different EPD displays of the biophysical data, we can see that the most stable region for formulations of L460D pneumolysoid is in the pH range of 6 to 7 and below 48 ℃.

5.3.2 Excipient Screening

Following the physical characterization of L460D pneumolysoid, a screening study was performed to identify stabilizers that enhance thermal stability and minimize aggregation in solution. Based on the EPD displays, pH 6 was used for this study (using a 10 mM histidine buffer). Tryptophan fluorescence spectroscopy and static light scattering techniques were used to screen for stabilizing compounds from a GRAS (Generally Regarded as Safe) library of excipients (see Table 1 and text below).

Results of fluorescence spectroscopy measurements of 0.1 mg/ml L460D pneumolysoid in the presence of selected destabilizers and stabilizers are shown in Figures 3A and B. The thermal transition of the protein is shifted to lower temperatures in the presence of destabilizers (e.g. guanidine), and is shifted to higher temperatures in the presence of stabilizers (e.g. trehalose, sucrose and sorbitol). Similar results were observed by static light scattering measurements (Figure 3C). In Figure 3C and Table 1, it can be seen that compared to the T_m of the L460D pneumolysoid alone, 0.3 M guanidine decreases the T_m by

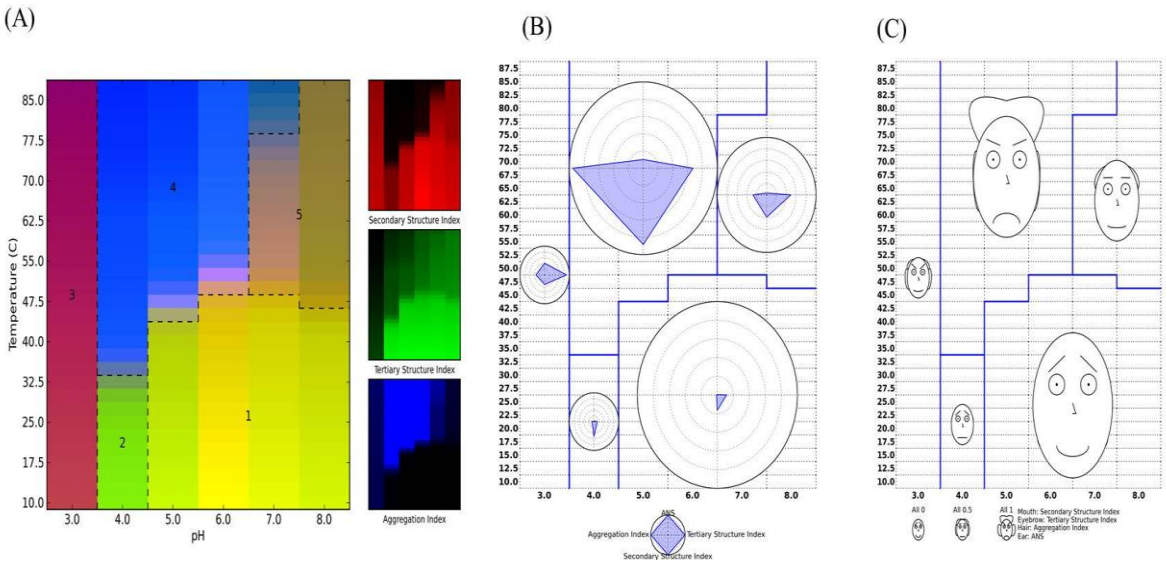

Figure 2. (A) Three-Index EPD, (B) clustered radar chart, and (C) clustered Chernoff face diagram for the conformational stability of L460D pneumolysoid. The three-index EPD was prepared from CD at 217 nm, intrinsic fluorescence (peak position) and static light scattering data. The radar chart and the chernoff face diagram use same three data sets but also include extrinsic (ANS) fluorescence as a fourth data set. Each cluster is represented as a radar chart or chernoff face diagram which averages the data of all images that belong to the cluster. For complete diagrams see supplementary Figure S1.

t

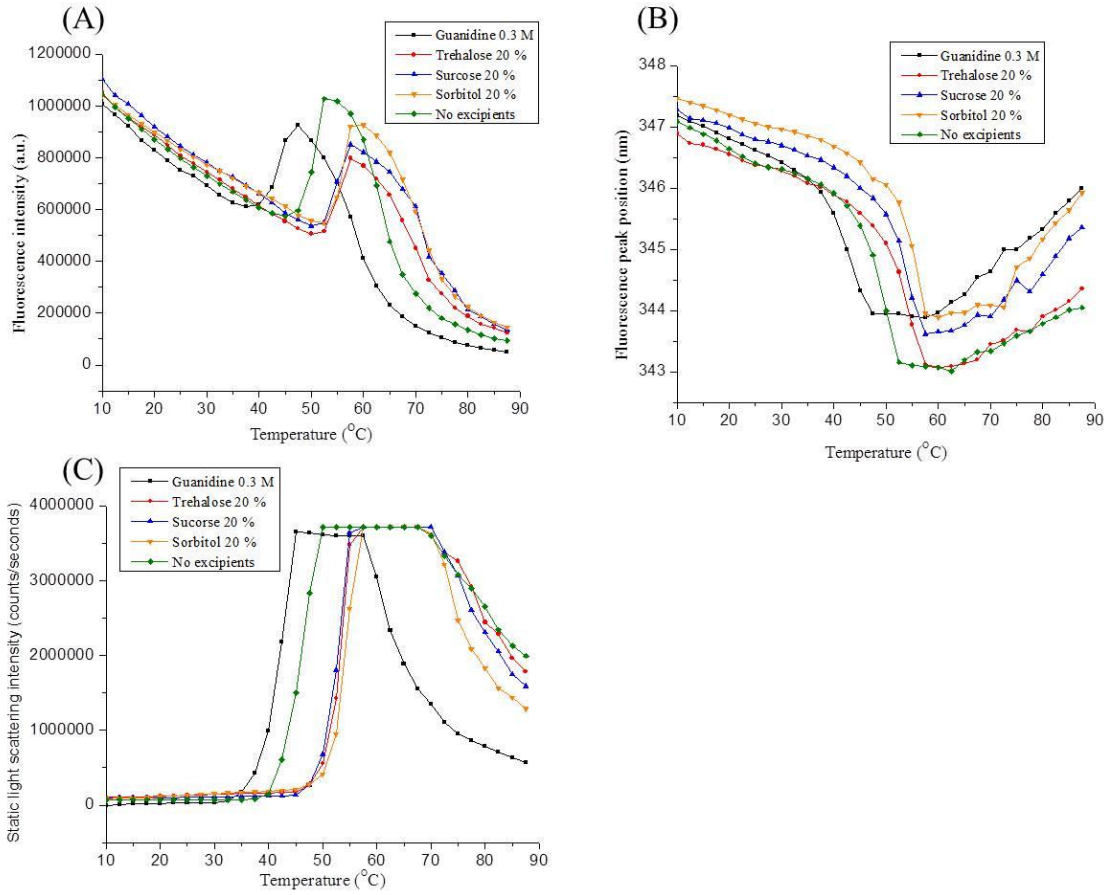

Figure 3. Conformational stability of L460D pneumolysoid in presence of various excipients. (A): The intrinsic Trp fluorescence emission maximum (peak position), (B): the emission peak intensity and (C): Static light scattering intensity of protein as a function of temperature with and without selected excipients. Protein concentration was 0.1 mg/ml in a 10mM histidine buffer at pH 6.

Excipient (Molarity (M) or weight percent (%))	Intrinsic fluorescence				Static light scattering	
	peak position T_m (^{O}C)	$\triangle T_m$ of peak position	emission peak intensity T_{onset} (^{O}C)	$\triangle T_{onset}$ (^{O}C) of emission peak intensity	T_m (^{O}C)	$\triangle T_m$ (^{O}C)
Protein without excipients (0.1mg/ml)	48.6		47.5		48.3	
Dextran T 70 ($7.5x10^{-6}$ M)	48.8	0.2	47.5	0	48.4	0.1
Aspartic Acid (0.075M)	49.1	0.5	47.5	0	49.5	1.2
Glutamic Acid (0.15M)	48.1	-0.5	47.5	0	48.3	0
Lactic Acid (0.15M)	48.7	0.1	47.5	0	48.6	0.3
Malic Acid (0.15M)	50.0	1.4	47.5	0	51.3	3.0
Dietanolamine (0.3M)	46.3	-2.3	45.0	-2.5	47.7	-0.6
Guanidine (0.3M)	41.5	-7	40.0	-7.5	41.7	-6.6
Histidine (0.2M)	47.4	-1.2	45.0	-2.5	47.8	-0.5
Proline (0.3M)	48.7	0.1	47.5	0	49.0	0.7
Glycine (0.3M)	48.6	0	47.5	0	47.8	-0.5
Calcium Chloride (0.015M)	48.1	-0.5	47.0	-0.5	47.8	-0.5
Sodium Citrate (0.2M)	49.7	1.1	47.5	0	51.0	2.7
Brij 35 (0.1%)	47.8	-0.8	47.0	-0.5	47.8	-0.5
Tween 20 (0.1%)	47.3	-1.3	46.0	-1.5	46.6	-1.7
Tween 80 (0.1%)	49.3	0.7	47.5	0	48.6	0.3
Pluronic F-68 (0.1%)	48.8	0.2	47.5	0	48.6	0.3
Lactose (20%)	51.8	3.2	51.0	3.5	53.6	5.3
Trehalose (20%)	51.9	3.3	52.0	4.5	53.5	5.2
Dextrose (20%)	52.2	3.6	52.0	4.5	54.8	6.5
Sucrose (20%)	51.6	3.0	52.0	4.5	52.5	4.2
Mannitol (10%)	51.8	3.2	52.0	4.5	52.6	4.3
Sorbitol (20%)	53.4	4.8	52.5	5.0	55.3	7.0
Glycerol (20%)	50.3	1.7	50.0	2.5	50.4	2.1
α Cyclodextrin(CD) (2.5%)	48.0	-0.6	47.5	0	48.3	0
2-OH propyl ɤ-CD (2.5%)	49.5	0.9	48.0	0.5	49.7	1.4

Table 1: The effect of various GRAS excipients on the tertiary structural stability (T_m and T_{onset}) of L460D pneumolysoid was determined by intrinsic fluorescence spectroscopy and static light scattering. Duplicate measurements were run for pneumolysin alone, and one measurement for pneumolysin with each excipient. The precision of the T values is estimated to be ±0.5 ℃. Protein concentration was 0.1 mg/ml in a 10 mM histidine buffer at pH 6.

about 6.6 ℃ (Table 1), while the other three excipients (20% trehalose, sucrose and sorbitol) increase the T_m significantly from 4 to 7 ℃ (Table 1). These results show that the two techniques are sensitive enough to investigate the stabilizing and destabilizing effects of excipients on the L460D pneumolysoid.

A complete list of excipients examined and their effect on L460D pneumolysoid tertiary structural stability and aggregation are shown in Table 1. The T_m and T_{onset} values of thermal unfolding curves were calculated and are listed in this table. Excipients such as diethanolamine and guanidine have destabilizing effects. Excipients such as sugars and sugar alcohols exhibit stabilizing effects. The more promising stabilizers (trehalose, sucrose and sorbitol) were then examined at different concentrations. Table 2 shows the T_m and T_{onset} values of 0.1 mg/ml L460D pneumolysoid using selected stabilizers at concentrations ranging from 5 to 20%. For the fluorescence measurements, the T_m and T_{onset} values increase with increasing amounts of trehalose and sucrose in solution. Sucrose shows slightly better stabilizing effects than trehalose at the same weight percent. Sorbitol shows the best stabilizing effects. For the static light scattering measurements, similar observations were obtained as the fluorescence results, although, the T_m obtained from the static light scattering is about 1-3 ℃ higher than the T_m obtained from the fluorescence technique. The increases in T_m and T_{onset} seen in the second round of screening experiments suggest that the selected stabilizers are good candidates to enhance the physical stability and minimize aggregation of L460D pneumolysoid at high temperatures and potentially at lower storage temperatures as well.

Excipient weight percent	Fluorescence (Flu) peak position T_m (^OC)	ΔT_m of flu peak position	Flu emission peak intensity T_{onset} (^OC)	ΔT_{onset} (^OC) of flu emission peak intensity	Static light scattering T_m (^OC)	ΔT_m (^OC) of static light scattering
Protein without excipients	47.9 ±1.1		47.0		46.6 ±0.5	
Trehalose (5%)	49.0 ±0.1	1.1	47.5	0.5	47.3 ±0.2	0.7
Trehalose (10%)	49.5 ±0.8	1.6	47.5	0.5	48.5 ±0.7	1.9
Trehalose (15%)	50.0 ±0.8	2.1	50	3.0	51.3 ±0.8	4.7
Trehalose (20%)	52.0 ±0.2	4.1	51	4.0	53.0 ±0.7	6.4
Sucrose (5%)	49.3 ±0.4	1.4	47.5	0.5	47.8 ±0.1	1.2
Sucrose (10%)	50.4 ±0.4	2.5	50	3.0	48.9 ±1.6	2.3
Sucrose (15%)	51.1 ±0.5	3.2	50	3.0	51.1 ±1.0	4.5
Sucrose (20%)	51.7 ±0.9	3.8	52.5	5.5	52.5 ±0.2	5.9
Sorbitol (5%)	49.2 ±0.3	1.3	47.5	0.5	47.8 ±0.02	1.2
Sorbitol (10%)	50.7 ±1.0	2.8	50	3.0	49.5 ±1.4	2.9
Sorbitol (15%)	52.4 ±0.3	4.5	52.5	5.5	52.1 ±0.03	5.5
Sorbitol (20%)	53.2 ±0.3	5.3	52.5	5.5	54.1 ±1.7	7.5

Table 2. The effect of stabilizer concentration on the tertiary structural stability and aggregation behavior of L460D pneumolysoid as measured by fluorescence spectroscopy and static light scattering. Duplicate measurements were run. The T_m value was calculated separately for each measurement, the values were averaged, and the standard deviation was determined. Protein concentration was 0.1 mg/ml in a 10 mM histidine buffer at pH 6.

The solution osmolarity was measured for buffers containing the selected stabilizers at various concentrations, and the results are summarized in Supplemental Table S1. Buffers containing sorbitol show much higher osmolarity than those containing sucrose or trehalose at the same concentration. Therefore, sorbitol was not examined further. Both 20% sucrose and 20% trehalose have relatively high osmotic pressure values that are not generally suitable for injection. Both 5% sucrose and 5% trehalose have reasonable osmotic pressure values, but formulations at these concentrations show a smaller increase in T_m values than those using 10 or 15% concentrations. Therefore, in further experiments, only 10% and 15% sucrose and trehalose were used. These two concentrations of excipients show good stabilizing effects on L460D pneumolysin, as observed by both fluorescence and static light scattering techniques (Table 2) and provide an acceptable range of osmotic pressures.

In the next experiment, the protein concentration was varied, and tryptophan fluorescence spectroscopy and static light scattering were again used to monitor protein stability. Four concentrations (0.1, 0.5, 1.0 and 4.0 mg/ml) of L460D pneumolysoid were selected. These samples were investigated with and without sucrose and trehalose (10% and 15% concentrations). For samples without excipients, typical fluorescence and static light scattering curves of L460D pneumolysoid at different protein concentrations are shown in Figure 4. For the fluorescence studies (Figures 4A-B), the thermal transition shifts of the emission peak position are similar at the different protein concentrations (Figure 4A), although 4.0 mg/ml L460D pneumolysoid shows an earlier transition shift of the emission peak intensity than the other concentrations (0.1, 0.5 and 1.0 mg/ml) (Figure 4B). For the static light scattering studies (Figures 4C), the thermal transitions observed at the lower

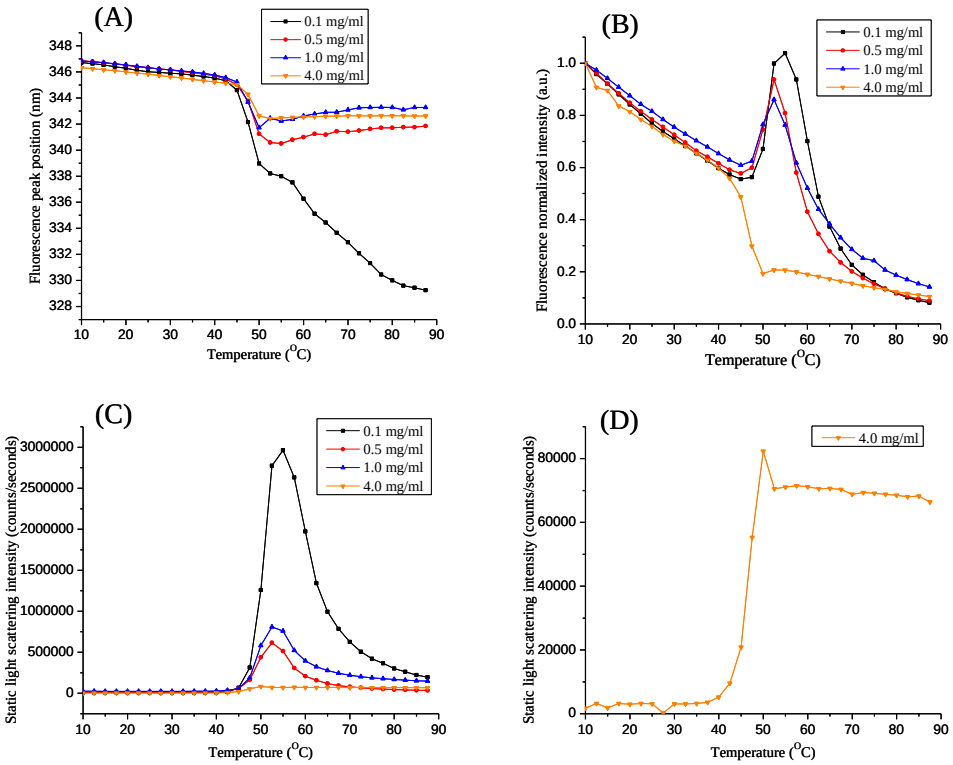

Figure 4. Effect of protein concentration on the conformational stability of L460D pneumolysoid (A): The intrinsic Trp fluorescence emission maximum (peak position), (B): the emission peak intensity, and (C) Static light scattering intensity of protein at different concentrations as a function of temperature. Due to different slit widths used in the experimental settings for lower and higher protein concentrations, the fluorescence intensity and scattering intensity data were normalized. Each data point represents the mean of two independent samples. Protein samples were prepared in a 10 mM histidine buffer at pH 6.

protein concentrations are similar, but, at 4.0 mg/ml, the protein aggregated at a lower temperature of about 40 ℃. Due to different slit widths used in the experimental settings for lower and higher protein concentrations, scattering intensity can't be compared directly between the samples, and the data was normalized. The T_m results for L460D pneumolysoid with and without excipients at different protein concentrations are shown in Supplemental Table S2. Overall, concentrations of 10% or 15% trehalose and sucrose have similar stabilizing effects on L460D pneumolysoid across the range of protein concentrations studied (0.1-4.0 mg/ml) using results from both intrinsic fluorescence spectroscopy and static light scattering as criteria. The T_m results show that the selected excipients have the weakest stabilizing effects on 4.0 mg/ml of protein and the strongest stabilizing effects on 0.1 mg/ml of protein. These excipients have intermediate and good stabilizing effects on the other two concentrations (0.5 and 1.0 mg/ml) of protein.

The stabilizing effects of various excipients on the L460D pneumolysoid at 1.0 mg/ml were further investigated using differential scanning calorimetry (DSC). A typical DSC thermogram of 1.0 mg/ml L460D pneumolysoid without excipients is shown in Supplemental Figure S2 (A). A sharp DSC peak is observed at 52.4 ℃. The T_m values from the DSC studies are summarized in Table 3, both sucrose and trehalose at concentrations of 10% and 15% increase the T_m values by about 2-3 ℃.

5.3.3 Adjuvant-Antigen studies

5.3.3.1 Adsorption Study

The binding of L460D pneumolysoid to alhydrogel (0.6 mg/ml) was investigated where the protein showed efficient binding to aluminum hydroxide adjuvant. An adsorption

Sample	T_m value from DSC study (^{O}C)	$\triangle T_m$ (^{O}C)
Pneumolysin	52.4 ±0.1	
Pneumolysin + 10% sucrose	54.3 ±0.2	1.9
Pneumolysin + 15% sucrose	54.9 ±0.1	2.5
Pneumolysin + 10% trehalose	54.7 ±0.1	2.3
Pneumolysin + 15% trehalose	55.2 ±0.1	2.8

Table 3: Thermal unfolding temperatures (T_m) of L460D pneumolysoid (1.0 mg/ml) with and without excipients. Data were obtained using differential scanning calorimetry. Duplicate measurements were run, the T_m value was calculated separately for each measurement, the values were averaged, and the standard deviation was determined. Protein concentration was 0.1 mg/ml in a 10 mM histidine buffer at pH 6.

isotherm of protein and adjuvant is shown in Supplemental Figure S3. For L460D pneumolysoid concentrations between 0.05 and 1.5 mg/ml, the protein binds completely to the surface of the aluminum hydroxide adjuvant. The adsorption isotherm reaches a plateau at a protein concentration greater than 2.5 mg/ml. Pneumolysin, with at pI of 4.9, has a negative charge at pH 6.0, and hence would be expected to bind to the positively charged alhydrogel presumably at least partially through electrostatic interactions.

5.3.3.2 Stability of L460D pneumolysoid on the Surface of the Aluminum Hydroxide Adjuvant

The conformational stability of L460D pneumolysoid bound to the surface of the alhydrogel adjuvant was investigated by front face fluorescence spectroscopy. Front face fluorescence was used to probe changes in the tertiary structure of the protein in solution and when adsorbed to adjuvant as a function of temperature. Results are shown in Figure 5 (no excipients), Supplemental Figure S4 (with 15% sucrose), and Supplemental Figure S5 (with 15% trehalose). The sharp blue shift of the emission peak position (T_{onset} around 45-47.5 ℃) that is observed for L460D pneumolysoid in solution (either with or without excipients) is not

evident in the samples containing adjuvant. This result suggests a significant effect of surface adsorption on the structural properties of protein antigen, although the exact nature of this phenomenon is currently unknown. For the samples containing adjuvant, the initial peak position was decreased by about 2 nm. The slopes of the pre-transition curves of samples with and without adjuvant, however, were similar (Figures 5B, Figure S4B and Figure S5B), and the observed transitions also do not seem to be affected by previously identified stabilizers. This observation may suggest that the adsorption of the protein on alhydrogel does not significantly affect its stability, although some effect of the adjuvant surface on the properties of the protein is clearly evident in the change in cooperativity of the thermal unfolding transitions. For samples with adjuvant, the increase in fluorescence intensity seen between 10 and 50 ℃ (Figures 5C, Figure S4C and Figure S5C) might be explained by fluorescence excitation and emission of a zone of protein molecules at higher concentration, because proteins packed on the surface of adjuvant are much more concentrated than they are in solution, although again, this idea is highly speculative. The heterogeneous distribution of protein on the adjuvant surface may be another reason for this observed increase in fluorescence intensity.

The stability of L460D pneumolysoid on the surface of alhydrogel was further examined by DSC. The DSC transition peak of pneumolysin with adjuvant is noisier and broader than the peak obtained with protein in solution due to the presence of adjuvant (Figure S2 (B)). This may suggest the presence of a heterogeneous population of proteins on the adjuvant surface and that a fraction of bound protein has been conformationally altered. The averaged

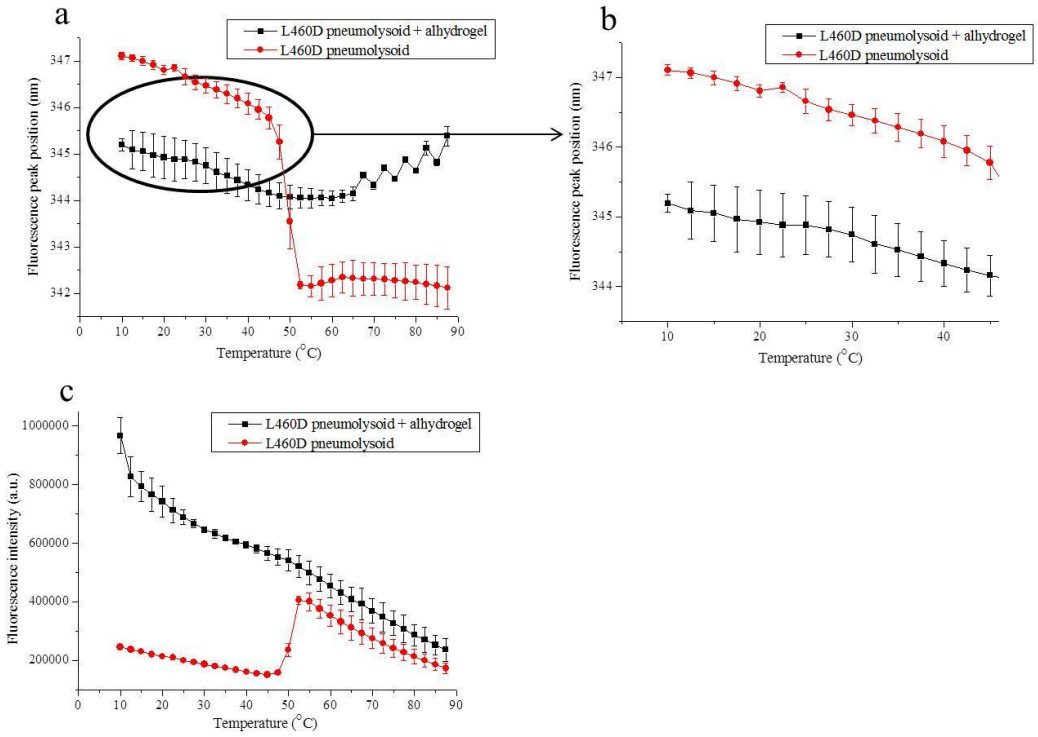

Figure 5. Comparison of tertiary structure stability of L460D pneumolysoid determined by front face fluorescence spectroscopy in solution and when adsorbed to alhydrogel adjuvant. (A): Fluorescence emission maximum (peak position) as a function of temperature. (B): Enlargement of part of the pre-transition regions from (A). (C): emission peak intensity as a function of temperature. Each data point represents the mean of two independent samples, and error bars show the standard deviation. Protein samples were prepared in a 10 mM histidine buffer at pH 6.

T_m value of the L460D pneumolysoid with adjuvant is 51.7 ± 2.1 ℃, which is similar to the average T_m value in solution (52.4 ± 0.1 ℃), however, T_{onset} value of the protein in solution is about 5 ℃ higher compared to the adjuvant–adsorbed protein. Although the similarity in T_m values suggests that there may be little effect of adsorption to alhydrogel on the structure and thermal stability of L460D pneumolysoid, differences in T_{onset} values may suggest some differences in conformational stability.

5.4 Summary and Discussion

The development of recombinant protein-based vaccines offers an alternative way to produce cheaper, robust and broader coverage pneumococcal vaccines in comparison to current polysaccharide and polysaccharide-conjugate based vaccines. Common pneumococcal proteins such as pneumococcal surface protein A (PspA), pneumococcal surface protein C (PspC), pneumococcal surface adhesion A (PsaA) and pneumolysin are currently being evaluated as vaccine candidates against *S. pneumoniae* infection.[4] Pneumolysin is a lead vaccine candidate which has been long known to be highly immunogenic. The protein can potentially be used as an antigen itself or as a carrier protein to the polysaccharides in current vaccine preparations, and in the case of the latter, it may increase the immunogenicity of conjugated vaccines.[8,30] By the use of site-directed mutagenesis, immunogenic pneumolysin mutants with reduced cytotoxicity have been constructed [16,17], with pneumolysoid (L460D) being one of these detoxified forms.

In this study, the conformational stability of the recombinant L460D pneumolysoid was characterized by various biophysical techniques. The overall secondary and tertiary structure of the protein antigen was highly sensitive to pH and temperature. The protein manifests the

highest stability at pH 6-7, much lower stability at pH 4, and at pH 3 the protein is significantly structurally altered even at low temperature (10 ℃). Both pH and temperature also affect the aggregation behavior of the L460D pneumolysoid. Samples at pH 4 to 8 have a strong tendency to aggregate at elevated temperatures as monitored by static light scattering. No aggregation behavior is observed at pH 3 presumably due to proteins' altered structure as this pH. Temperature induced structural changes of L460D pneumolysoid at pH 6 were also monitored by FTIR. We observed that thermal unfolding leads to a loss of native structural bands at 1655 (α-helix), and 1636 cm^{-1} (β-sheet), and the appearance of a new band near 1620 cm^{-1} (data not shown). The latter observation is indicative of the formation of intermolecular beta sheets with increases in temperature. The results obtained from multiple techniques thus provide a comprehensive overview of physical stability of L460D pneumolysoid as a function of pH and temperature.

Excipients such as trehalose, sucrose and sorbitol induce stabilizing effects on L460D pneumolysoid with respect to improving thermal transition temperatures and minimizing its aggregation. These excipients are generally known to stabilize the proteins in solution by the mechanism of preferential hydration.[31,32,33] The effect of protein concentration on stability was also examined, because rates of degradation may vary as a function of protein concentration. Stabilizing excipients had the weakest effect on 4.0 mg/ml of protein (by increasing the T_m by only 1-3 ℃), and had the strongest effect on 0.1 mg/ml protein (by increasing the T_m by 3-5 ℃). The observed lower stabilizing effect produced by excipients at high protein concentrations could be a natural consequence of increased aggregation rates at higher protein concentrations[34] and/or changes of the key ratio of protein:excipient.[35,36]

Finally, an optimized formulation candidate containing 15% trehalose in 10 mM histidine buffer at pH 6 was identified, which balances the effects of increased conformational stability, decreased tendency to aggregate, and solution osmolality.

Adjuvant-antigen interaction studies were also performed using aluminum hydroxide adjuvant. L460D pneumolysoid binds efficiently to alhydrogel. For protein samples with and without adjuvant, the slopes of the pre-transition curves of front-face fluorescence data were similar. Furthermore, similar T_m values were also obtained in a DSC study. Therefore, the stability of L460D pneumolysoid on the surface of alhydrogel does not seem to be affected in a major way by adsorption to the alhydrogel, either with or without excipients, although the noncooperative nature of the surface transition remains unexplained. In addition, the adsorbed antigen shows greater heterogeneity than that of unadsorbed antigen as observed by a noisier and broader DSC thermogram.

In summary, this study provides a better understanding of the inherent characteristics of a vaccine candidate pneumolysin mutant (L460D). This protein antigen has the potential to be developed as an alternative, more broadly immunogenic, yet less expensive pneumococcal vaccine. The effects of various pH /temperature conditions, buffers and excipients on the physical stability of the L460D pneumolysoid were illustrated and optimal stabilizers were identified. The interaction of the protein antigen with aluminum adjuvant was also characterized. This preformulation work provides the basis for the development of a rational strategy in the next stage of formulation development, which should include chemical stability studies (e.g., Asn deamidation and Met oxidation) as well as the effect of

other environmental stresses such as agitation, freeze-thaw cycling and material compatibility on protein stability. In addition, studies to evaluate the immunogenicity and long-term storage stability of adjuvanted candidate formulations of the pneumolysin mutant (L460D) are also needed.

5.5. ASSCOCIATED CONTENT

Supporting Information. Supplemental Tables 1-2 and Supplemental Figures 1-5.

5.6 REFERENCES

1.Gray BM, Converse GM, Dillon HC 1980. Epidemiologic studies of Streptococcus pneumoniae in infants: acquisition, carriage, and infection during the first 24 months of life. Journal of infectious diseases 142(6):923-933.
2. Johnston Jr RB. 1991. Pathogenesis of pneumococcal pneumonia. Review of Infectious Diseases 13(Supplement 6):S509-S517.
3. O'Brien KL, Wolfson LJ, Watt JP, Henkle E, Deloria-Knoll M, McCall N, Lee E, Mulholland K, Levine OS, Cherian T. 2009. Burden of disease caused by Streptococcus pneumoniae in children younger than 5 years: global estimates. The Lancet 374(9693):893-902.
4. Black S, Eskola J, Whitney C, Shinefield H. 2008. Vaccines. 5 ed., Philadelphia: W.B.Saunders Co. p 531-567.
5. Jackson LA, Neuzil KM. 2008. Vaccines. 5 ed., Philadelphia: W.B.Saunders Co. p 569-604.
6. Iyer V, Hu L, Liyanage MR, Esfandiary R, Reinisch C, Meinke A, Maisonneuve J, Volkin DB, Joshi SB, Middaugh CR. 2012. Preformulationi characterization of an aluminum salt-adjuvanted trivalent recombinant protein-based vaccine candidate against streptococcus pneumoniae.
Journal of pharmaceutical sciences in 101(9): 3078-3090.
7. Rubins JB, Janoff EN. 1998. Pneumolysin: a multifunctional pneumococcal virulence factor. Journal of Laboratory and Clinical Medicine 131(1):21-27.
8. Jedrzejas MJ. 2001. Pneumococcal virulence factors: structure and function. Microbiology and molecular biology reviews 65(2):187-207.
9. Mitchell A, Mitchell T. 2010. Streptococcus pneumoniae: virulence factors and variation. Clinical Microbiology and Infection 16(5):411-418.
10. Molloy S. 2010. Bacterial pathogenicity: Pneumolysin: stimulating protection. Nature Reviews Microbiology 9(1):4-4.
11. Paton JC, Lock RA, Hansman DJ. 1983. Effect of immunization with pneumolysin on survival time of mice challenged with Streptococcus pneumoniae. Infection and immunity 40(2):548-552.

12. Lock RA, Hansman D, Paton JC. 1992. Comparative efficacy of autolysin and pneumolysin as immunogens protecting mice against infection by Streptococcus pneumoniae. Microbial pathogenesis 12(2):137-143.
13. Alexander JE, Lock RA, Peeters C, Poolman JT, Andrew PW, Mitchell TJ, Hansman D, Paton JC. 1994. Immunization of mice with pneumolysin toxoid confers a significant degree of protection against at least nine serotypes of Streptococcus pneumoniae. Infection and immunity 62(12):5683-5688.
14. Paton JC, Ferrante A. 1983. Inhibition of human polymorphonuclear leukocyte respiratory burst, bactericidal activity, and migration by pneumolysin. Infection and immunity 41(3):1212-1216.
15. Ferrante A, Rowan-Kelly B, Paton JC. 1984. Inhibition of in vitro human lymphocyte response by the pneumococcal toxin pneumolysin. Infection and immunity 46(2):585-589.
16. Kirkham LAS, Kerr AR, Douce GR, Paterson GK, Dilts DA, Liu DF, Mitchell TJ. 2006. Construction and immunological characterization of a novel nontoxic protective pneumolysin mutant for use in future pneumococcal vaccines. Infection and immunity 74(1):586-593.
17. Oloo EO, Yethon JA, Ochs MM, Carpick B, Oomen R. 2011. Structure-guided antigen engineering yields pneumolysin mutants suitable for vaccination against pneumococcal disease. Journal of Biological Chemistry 286(14):12133.
18. Soltani CE, Hotze EM, Johnson AE, Tweten RK. 2007. Specific protein-membrane contacts are required for prepore and pore assembly by a cholesterol-dependent cytolysin. Journal of Biological Chemistry 282(21):15709-15716.
19. Farrand AJ, LaChapelle S, Hotze EM, Johnson AE, Tweten RK. 2010. Only two amino acids are essential for cytolytic toxin recognition of cholesterol at the membrane surface. Proceedings of the National Academy of Sciences 107(9):4341-4346.
20. Mitchell LM, King J, Hale J, Tweten R, Briles D. 2011. Protective immune responses to streptococcus pneumoniae pneumolysoids. American society for microbiology, New Orleans.
21. Mann B, Tweten R, Gao G, Thornton J, Heath R, Maisonneuve J, Tuomanen E. 2012. Broadly protective protein based pneumococcal vaccine comprised of pneumolysin toxoid-CbpA peptide fusion. International symposium on pneumococci and pneumococcal diseases, Iguacu Falls, Brazil.
22. Wilson-Welder JH, Torres MP, Kipper MJ, Mallapragada SK, Wannemuehler MJ, Narasimhan B. 2009. Vaccine adjuvants: current challenges and future approaches. Journal of pharmaceutical sciences 98(4): 1278-1316.
23. Iyer V, Liyanage MR, Shoji Y, Chichester JA, Jones RM, Yusibov V, Joshi SB, Middaugh CR. 2012. Formulation development of a plant-derived h1n1 influenza vaccine containing purified recombinant hemagglutinin antigen. Human vaccines & immunotherapeutics 8(4) 453-464.
24. Kueltzo LA, Ersoy B, Ralston JP, Middaugh CR 2003. Derivative absorbance spectroscopy and protein phase diagrams as tools for comprehensive protein characterization: A bGCSF case study. Journal of pharmaceutical sciences 92(9):1805-1820.
25. Maddux NR, Joshi SB, Volkin DB, Ralston JP, Middaugh CR 2011. Multidimensional methods for the formulation of biopharmaceuticals and vaccines. Journal of pharmaceutical sciences. 100(10), 4171-4197.

26. Hu L, Olsen CM, Maddux NR, Joshi SB, Volkin DB, Middaugh CR 2011. Investigation of Protein Conformational Stability Employing a Multimodal Spectrometer. Analytical chemistry. 83(24), 9399-9405.
27. Maddux NR, Rosen IT, Hu L, Olsen CM, Volkin DB, Middaugh CR 2012. An improved methodoloy for multidimensional hig-throughput preformulation characterization of protein conformational stabiliity. Journal of pharmaceutical sciences. 101(6), 2017-2024.
28. Kim JH, Iyer V, Joshi SB, Volkin DB, Middaugh CR 2012. Improved data visualization techniques for analyzing macromolecule structrual changes Protein Science. 21(10): 1540-1553.
29. Böhm G, Muhr R, Jaenicke R 1992. Quantitative analysis of protein far UV circular dichroism spectra by neural networks. Protein engineering 5(3):191-195.
30. Kuo J, Douglas M, Ree HK, Lindberg AA 1995. Characterization of a recombinant pneumolysin and its use as a protein carrier for pneumococcal type 18C conjugate vaccines. Infection and immunity 63(7):2706-2713.
31. Kaushik JK, Bhat R 2003. Why is trehalose an exceptional protein stabilizer? Journal of Biological Chemistry 278(29):26458-26465.
32. Kendrick BS, Chang BS, Arakawa T, Peterson B, Randolph TW, Manning MC, Carpenter JF 1997. Preferential exclusion of sucrose from recombinant interleukin-1 receptor antagonist: Role in restricted conformational mobility and compaction of native state. Proceedings of the National Academy of Sciences 94(22):11917.
33. Ohtake S, Wang YJ 2011. Trehalose: current use and future applications. Journal of pharmaceutical sciences 100(6):2020-2053.
34. Wang W, Nema S, Teagarden D 2010. Protein aggregation—Pathways and influencing factors. International journal of pharmaceutics 390(2):89-99.
35. Costantino HR, Carrasquillo KG, Cordero RA, Mumenthaler M, Hsu CC, Griebenow K 1998. Effect of excipients on the stability and structure of lyophilized recombinant human growth hormone. Journal of pharmaceutical sciences 87(11):1412-1420.
36. Cleland JL, Lam X, Kendrick B, Yang J, Yang T, Overcashier D, Brooks D, Hsu C, Carpenter JF 2001. A specific molar ratio of stabilizer to protein is required for storage stability of a lyophilized monoclonal antibody. Journal of pharmaceutical sciences 90(3):310-321.

Chapter 5

Supporting Information

Table of Contents

Supplemental Table 1: ΔT_m (℃) and osmolarity values for L460D pneumolysoid in the selected stabilizers at various concentrations

Supplemental Table 2: T_m results of L460D pneumolysoid (0.1, 0.5, 1.0 and 4.0 mg/ml) with and without excipients

Supplemental Figure 1: (A) Radar chart and (B) Chernoff face diagram of the conformational stability of L460D pneumolysoid.

Supplemental Figure 2: DSC thermograms of L460D pneumolysoid alone and L460D pneumolysoid adsorbed to alhydrogel adjuvant at pH 6

Supplemental Figure 3: L460D pneumolysoid adsorption isotherm

Supplemental Figure 4: Comparison of tertiary structure stability determined by front face fluorescence spectroscopy of proteins in solution and adsorbed proteins, both with 15 % sucrose

Supplemental Figure 5: Comparison of tertiary structure stability determined by front face fluorescence spectroscopy of proteins in solution and adsorbed proteins, both with 15 % trehalose

	Weight percent	Osmotic pressure (mosm/kg H_2O)	$\triangle T_m$ of fluorescence peak position	$\triangle T_m$ (^{O}C) of static light scattering
Trehalose	5%	151.5 ±2.1	1.1	0.7
	10%	291.5 ±3.5	1.6	1.9
	15%	459.0 ±1.4	2.1	4.7
	20%	683.5 ±3.5	4.1	6.4
Sucrose	5%	168.5 ±3.5	1.4	1.2
	10%	322.5 ±2.1	2.5	2.3
	15%	502.5 ±2.1	3.2	4.5
	20%	768.5±17.7	3.8	5.9
Sorbitol	5%	298.3 ±4.7	1.3	1.2
	10%	597.7 ±11.0	2.8	2.9
	15%	953.3 ±24.6	4.5	5.5
	20%	1361.7 ±8.0	5.3	7.5

Supplemental Table S1. ΔT_m (℃) and osmolarity values for L460D pneumolysoid in the selected stabilizers at various concentrations. For osmotic pressure values, triplicate measurements were run, the results were averaged, and the standard deviation was determined. The ΔT_m (℃) values are the same as those in Table 3. Protein concentration is 0.1 mg/ml in a 10 mM histidine buffer at pH 6.

Excipient weight percent	Fluorescence peak position T_m (^{O}C)	△ T_m of fluorescence peak position	Static light scattering T_m (^{O}C)	△T_m (^{O}C) of static light scattering
Pneumolysin 0.1 mg/ml	47.7±0.5		49.9±0.4	
0.5 mg/ml	47.7±0.9		49.4±0.5	
1.0 mg/ml	47.1±0.6		48.9±0.2	
4.0 mg/ml	47.8±0.1		47.1±0.1	
0.1 mg/ml protein	47.7±0.5		49.9±0.4	
Trehalose (10%)	51.2±0.2	3.5	52.7±0.2	2.8
Trehalose (15%)	51.8±0.1	4.1	53.2±0.1	3.3
Sucrose (10%)	51.7±0.5	4.0	52.5±0.4	2.6
Sucrose (15%)	52.6±0.4	4.9	53.1±0.1	3.2
0.5 mg/ml protein	47.7±0.9		49.4±0.5	
Trehalose (10%)	50.6±0.2	2.9	52.0±0.004	2.6
Trehalose (15%)	51.2±0.1	3.5	52.9±0.04	3.5
Sucrose (10%)	50.6±0.3	2.9	51.8±0.1	2.4
Sucrose (15%)	51.1±0.2	3.4	52.5±0.1	3.1
1.0 mg/ml protein	47.1±0.6		48.9±0.2	
Trehalose (10%)	50.4±0.04	3.3	51.6±0.1	2.7
Trehalose (15%)	51.0±0.2	3.9	52.2±0.1	3.3
Sucrose (10%)	50.1±0.2	3.0	51.3±0.1	2.4
Sucrose (15%)	50.2±0.2	3.1	51.4±0.03	2.5
4.0 mg/ml protein	47.8±0.1		47.1±0.1	
Trehalose (10%)	49.5±0.7	1.7	48.0±0.7	0.9
Trehalose (15%)	50.2±0.1	2.4	49.1±0.2	2.0
Sucrose (10%)	49.3±0.1	1.5	47.9±0.4	0.8
Sucrose (15%)	50.7±0.3	2.9	49.7±0.5	2.6

Supplemental Table S2: T_m results of L460D pneumolysoid (0.1, 0.5, 1.0 and 4.0 mg/ml) with and without excipients. Data were obtained from the intrinsic fluorescence spectroscopy and static light scattering techniques. Duplicate measurements were run, the T_m value was calculated separately for each measurement, the values were averaged, and the standard deviation was determined. Protein was prepared in a 10 mM histidine buffer at pH 6.

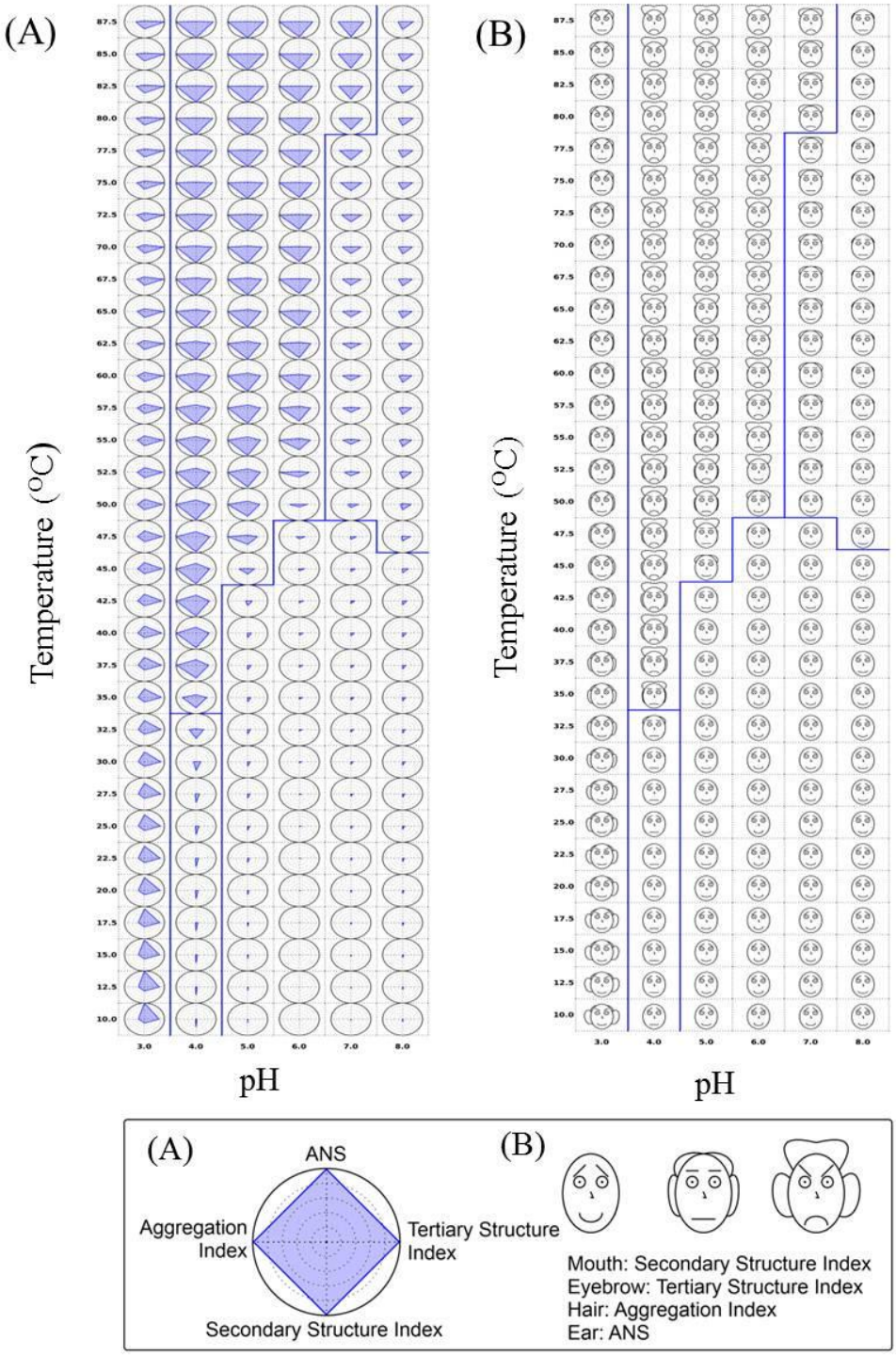

Figure S1. (A) Radar chart and (B) Chernoff face diagram of the conformational stability of L460D pneumolysoid. The diagrams were prepared from CD at 217 nm, intrinsic fluorescence (peak position), static light scattering and ANS fluorescence data. All data were adjusted represent to the native state as (A) a dot and (B) a smiling face. Blue lines indicate an example of clustering results.

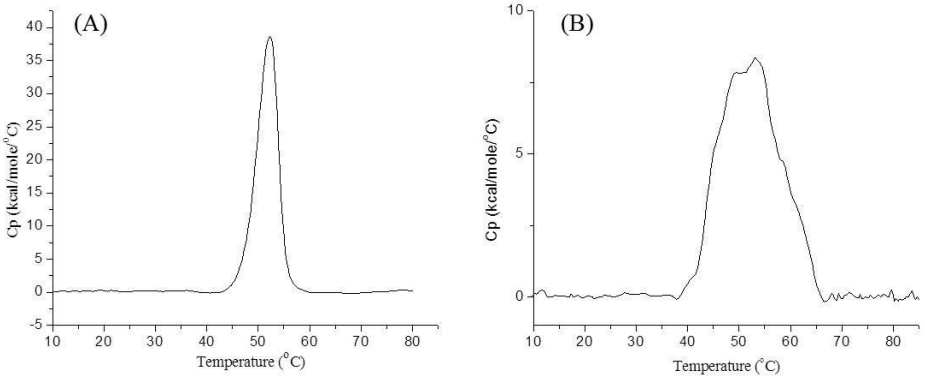

Supplemental Figure S2. Representative DSC thermograms. (A) 1.0 mg/ml L460D pneumolysoid alone and (B) L460D pneumolysoid adsorbed to alhydrogel adjuvant in 10 mM histidine buffer at pH 6. Duplicate measurements were run, each T_m value was calculated separately, and then the values were averaged and reported in the text.

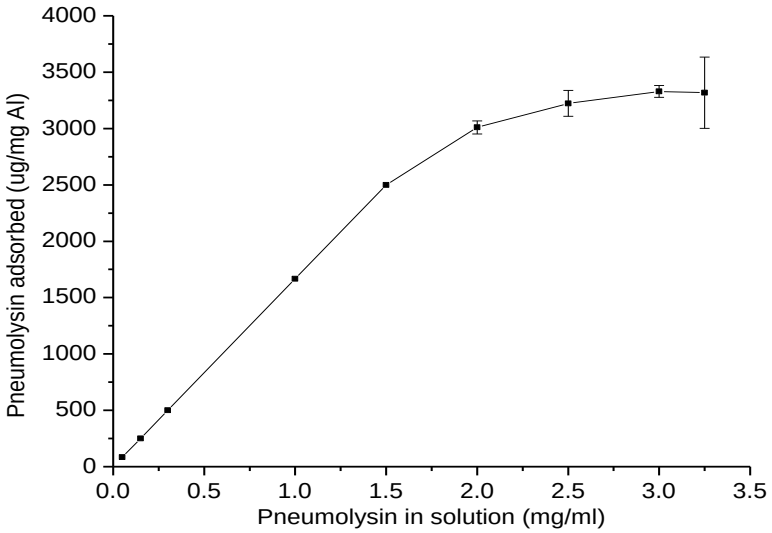

Supplemental Figure S3. Adsorption isotherm of L460D pneumolysoid to alhydrogel adjuvant. Protein concentrations were 0.05, 0.15, 0.3, 1.0, 1.5, 2.0, 2.5, 3.0 and 3.25 mg/ml. The alhydorgel concentration was 0.6 mg/ml. Sample volume was 200 µl. The amount of protein bound to adjuvant was determined by subtracting the amount of protein remaining in solution from the amount of protein added. Each data point represents the mean of two independent samples, and error bars show the standard deviation. Protein samples were prepared in a 10 mM histidine buffer at pH 6.

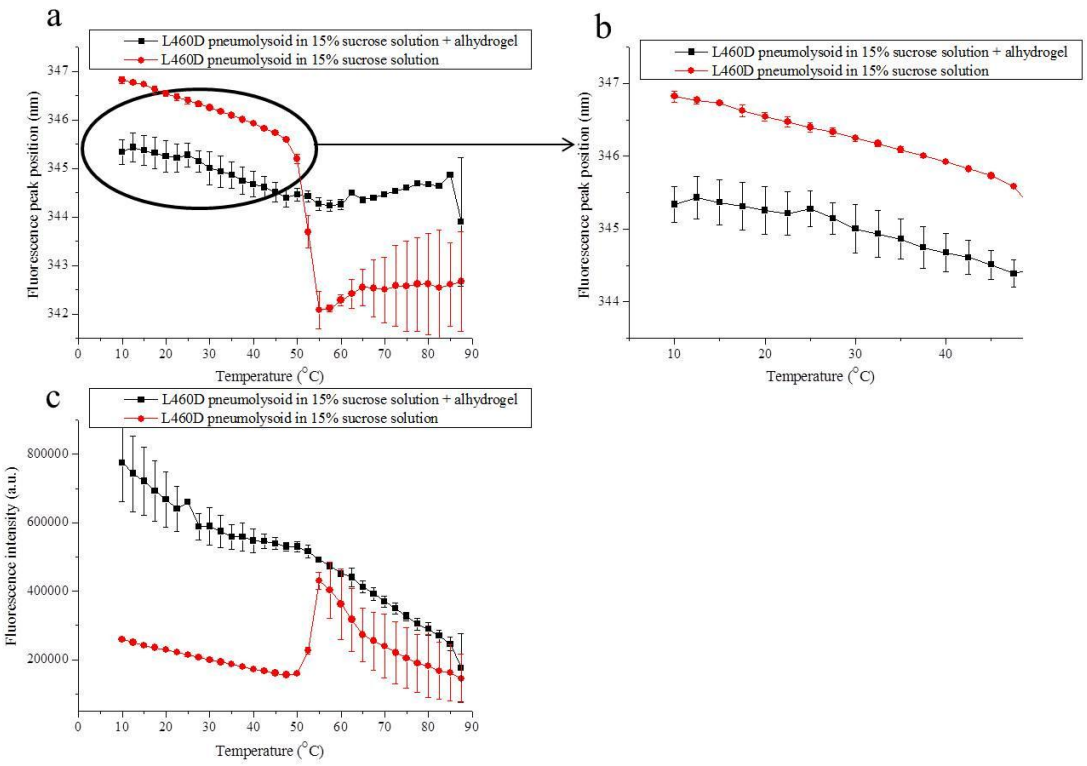

Supplemental Figure S4. Comparison of tertiary structure stability of L460D pneumolysoid determined by front face fluorescence spectroscopy in solution and when adsorbed to alhydrogel adjuvant in the presence of 15 % sucrose. (A): Fluorescence emission maximum (peak position) as a function of temperature. (B): Enlargement of part of the pre-transition regions from (A). (C): emission peak intensity as a function of temperature. Each data point represents the mean of two independent samples, and error bars show the standard deviation. Protein samples were prepared in a 10 mM histidine buffer at pH 6.

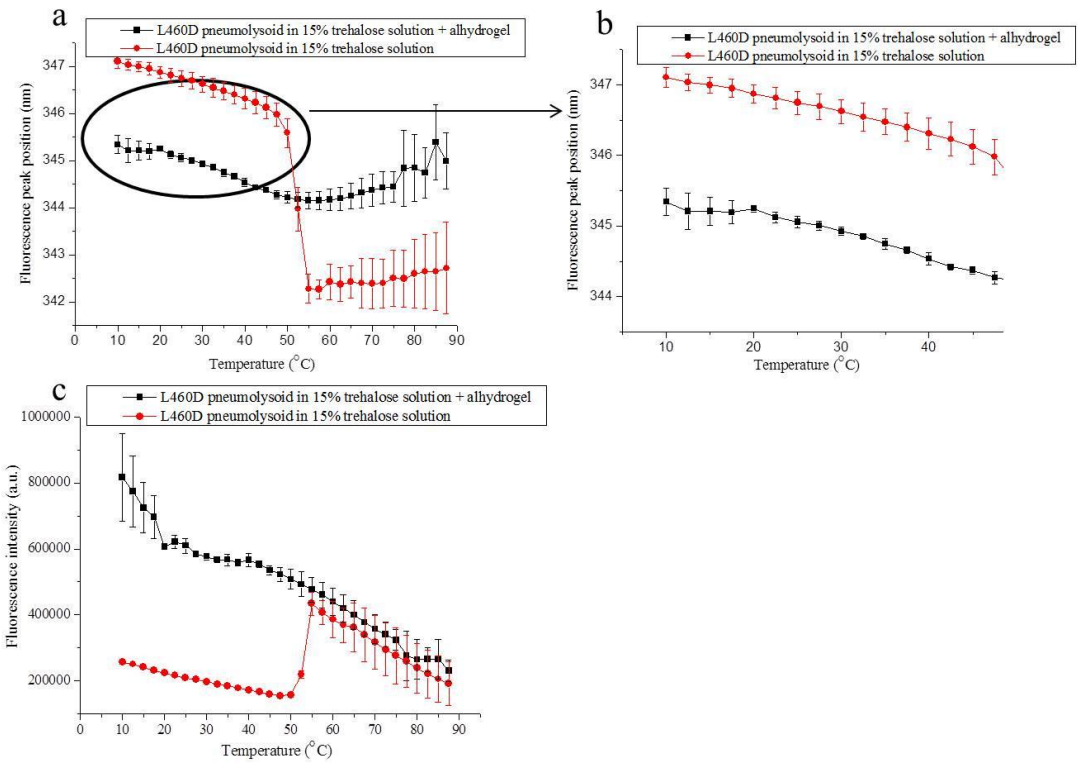

Supplemental Figure S5. Comparison of tertiary structure stability of L460D pneumolysoid determined by front face fluorescence spectroscopy in solution and when adsorbed to alhydrogel adjuvant in the presence of 15 % trehalose. (A): Fluorescence emission maximum (peak position) as a function of temperature. (B): Enlargement of part of the pre-transition regions from (A). (C): emission peak intensity as a function of temperature. Each data point represents the mean of two independent samples, and error bars show the standard deviation. Protein samples were prepared in a 10 mM histidine buffer at pH 6.

Chapter 6 Biophysical Characterization and Conformational Stability of Ebola and Marburg Virus-like Particles

6.1 INTRODUCTION

The Ebola (EBOV) and Marburg (MARV) viruses infect both humans and nonhuman primates and cause severe hemorrhagic fevers. They are members of the Filoviridae family, which consists of filamentous, enveloped, nonsegmented, negative-sense RNA viruses.[1-3] Mortality rates in humans are as high as 90% for EBOV and MARV.[1,4] Viral infection is zoonotic, with African fruit bats recently identified as a potential natural reservoir.[5-7] Person-to-person transmission occurs primarily through physical contact with body fluids of infected animals or patients.[8,9] The filoviruses have a low lethal infectious dose and can be transmitted by droplets or small-particle aerosols.[10] Furthermore, there is a concern for their potential use as biological weapons because of their high virulence, weaponization in form of aerosol in former USSR, and potential to be produced in large quantities.[11-14]

The EBOV and MARV viruses share a common morphology and are similar in structure. Their genomes have a length of approximately 18.9 kb for EBOV and 19.1 kb for MARV, which are two of the largest known negative-stranded RNA virus genomes.[1] Their linear genomes encode seven major structural proteins: nucleoprotein (NP), virion protein 35 (VP) 35, VP40, glycoprotein (GP), VP30, VP24 and polymerase (L) protein. Four of them (NP, VP30, VP35, and L) are nucleoproteins, which are essential for transcription and replication. The remaining three are membrane-associated.[1,15,16]

Vaccines are needed for protection against filovirus infections. Currently, there are no licensed vaccines or chemotherapeutic agents available for the treatment of prevention of these viral infections. Thus, development of an efficacious vaccine to protect public health is crucial. In the last ten years, significant progress has been made and several vaccine strategies

have been used to protect immunized animals against filovirus challenge with varying efficacy. These strategies include inactivated or attenuated viruses, individual viral protein, DNA and recombinant viral-vector-based vaccines, as well as virus-like particles (VLPs).[17-21] Among these vaccine strategies, vector-based vaccines and VLPs are the most promising strategies to date. VLPs have several potential advantages over other candidate vaccines. VLPs lack viral genomic material (and, thus, cannot replicate), lack issues involving pre-existing immunity to a viral vector vaccine, are relatively easy to produce in large quantities, and can be administrated repeatedly to boost the levels of immune responses.[22] As shown by the two currently available VLP based vaccines, hepatitis B and human papillomavirus vaccines, their multimeric nature is especially conducive to strong humoral responses.[23-25]

Recent studies have demonstrated that monovalent and multivalent VLP vaccine strategies are efficacious and offer protection to several species, including mice, guinea pigs, and nonhuman primates (monkeys), against lethal dose challenge by Ebola and/or Marburg viruses.[26-32] These VLP particles have been produced in both mammalian and insect cell cultures. Expression and production of viral structural proteins lead to the assembly and release of VLPs which resemble virions in size and morphology. [26,30-38] The Ebola VLPs (eVLPs) and Marburg VLPs (mVLPs), comprised of the homologous GP, VP40, and NP, elicited strong neutralizing antibody responses as well as cellular immune responses against filoviruses in animal models.[22,30,31] These studies have convincingly demonstrated the potential of a VLP vaccine strategy for use against human filovirus infection.

The formulation of viral antigens into stable, efficacious protein-based vaccine dosage form is critical to their successful development into commercial vaccines. The long term storage stability of such vaccines in liquid formulations can be maximized by optimizing the properties of the solution (e.g. antigen concentration, solution pH, and addition of excipients such as buffers, salts, and stabilizers). Characterization of the stability of these vaccines by a number of biophysical methods will help us better understand potential structural changes produced by various types of environmental stresses. This work focuses on the characterization of the temperature and pH stability of the eVLPs and mVLPs with the goal of developing stable vaccine formulations as a next step. Various spectroscopic techniques were employed to investigate the conformational stability of these two enveloped VLPs in solution. These techniques include intrinsic fluorescence, extrinsic (laurdan) fluorescence, and circular dichroism (CD) over a wide range in pH and temperature, from pH 3 to 8 and 10 to 87.5 ℃, respectively. Temperature-induced aggregation of the VLPs at various pH values was monitored by static and dynamic light scattering. These large biophysical data sets were summarized through the use of empirical phase diagrams (EPDs) for both the eVLPs and mVLPs. The EPDs describe physical changes in the enveloped VLP particles under stressed environmental conditions, including elevated temperature and acidic pH. From the results of each biophysical technique and the resultant EPDs, a temperature/pH stability profile of each VLP was created. This information can be used as a starting point in the development of stable formulations for these two enveloped VLPs.

6.2 MATERIALS AND METHODS

6.2.1 Generation of VLPs

For expression in the insect cell system, the homologous Ebola virus (Zaire strain) (ZEBOV) or Marburg virus (Musoke strain of Lake Victoria) (MMARV) glycoprotein (GP), nucleoprotein (NP), and viral protein 40 (VP40) genes were inserted into a baculovirus vector system (Bac-to-Bac, Invitrogen) for expression in insect cells. Integrated Biotherapeutics Inc. (IBT) produced a three-gene bacmid construct to allow a single baculovirus to produce each respective ZEBOV or MMARV VLP particle type. The triple construct has each gene (ordered NP, VP40, and GP) flanked by the polyhedrin promoter and SV40 polyadenylation sequence for high expression of these genes. Recombinant baculoviruses containing the filovirus proteins of interest were recovered and amplified with another passage through Sf9 cells. The final viruses were introduced into Sf9 insect cells for VLP production, and the VLPs were recovered from the culture supernatants by high-speed concentration, purified on sucrose gradients, and resuspended in phosphate buffered saline. Purified VLPs were characterized by SDS-PAGE followed by Western blot using antibodies against ZEBOV or MMARV viral proteins. The total concentrations of the VLPs preparations were determined by using a BCA protein assay (Thermo Scientific).

6.2.2 Preparation of virus-like particles for biophysical analysis

Individual VLPs solutions at pH 3-8 were prepared by centrifuging 1.0 ml of the concentrated stock solutions of the VLPs (2.0 mg/ml) for 10 minutes at 13,000 x g at 4 ℃ using a Fisher Scientific accuSpin^{TM} Micro centrifuge (Fisher Scientific., Pittsburgh, PA). The resulting pellet was resuspended in 1.0 ml of 20 mM citrate-phosphate buffer with an

ionic strength of 0.15 M adjusted with sodium chloride. The buffer exchange process was repeated three times in total. Samples at pH 3 and 4 contained 30% sucrose to retard particulate settling seen at low pH. Experimental concentrations were 0.1 mg/ml for all fluorescence and light scattering measurements, and was 0.4 mg/ml for circular dichroism studies to increase the strength of the CD signals.

6.2.3 Electron microscopy

The eVLPs and mVLPs at pH 7 (20 mM citrate-phosphate buffer) were examined on a JEOL EX transmission electron microscope at 80 kV after the samples were negatively stained with 1% uranyl acetate, as previously described, for the electron microscopy study.[26,29] These studies were performed as a service by the Pathology Division at the United States Army Research Institute of Infectious Diseases.

6.2.4 Far-UV Circular Dichroism Spectroscopy

Circular dichroism study was performed with a Jasco-810 spectrophotometer equipped with a Peltier temperature controller and a 6-position cuvette holder (Jasco Inc., Easton, MD). Far UV spectra of eVLPs and mVLPs (0.4 mg/ml) were collected in the range of 190-260 nm using a 0.1 cm path length cuvette sealed with a Teflon stopper. A scanning speed of 20 nm/min with a response time of 1 s and a bandwidth of 1 nm were used. The CD signals of eVLPs and mVLPs at 225 nm were monitored as a function of temperature at 0.5 ℃ intervals from 10 to 87.5 ℃. The heating rate was 15 ℃/h. At minimum, duplicate samples at each pH were measured. Baseline measurements of buffers were taken and subtracted from sample measurements prior to data analysis.

6.2.5 Intrinsic Fluorescence Spectroscopy

The intrinsic fluorescence of eVLPs and mVLPs (0.1 mg/ml) was measured using QuantaMaster 810 spectrofluorometer (Photon Technology International, Inc., Birmingham, NJ) equipped with a 4-position cell holder and Peltier temperature control device. Fluorescence emission spectra of eVLPs and mVLPs were recorded as a function of temperature (10-87.5 ℃) and pH (3-8). Triplicate samples were measured using an excitation wavelength of 295 nm (> 95% tryptophan emission). Emission spectra were collected from 310 to 400 nm with a step size of 1 nm and 1 s integration time. The excitation and emission slits were set at 3 nm and 8 nm respectively, for eVLPs, and 3 nm and 12 nm for the mVLPs. The spectra were collected at 2.5 ℃ intervals with a 5 min equilibration time at each temperature. A 1 cm path length quartz cuvette was used in all experiments. To maintain solution homogeneity during measurements, samples were stirred using a magnetic stirrer. Buffer baselines were subtracted from each spectrum before data analysis. Data analysis was performed using FelixTM (Photon Technology International, Inc.) software. The position of the emission wavelength maximum was determined using a polynomial derivative fitting method executed in *Origin 7.0* software. The fluorescence emission intensity data were normalized between 0 and 1 for each sample.

6.2.6 Extrinsic Fluorescence Spectroscopy

Laurdan (2-dimethylamino-6-lauroylnaphthalene) was used as an extrinsic fluorescent probe to study changes in membrane fluidity of eVLPs and mVLPs. The interaction of laurdan with the membranes was monitored as a function of temperature (10-87.5 ℃) and pH (3-8) using the PTI Quanta Master 810 spectrophotometer. Triplicate samples were measured,

and samples were stirred using a magnetic stirrer. A stock solution of laurdan was prepared by dissolving 1.0 mg of the laurdan into 1.5 ml of dimethylsulfoxide (DMSO). Each sample solution containing 10 μM diluted laurdan was incubated at 10 ℃ in the dark for 20 minutes before measurement. Samples were excited at 340 nm and spectra were collected from 400-500 nm at 2.5 ℃ intervals with a 5 min equilibration time at each temperature in a 1 cm path length quartz cuvette. Emission peak intensities at 440 nm and 480 nm (I_{440} and I_{480}) were used to calculate the generalized polarization (GP) of laurdan fluorescence, where GP = (I_{440}-I_{480}) / (I_{440}+I_{480}). Buffer baselines containing 10 μM laurdan were subtracted from each sample spectrum prior to analysis.

6.2.7 Static Light Scattering

The static light scattering intensities of eVLPs and mVLPs (0.1 mg/ml) were recorded simultaneously using a 1 nm slit width during the intrinsic fluorescence experiments by employing a second photomultiplier located 180 ° to the fluorescence detector. The scattering intensities at 295 nm were plotted as a function of temperature (10-87.5 ℃) to monitor the aggregation behavior of the VLPs. Buffer baselines were subtracted from each sample spectrum before analysis.

6.2.8 Dynamic Light Scattering

The mean effective hydrodynamic diameters of the VLPs (0.1 mg/ml) were monitored by dynamic light scattering from 10 to 87.5 ℃. Measurements were recorded at 2.5 ℃ intervals with a 5 min equilibration time at each temperature. Five measurements were taken at each temperature. Incident light at 532 nm was generated by a 125 mW diode-pumped laser, and the scattered light was monitored at 90 ° to the incident beam. A digital autocorrelator

(BI-9000 AT) was used to create the autocorrelation function (Brookhaven Instrument Corp., Holtzille, NY). The diffusion coefficients of the particles were extracted by cumulant analysis of the auto correlation functions. The effective hydrodynamic diameter was calculated from the diffusion coefficients by the Stokes-Einstein equation. Viscosity and refractive index corrections were applied to each measurement using the NanoDLS Particle Sizing software (Brookhaven Instrument). In addition, viscosities of the buffers at pH 3 and 4 containing 30% sucrose were measured using the SVM 3000 viscometer (Anton Parr USA Inc., Ashland, VA). Measurements were recorded from 10 to 87.5 ℃ at 2.5 ℃ intervals, and the average values of three replicates at each temperature were applied to viscosity correction.

6.2.9 Empirical Phase Diagrams

Conformational changes can be determined independently by each of the above described techniques. The large sets of data obtained can be combined to construct empirical phase diagrams (EPDs) that connect similar data correlated with similar structure. The data sets are initially ordered by environmental parameter (e.g., temperature, pH). Each biophysical technique uses identical environmental parameters over the same ranges (e.g., pH from 3 to 8, temperature from 10 ℃ to 87.5 ℃) at regular increments. The raw data sets from all of the measurements are defined as multi-dimensional vectors. These vectors are analyzed by principal components analysis in which the components with the three largest contributions are combined to construct an empirical phase diagram using a red, green, and blue (RGB) color system as described in detail elsewhere.[39] The EPDs are used to identify coherent parameter regions that define VLP structural states as a function of solution variables (temperature and pH in this case) as described below. Note that these are not

thermodynamic phases and no equilibrium is implied across any of the observed apparent phase boundaries.

6.3 RESULTS

6.3.1Biophysical Characterization of Purified VLPs Produced in Insect Cells

SDS-PAGE profile (Figure 1A) revealed that the major bands were VP40 and NP proteins in both VLPs. The glycoprotein (GP) was not visible in either of the eVLPs and mVLPs preparations, probably because of the mobility over a wider range due to multiple glycosylated forms and relatively low level of GP in VLPs. A protein band of about 64 KDa in molecular weight was also detected in both VLPs, which is likely a baculovirus GP64 protein that co-purified with the VLPs.[28,32] Western blot analysis was performed by using monoclonal antibodies against Ebola and Marburg viral proteins and revealed that GP, NP and VP40 are present in the two VLPs preparation (Figure 1B1-B6). The purified eVLPs and mVLPs in pH 7 citrate phosphate buffer were also examined by electron microscopy (Figure 2). Both VLPs displayed filamentous morphology similar to filovirus. These filamentous VLPs at pH 7 have a diameter of 60-80 nm and are about 350 nm to 5000 nm in length. As discussed in detail in the following sections, the eVLPs and mVLPs displayed an effective hydrodynamic diameter of 250 – 400 nm in solution (pH 7, 10 ℃), as measured by dynamic light scattering. In addition, the proteins in the VLP samples were primarily α-helical in structure in solution (pH 7, 10 ℃), as measured by circular dichroism.

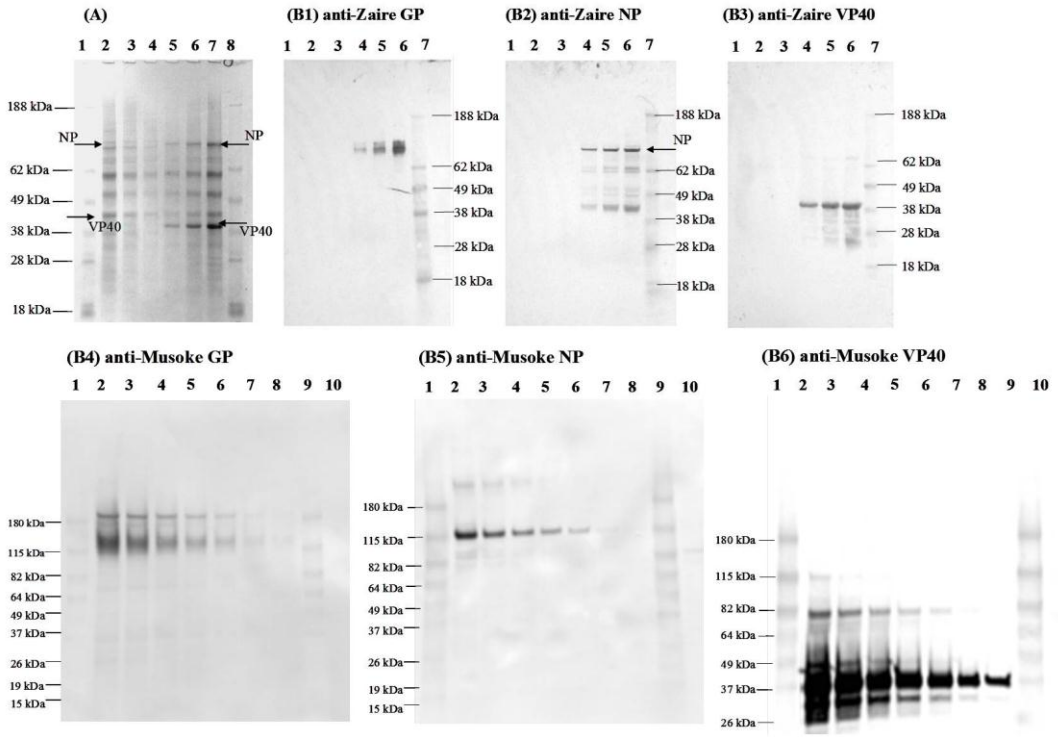

Figure 1. (A): SDS-PAGE analysis of EBOV Zaire VLPs (eVLPs) and MARV Musoke VLPs (mVLPs) preparations stained with Coomassie blue. 4, 2 and 1 μg of VLP preparations were mixed with reducing protein sample buffer, heated at 90 ℃ for 10 min, and then subjected to SDS-PAGE. Lanes 1 and 8, molecular weight markers; lanes 2, 3 and 4, MARV Musoke VLPs 4, 2 and 1 μg; lanes 5, 6 and 7, EBOV Zaire VLPs 1, 2 and 4 μg. (B1-B6): Western blot analysis of EBOV Zaire VLPs and MARV Musoke VLPs. All primary antibodies diluted 1:1000, (B1) anti-Zaire GP, (B2) anti-Zaire NP, and (B3) anti-Zaire VP40 antibodies were used. Lanes 1, 2 and 3, MARV Musoke VLPs 4, 2 and 1 μg; lanes 4, 5 and 6, EBOV Zaire VLPs 1, 2 and 4 μg; lane 7, molecular weight marker. (B4) anti-Musoke GP, (B5) anti-Musoke NP, and (B6) anti-Musoke VP40 antibodies were used. Lanes 1 and 9, molecular weight markers; lanes 2 to 8, MARV Musoke VLPs 8, 4, 2, 1, 0.5, 0.25 and 0.1 μg; lane 10, EBOV Zaire VLPs 8 μg.

(A) eVLPs

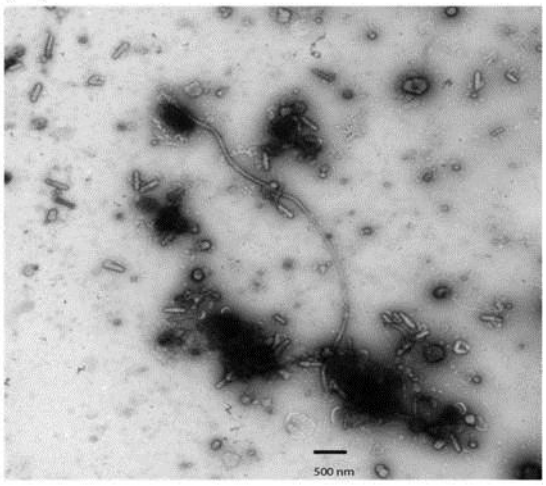

(B) mVLPs

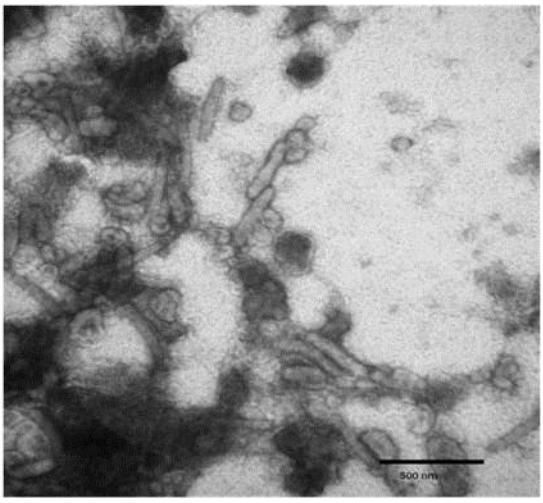

Figure 2. EVLPs (A) and mVLPs (B) in 20mM citrate phosphate buffer at pH 7 were analyzed by electron microscopy.

6.3.2 Dynamic Light Scattering

The hydrodynamic properties of the VLPs were measured by dynamic light scattering (DLS) (Figure 3). Because the eVLPs and mVLPs are filamentous in shape, the effective diameter was measured primarily for qualitative purpose to evaluate the effect of pH and temperature on the size of the VLPs. For both VLPs, the particle size increased with increasing temperature (in the pH range of 6-8 and 3-8 for eVLPs and mVLPs, respectively).

For eVLPs (Figure 3A), the average hydrodynamic diameters at pH 3 and 4 were significantly larger than those at higher pH values, even at low temperatures. The measured values were around 1700 nm which exceeded the measuring range of the instrument employed in this study. These particles formed at low pH appeared to decrease in size as the temperature increased (data not shown). This result suggests a disruption of the particles, or their aggregates, at elevated temperature and low pH. In contrast, there was little temperature-dependence on the size of the eVLPs at pH 5. For eVLPs at pH 6-8, an increase in the size of the particles with increasing temperature was observed.

In case of mVLPs (Figure 3B), samples at pH 3 and 4 demonstrated the fastest rates of size increase and aggregated significantly at elevated temperature. The diameter of the sample at pH 5 was largest at low temperatures, which suggests structural alteration with an expansion in size. The effective diameters of the particles increased as the temperature was raised and at least tripled in size for all samples at higher temperatures. It should be noted that particle sizes greater than a micron are not accurately measured by DLS instrumentation,

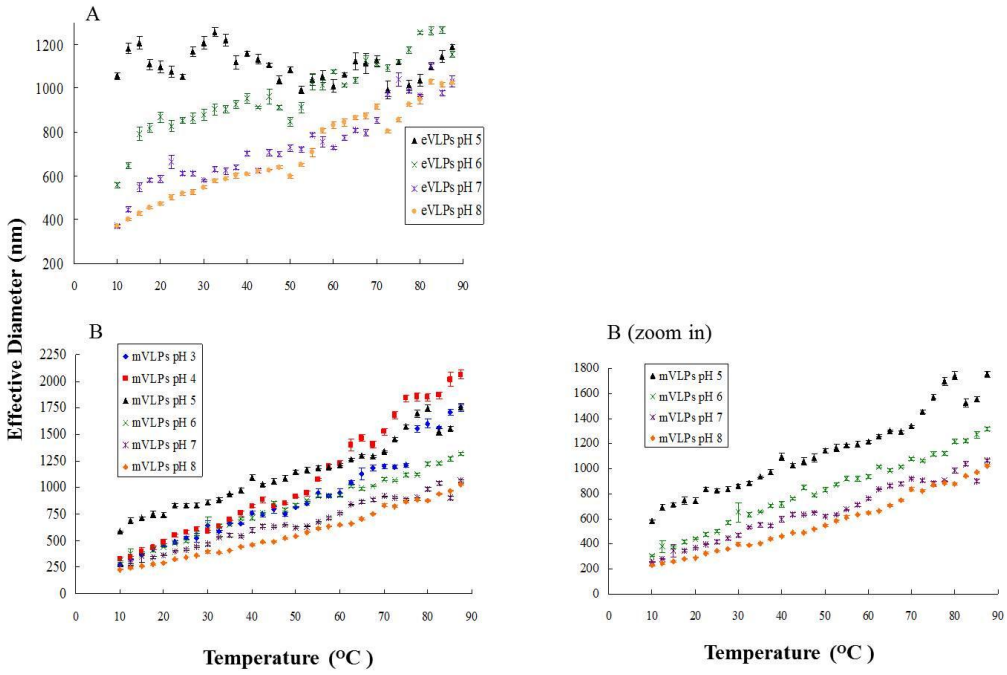

Figure 3. Effective diameters of eVLPs (A) and mVLPs (B) as a function of temperature and solution pH as measured by dynamic light scattering. Each data point represents the mean of five accumulations at each temperature point, and error bars show the standard deviation.

however, they are reported here to continue the observation of stability trends at higher temperatures. At pH 7 and 8, both VLP types manifested smaller particle sizes than those prepared at pH 5 and 6 over the entire temperature range. This result implies decreased stability of the VLPs at pH 5 and 6 due to particle aggregation.

6.3.3 Static Light Scattering

A static light scattering study was performed to monitor the aggregation behavior of the VLPs in solution as a function of temperature and pH. Increased scattering intensity is typically a consequence of protein association-related behavior (for example, aggregation). Decreased scattering intensity observed after the increased intensity is typically due to the precipitation of the aggregated VLP particles or a reduction of the refractive index of particles, as a result of decreased densities.

For the eVLPs (Figure 4A), samples at pH 3 and 4 exhibited lower scattering intensities and demonstrated little change over the temperature range examined, in comparison to those prepared at other pH values. The change in scattered light intensity peaked at pH 6, with intermediate values at pH 5, 7 and 8. Weak transitions in apparent particle size are seen for the eVLPs at pH 5-8, with some variation in behavior over this pH range. For example, a double transition is observed at pH 5.

Like the eVLPs, the mVLPs also display a complex effect of solution pH on scattering intensity (Figure 4B). For this case, the optimum scattering at lower temperatures is near pH 5. Again, transitions are seen at all pH values although only a weak effect is observed at pH 8. For both the eVLPs and the mVLPs, the thermal transitions generally indicate small increases in size, followed by a maximum, and then a decrease at higher temperatures. Interestingly, for

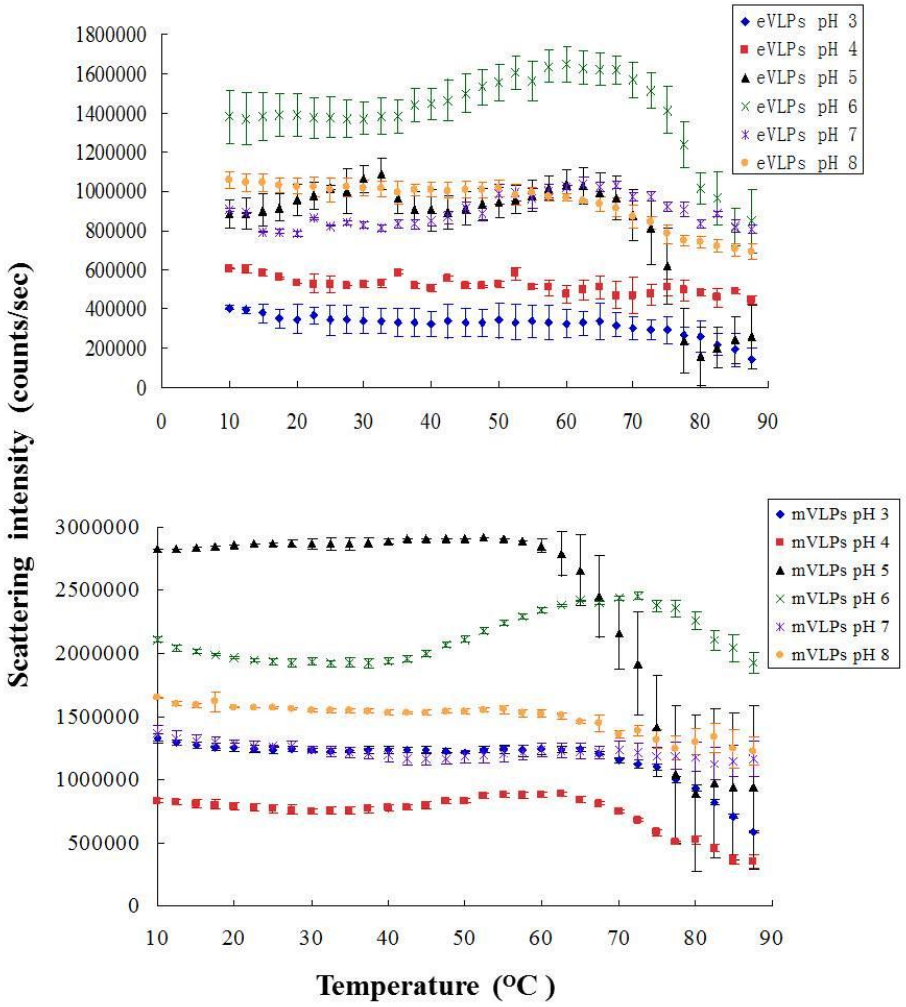

Figure 4. Static light scattering intensities of eVLPs (A) and mVLPs (B) as a function of temperature and solution pH. Each data point represents the mean of three independent samples, and error bars show the standard deviation.

both VLP types the difference in initial scattering intensity at 10 ℃ suggests that there may be temperature-independent difference in VLPs sizes due to solution pH. The DLS results (Figure 3) are consistent overall with the observations made from static light scattering (Figure 4).

6.3.4 Far-UV Circular Dichroism Spectroscopy

Far-UV CD is frequently used to study the conformational changes of proteins, and thus can be applied to VLPs with appropriate consideration for absorption flattening and differential scattering artifacts. The far UV region (190-250 nm) mainly reflects peptide bond absorption, and thus provides information about the secondary structure of proteins. For eVLPs and mVLPs in this study, several proteins contribute to the observed spectrum. Thus, the CD spectrum is a sum of the CD signals from all these proteins, although it may be dominated by contributions from the most abundant protein(s).

The CD spectra of eVLPs and mVLPs at different pH values at 10 ℃ are shown in Figures 5 (A) and (B). Spectra of both VLPs showed a shoulder at 210 nm and a broad peak at approximately 223-225 nm from pH 6 to 8. This result suggests that proteins in both VLPs contain significant amount of α-helical secondary structures, as may be expected for protein associated with lipids. In general, the ellipticity of the VLPs decreased with decreasing pH indicating a reduction in α-helical content. The minima at 210 nm and 225 nm were strongest at pH 7 and 8, and became more poorly resolved as the pH decreased. Spectra of both VLPs at pH 5 showed a shifted minimum to 227-228 nm while the mVLPs at pH 5 also produced stronger CD signals than samples at pH 6 and 7. These results argue for altered secondary

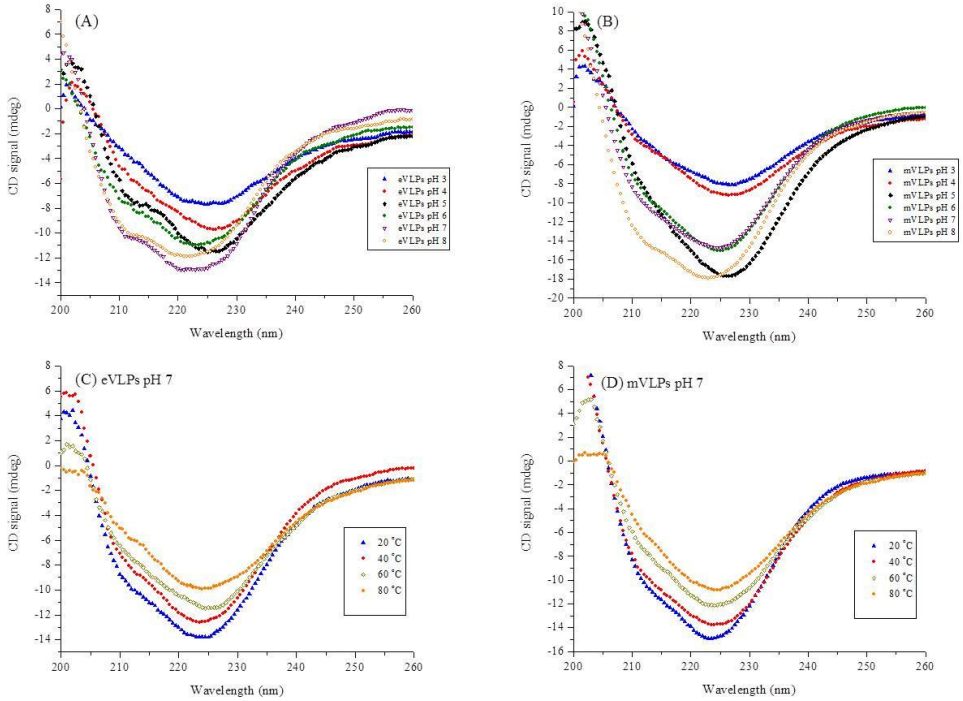

Figure 5. Far-UV circular dichroism (CD) spectra of eVLPs (A) and mVLPs (B) at 10 ℃. Samples were examined from pH 3 to 8 at one pH unit intervals. The CD spectra of eVLPs at pH 7 (C) and mVLPs at pH 7 (D) were collected at the indicated temperatures.

structure of the VLPs at pH 5 in contrast to those at pH 6-8. The spectra at pH 3 and 4 exhibited much lower CD signals compared to samples at higher pH values. These spectra are broadened and the minimum at 223-225 nm is red-shifted. These observations suggested that the VLPs have lost secondary structures and/or are displaying absorption flattening due to aggregation at lower pH.

Figures 5 (C) and (D) demonstrate the loss of secondary structure with increasing temperature for both VLPs at pH 7. Samples at other pH values display similar behavior (data not shown). Temperature-induced changes in secondary structure of the VLPs were also monitored at 225 nm from 10 to 87.5 ℃. Both eVLPs (Figure 6) and mVLPs (Figure 7) gradually lost secondary structure with increasing temperature, with significant pH dependent behavior. At pH 3 and 4, much weaker CD signals were observed at low temperature and the accompanying thermal transitions were quite broad. At pH 5 and 6, stronger CD signals are seen and the ranges of signal change are greater (8-10 mdeg units) when compared to the other conditions. The VLPs at pH 7 and 8 also demonstrated strong initial CD signals, but displayed smaller magnitudes of signal change (about 4 mdeg units) over the entire temperature range. These findings suggest that eVLP and mVLP samples at pH 5 and 6 demonstrated greater structural sensitivity to temperature. Thus, they are more easily altered to produce thermal-induced non-native states compared to VLPs under neutral pH solutions. The breadth of the melting curves, however, does not permit a quantitative analysis of stability in terms of T_m changes. Most transitions appear to initiate between 40 - 45 ℃.

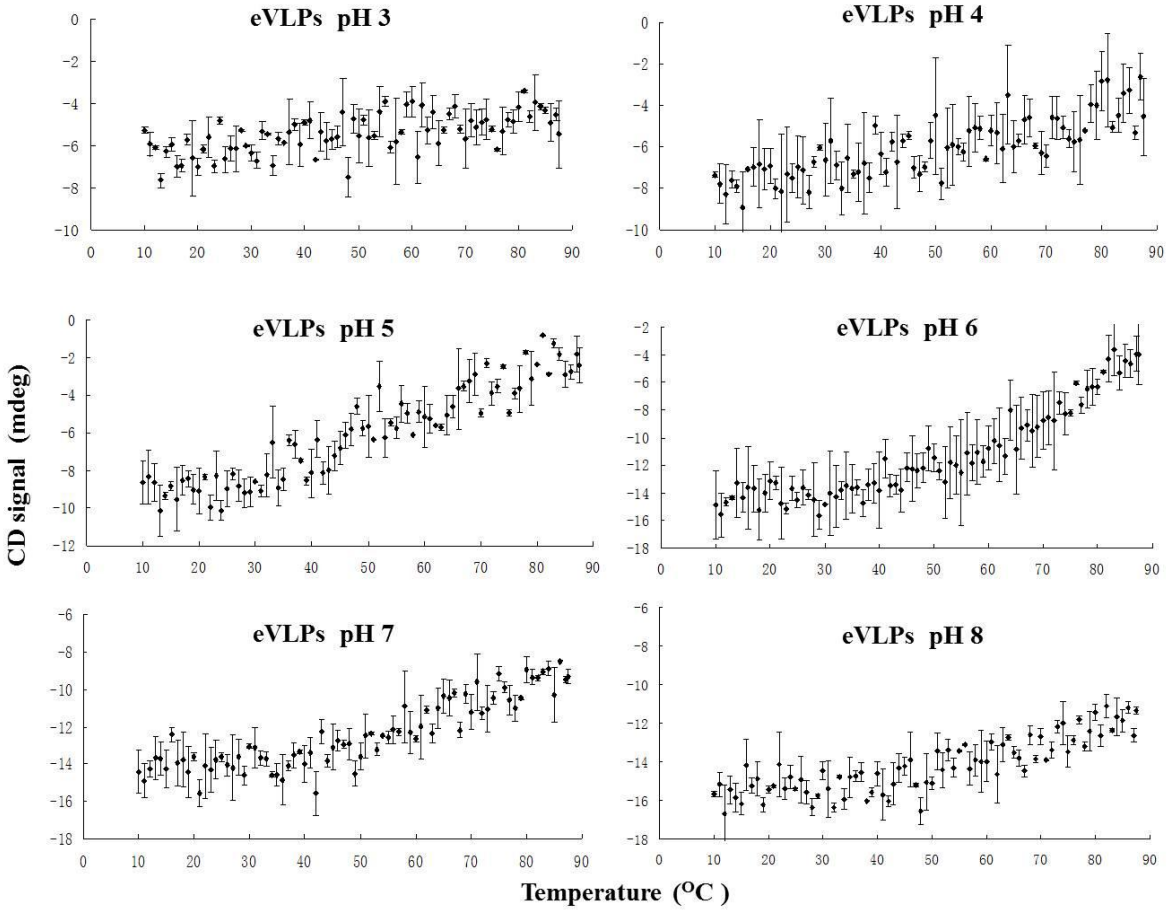

Figure 6. The CD signal of the eVLPs at 225 nm as a function of temperature and solution pH. Data were collected at 0.5 ℃ intervals and are shown here at 1 ℃ increments. Each data point represents the mean of two independent runs with error bars showing the standard deviation.

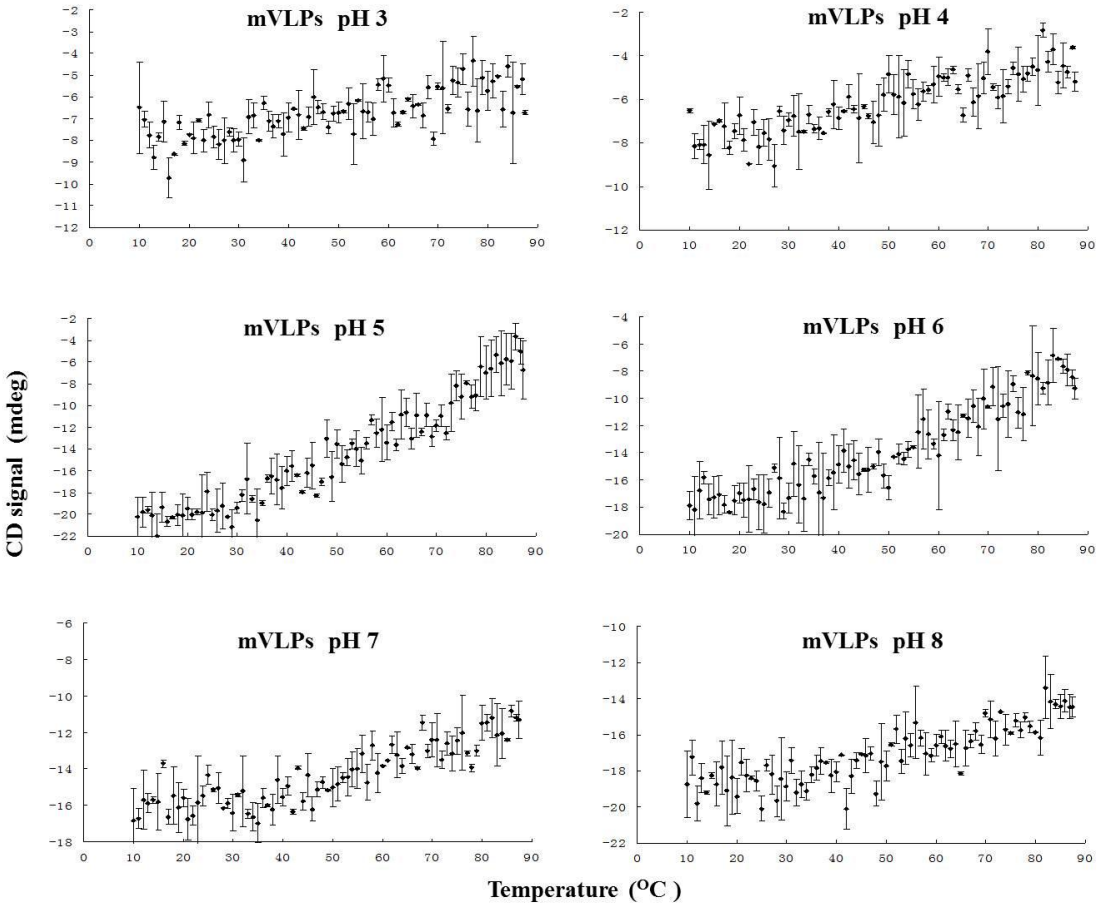

Figure 7. The CD signal of the mVLPs at 225 nm as a function of temperature and solution pH. Data were collected at 0.5 ℃ intervals and are shown here at 1 ℃ increments. Each data point represents the mean of two independent runs with error bars showing the standard deviation.

6.3.5 Intrinsic Fluorescence

Intrinsic fluorescence spectroscopy is often employed to examine tertiary structural changes in proteins. The fluorescence of tryptophan (Trp) residues, which tend to dominate protein fluorescence spectra, is strongly dependent on their local environment. Tertiary structure changes in the eVLPs and mVLPs were monitored for changes in the position and intensity of their tryptophan emission peak.

A slight shift to longer wavelength in peak position is seen with increasing temperature at pH 5-8 (eVLPs) and at pH 7-8 (mVLPs), although the results are pH dependent with increases in thermal stability generally observed at higher pH values (Figures 8 and 9). This observation suggests a pH-dependent partial unfolding of the VLP proteins at elevated temperature. A much sharper blue shift in peak position was observed for both the eVLPs and mVLPs at most temperatures higher than 70 ℃, including an increase in noise of the data above this temperature (data points shown in the figures were cut off at 82.5 ℃ and 80 ℃ for eVLPs and mVLPs, respectively). These results most likely reflect aggregation of the VLPs at higher temperatures (similar to the observations discussed in the previous section with the light scattering experiments).

The initial emission peak positions of eVLP samples at pH 3 and 4 were around 329-330 nm (Figure 8), a value several nanometers less than that seen at higher pH (~332nm). This result suggests a more apolar environment for the Trp residues, presumably as a consequence of aggregation or increase in size (i.e., expansion). No clear thermal transition is seen at pH 3 and 4, although a small transition may be present at approximately 50 ℃. Small thermal transitions were also observed for eVLPs at pH 7 at 52.5 ℃ and 65 ℃. For eVLPs at pH 8,

however, similar significant blue shifts were not observed, although two small transitions were seen near 45 and 55 ℃.

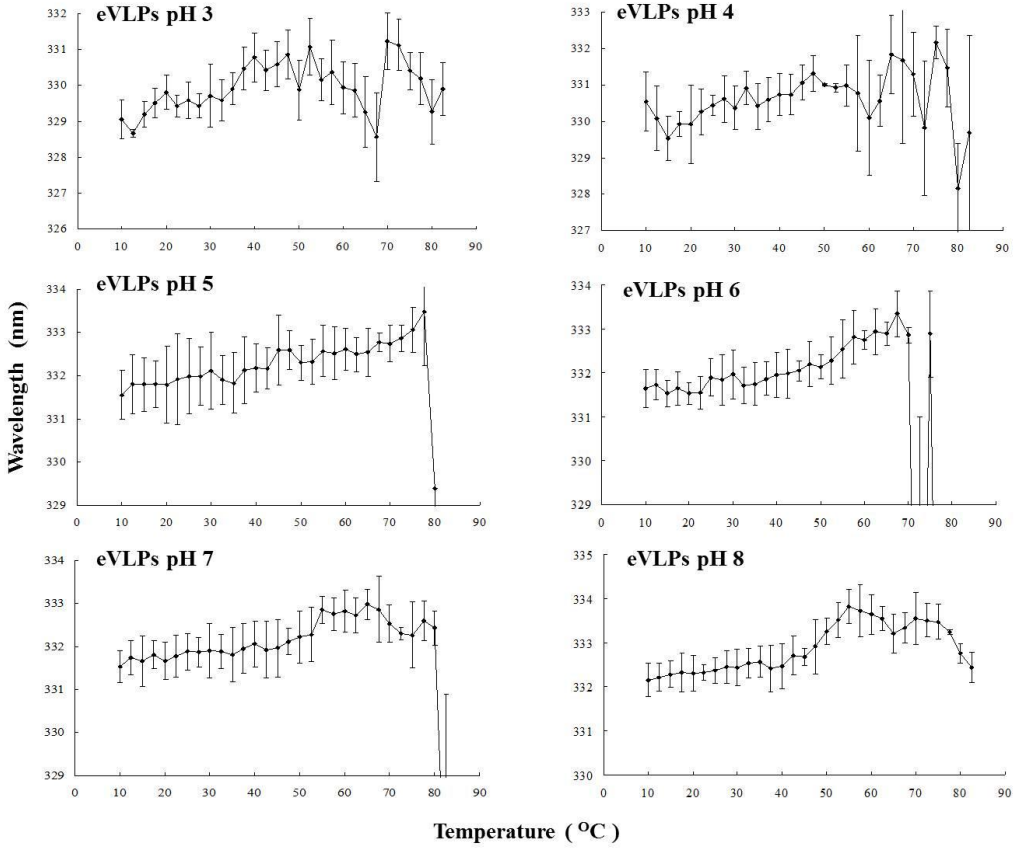

Figure 8. The change in intrinsic Trp fluorescence emission maximum (peak position) for eVLPs as a function of temperature and solution pH. Each data point represents the mean of three independent samples, and error bars show the standard deviation.

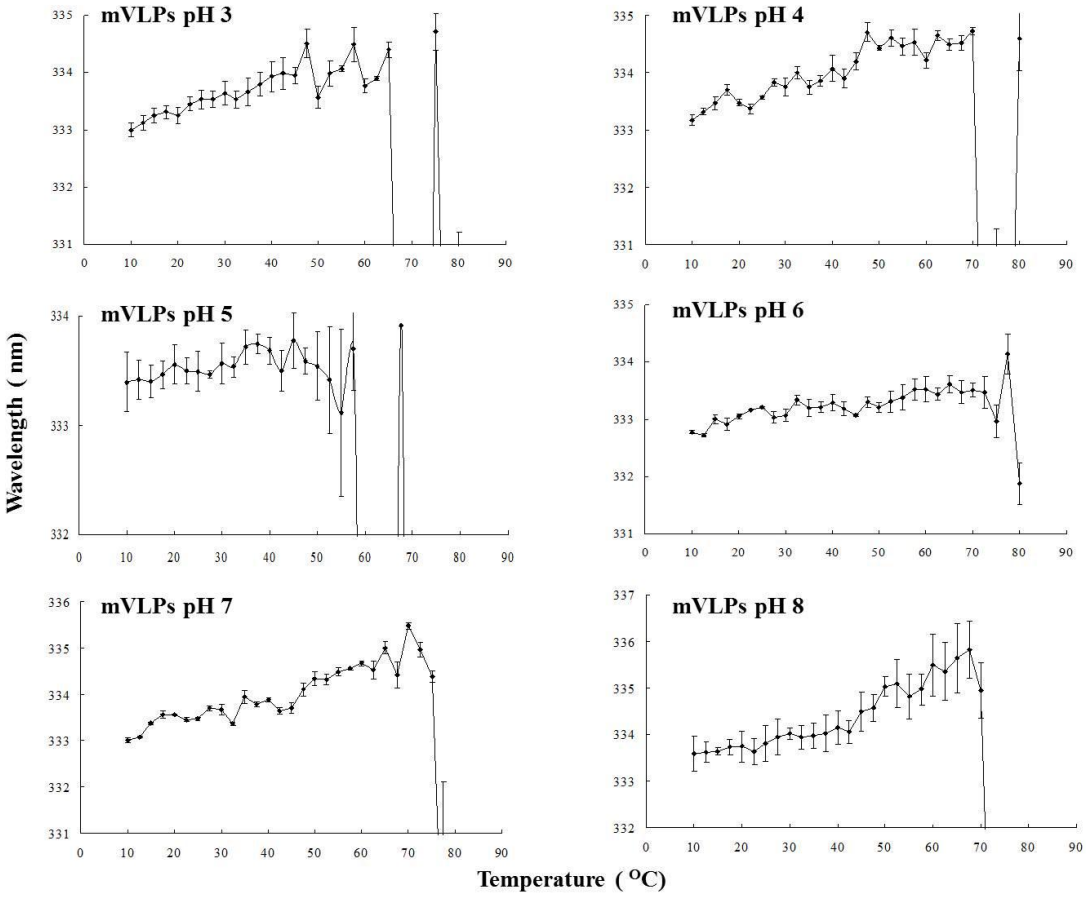

Figure 9. The change in intrinsic Trp fluorescence emission maximum (peak position) of mVLPs as a function of temperature and solution pH. Each data point represents the mean of three independent samples, and error bars show the standard deviation.

For mVLPs (Figure 9), the initial emission peak positions were observed around 333 nm over the entire pH range (3-8) suggesting an unchanged environment for Trp residues. Blue shifts occurred at approximately 65, 67, 57, 70, 72 and 70 ℃, respectively, as the solution pH ranged from pH 3 to 8. Samples at pH 7 and 8 also showed a transition in emission peak position near 45 ℃.

Figures 10 (A) and (B) illustrate the effect of temperature and pH on the fluorescence emission intensity of the eVLPs and mVLPs, respectively. There are no major thermal transitions observed except for samples at pH 5. Small transitions do occur, however, at lower temperatures for some pH values. Both VLPs at pH 7 and 8 manifest a linear response to temperature (decrease) as expected due to the intrinsic effect of temperature on fluorescence. Both VLPs at pH 6 show slight deviations from linearity. The transitions in fluorescence intensity measurements occurring at pH 5 and 6 appear to correspond to the shaper transitions present in the CD (225 nm) (Figures 6 and 7) and the static light scattering measurements (Figure 4). VLPs at pH 3 and 4 exhibited broad changes in fluorescence emission intensity with increasing temperature, except for the slight deviation from linearity of the eVLPs at pH 4 from 30 to 50 ℃. In summary, the effects of pH and temperature on the fluorescence of the VLPs are quite complex, reflecting a similar complex response of the overall conformational structure of the VLPs to these two forms of environmental stress.

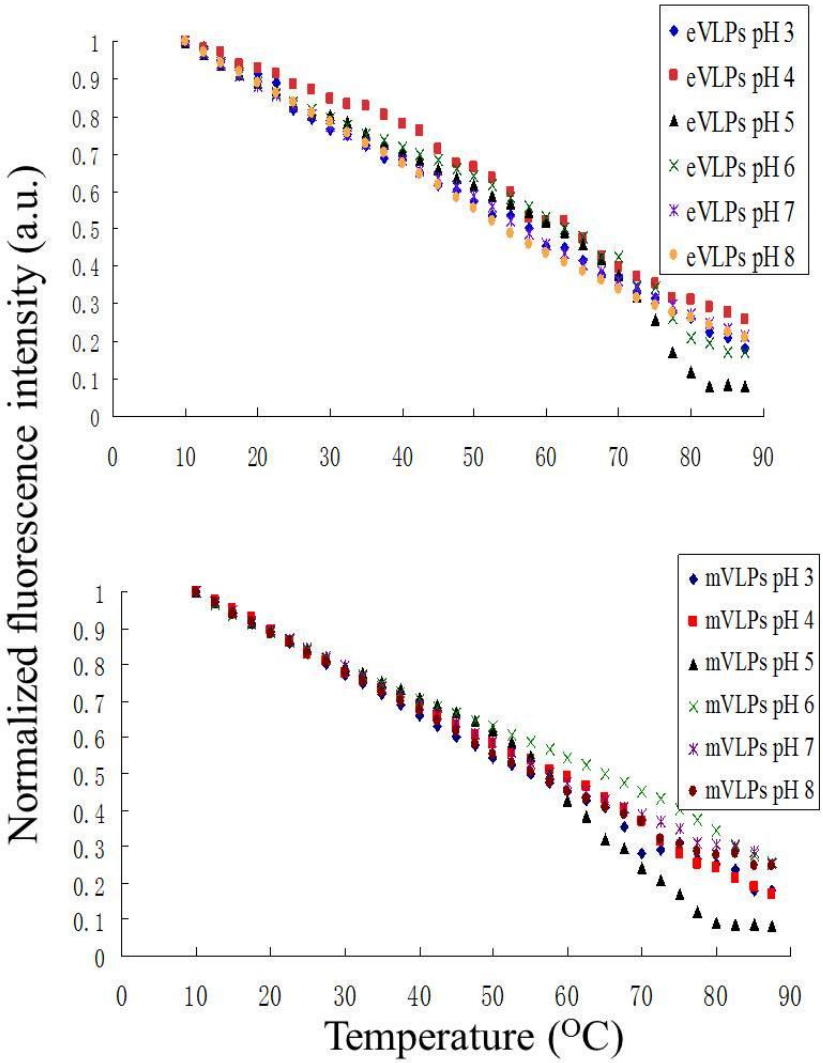

Figure 10. The intrinsic Trp fluorescence normalized intensities for eVLPs (A) and mVLPs (B) as a function of temperature and solution pH. (A): eVLPs from pH 3 to pH 8 on one plot. (B): mVLPs from pH 3 to pH 8 on one plot. Each data point represents the mean of three independent samples, and error bars show the standard deviation.

6.3.6 Extrinsic (Laurdan) Fluorescence

Emission from the fluorescent probe laurdan (2-dimethlyamino-6-lauroylnaphthalene) is sensitive to the polarity of its environment, in this case, the lipid component of the VLPs. Such immediate analyses are typically performed by measuring the relative intensities of two of the fluorophore's peaks in the form of a parameter known as the generalized polarization. Laurdan was used to characterize the membrane fluidity of the eVLPs and mVLPs under varying pH and temperature conditions. As the temperature was increased, the lipid bilayer became more fluid. The increased mobility within the membrane shifted the probe emission peak from 440 nm to around 480-490 nm, with excitation at 340 nm (data not shown). Thus, a decreased generalized polarization value with increasing temperature was observed for both VLPs as shown in Figures 11 and 12.

Broad thermal transitions (generalized polarization vs. temperature) were observed for both VLPs across the range of solution pH 3-8. Initial generalized polarization values at 10 ℃ varied for all pH values. The difference in initial generalized polarization values at 10 ℃ suggests differences in membrane fluidity as a function of pH. Samples at pH 3 had the highest initial generalized polarization values in both VLPs suggesting the lowest water density in the apolar interface environment. The eVLPs at pH 8 and mVLPs at pH 7 exhibited the greatest extent of membrane hydration at high temperatures (above 70 ℃). Both VLPs at pH 7 demonstrated a slower change of GP values with increasing temperature. A slower rate of change in generalized polarization values implies that membrane fluidity is less sensitive to temperature effects at these pH values.

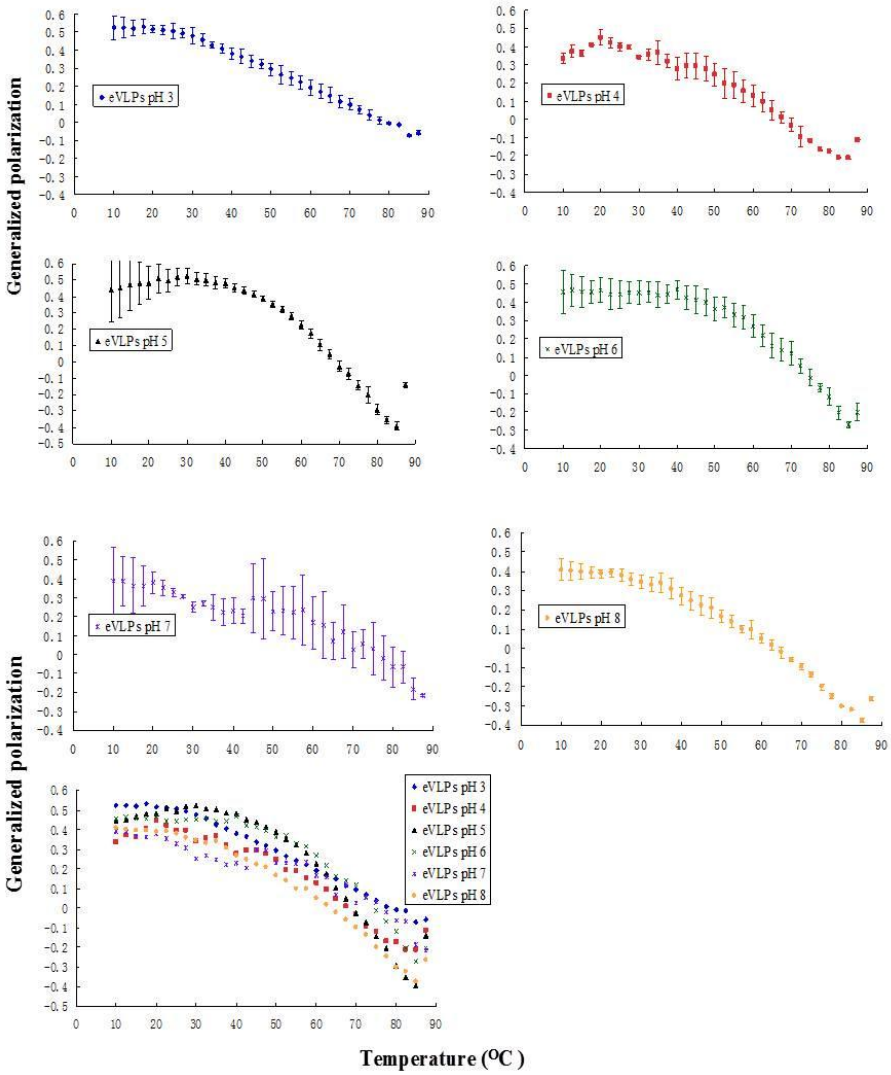

Figure 11. Generalized polarization (GP) of laurdan fluorescence in the presence of eVLPs as a function of temperature and solution pH. Each data point represents the mean of three independent samples, and error bars show the standard deviation. See methods section for determination of GP values.

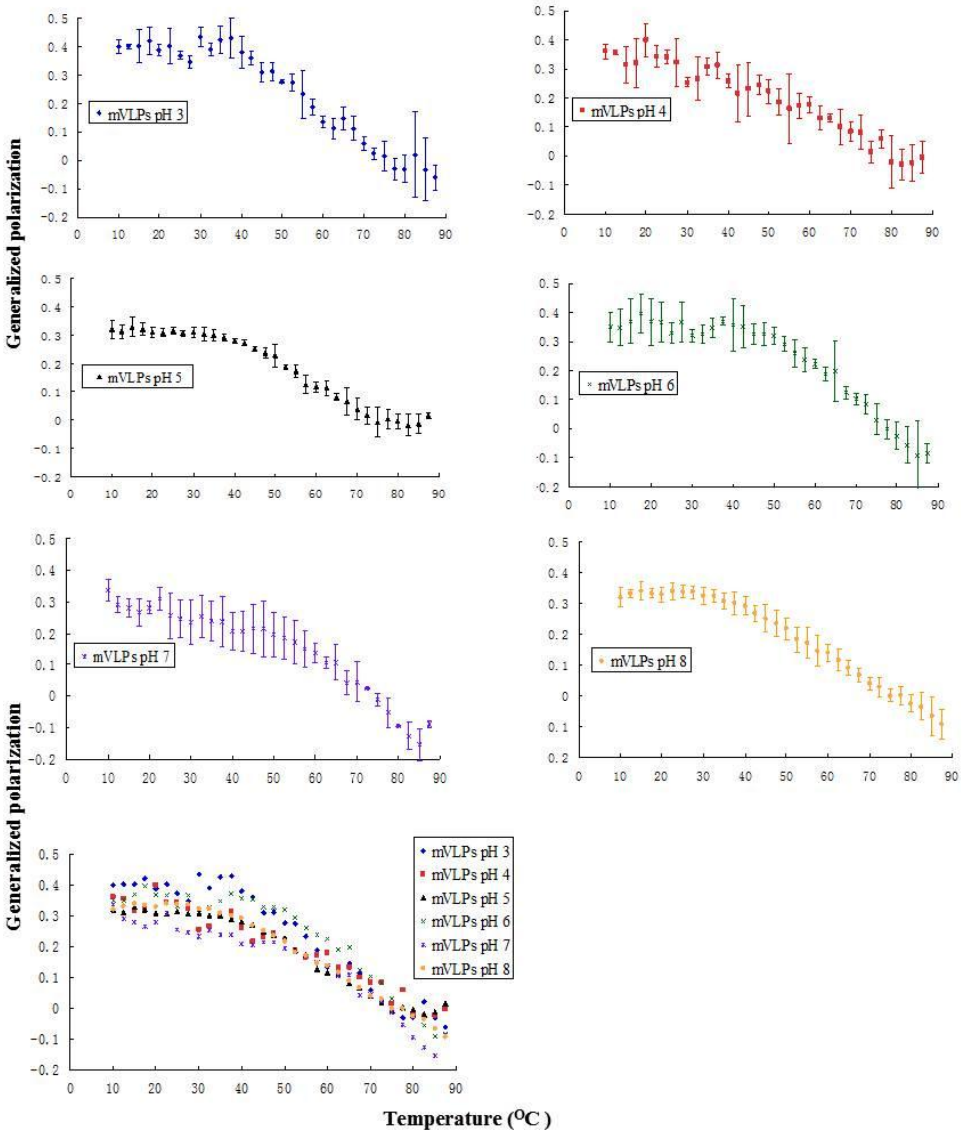

Figure 12. Generalized polarization (GP) of laurdan fluorescence in the presence of mVLPs as a function of temperature and solution pH. Each data point represents the mean of three independent samples, and error bars show the standard deviation. See methods section for determination of GP values.

6.3.7 Empirical Phase Diagrams

Empirical phase diagrams of eVLPs and mVLPs generated by the experiments (pH 3 to 8) without DLS results and produced from all experiments described (pH 5-8) were shown in Figures 13A-D. EPDs of two VLPs generated from all experiments (Figures 13 (B) and (D)) show similar defined "apparent" phases comparing those EPDs constructed without DLS results at the pH range of 5 to 8 (Figures 13 (A) and (C)). EPDs provide a convenient effective way to summarize large amounts of complementary data and provide a comprehensive view of VLP structural changes induced by change in environmental factors.[40,41] Due to the gradual signal changes observed in many of the techniques utilized in the study, especially for samples around neutral pH, there was some difficulty in defining the apparent phase boundaries to delineate the clear structural changes of eVLPs and mVLPs under neutral pH conditions.

In the case of eVLPs, there are approximately 4 different phases existing at low temperature (Figure 13A). In region 1, samples at pH 7 and 8 manifest a similar color (reddish blue) below 50 ℃. An intermediate phase is apparent at pH 5 and 6 (phase2/3), and a fourth phase is observed at pH 3 and 4. The distinction between these regions, and those at elevated temperatures, is evident with an apparent phase boundary progressing to a lower temperature as the pH is lowered. More heterogeneous region is present at elevated temperature with unique behavior at pH 6. Regions of gradual color change typically correspond to the broad, shallow transitions observed by different techniques.

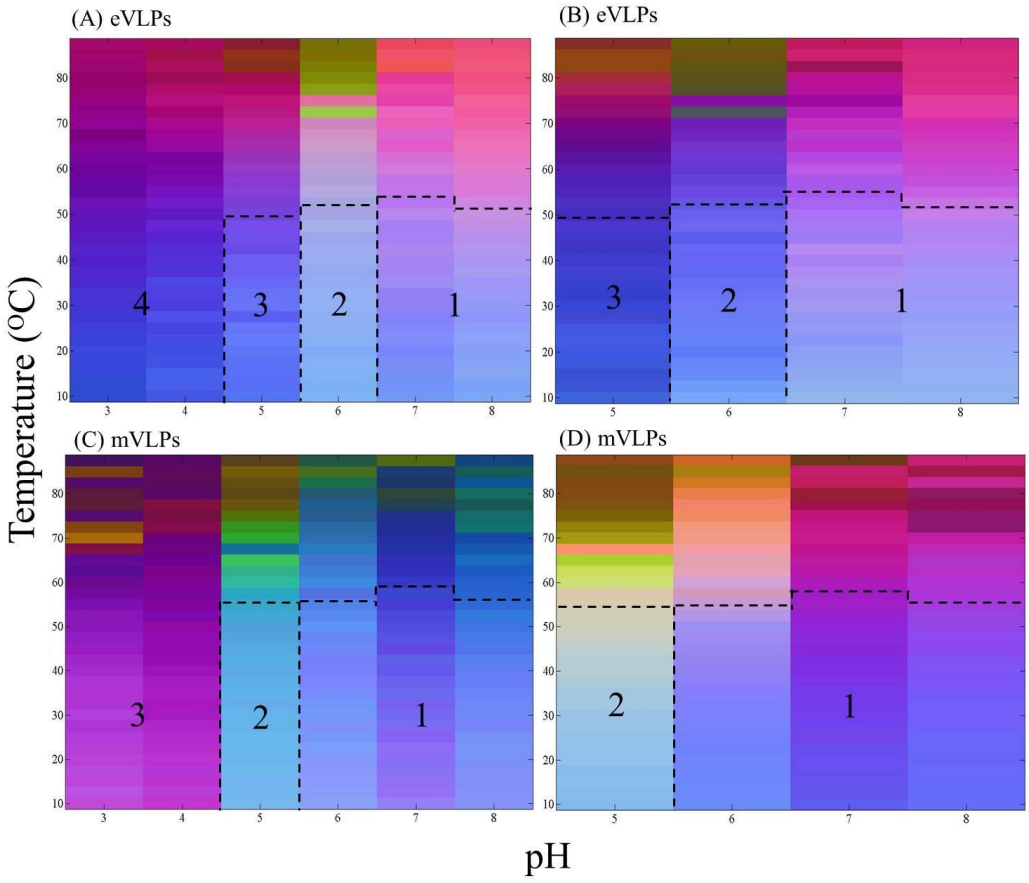

Figure 13. Empirical phase diagrams (EPDs) of the eVLPs (A and B) and mVLPs (C and D). EPDs in Figures A and C were constructed without using the DLS data, EPDs in Figures B and D were constructed using all data sets including DLS data. In the eVLPs (A), 1: Native like state and thermally stable; 2 and 3: Intermediate phase with marginal stability; 4: Structurally altered and prone to aggregation. In the mVLPs (C), 1: Native like state and thermally stable (less stable in sample at pH 6); 2: Intermediate phase with marginal stability; 3: Structurally altered and prone to aggregation. In original images, the color changes delineated by the dotted lines are more apparent. In addition, these transitions are also more evident in the data from specific techniques (see previous figures 3, 4 and 6 to 10). The EPDs were prepared from dynamic light scattering, static light scattering, CD at 225 nm, intrinsic fluorescence (peak position and normalized intensity), and extrinsic (Laurdan) fluorescence data collected across the pH range from 3 to 8 and temperature range from 10 ℃ to 87.5 ℃.

There are approximately 3 different apparent phases present at low temperatures observed for the mVLPs (Figure 13C). The pH and temperature behavior observed in the EPD for mVLPs is somewhat similar to the EPDs of the eVLPs. The heterogeneous nature of the high temperature region clearly reflects the presence of aggregates. A decrease in stability with the lowering of pH is also apparent for the mVLPs. In region 1, light scattering and CD (225 nm) data revealed that the mVLPs prepared at pH 6 were less thermally stable than those prepared at pH 7 and 8. In both cases, pH 7-8 appears to produce maximum stability.

6.4 DISCUSSION

The stability of proteins is generally investigated by a variety of spectroscopic, calorimetric, and hydrodynamic techniques that provide a diverse perspective on the response of protein structure to environment stress. These techniques can provide insight into different levels of protein structure (primary, secondary, tertiary, and quaternary), but no single spectroscopic or hydrodynamic technique can provide all of the desired information about protein structure and conformation. Therefore, several methods are typically combined to monitor various aspects of protein structure to obtain a better understanding of protein stability. In this work, several different spectroscopic and hydrodynamic techniques were employed to characterize the conformational stability of eVLPs and mVLPs over a wide range of temperature and pH. The physical data were combined to generate EPDs which provide a visual tool for characterizing structural alternations of macromolecules and their complexes under stress, caused by shift in pH and temperature.

The particles examined in this study primarily contain the NP, GP, and VP40 proteins of the corresponding viruses. Based on the estimated relative abundance of the three proteins in

the VLPs, their tryptophan contents, and with the assumption of similar emission from each indole side chain, their approximate contribution to the total Trp fluorescence would be about 50% (NP), 10% (GP) and 40% (VP40). Both NP and GP are highly helical proteins containing coils,[42-47] while VP 40 possesses approximately twice as much beta-sheet (30%) as helix (15%).[48] Based on these considerations, the intrinsic fluorescence spectra of the particles will primarily reflect the behavior of the NP and VP proteins while CD spectra should reflect primarily helical contributions from the NP protein. Contribution from the contaminating 64 KDa protein may also be significant but are unclear at this time.

Both eVLPs and mVLPs undergo conformational alternations induced by changes in temperature and pH. The EPDs reveal that the eVLPs and mVLPs have similar pH- and temperature-dependent stability profiles. At pH 3 and 4, both VLPs are structurally altered and highly aggregated at elevated temperatures. The VLPs are slightly more stable at pH 5 compared to those at pH 3 and 4, but undergo structural transitions at lower temperatures compared to samples at pH 6-8. These observations depict a phase in which the protein structure is highly altered. Furthermore, both VLPs at pH 6 are less stable than those prepared at pH 7 and 8, which can be illustrated by a shaper change of CD signal (225nm); earlier transition was observed using static light scattering and larger effective diameter was measured by DLS.

Greater stability and structural similarity are observed for eVLPs and mVLPs at pH 7 and 8. Both VLPs at pH 7 and 8 presumably contain folded protein components and a lipid bilayer demonstrating mild thermal resistance, as evidenced by the very low thermal

sensitivity; no detectable transitions were observed, as assessed by the techniques used in this study (except aggregation observed at high temperatures). Based on the analysis of EPDs and individual data sets, as measured by the different biophysical techniques, the overall stability results show that both VLPs manifest the highest stability at pH 7. The similarity of the physical characteristics of the two VLPs is not surprising, since previous studies have shown that they are nearly identical in structure and biochemical properties. Additionally, the actual EBOV and MARV show high similarities in the amino acid sequences of NP and VP40 structural proteins. Similarity is also evident in the N- and C- terminal regions of the GP protein.[15,16]

The overall secondary structure of both the eVLP and mVLP proteins were highly sensitive to pH as suggested by the different CD signal intensities and the shape of their CD spectra at different pH values. As indicated above, the presence of the minimum observed near 224 nm and a shoulder around 210 nm reflects the presence of the expected helical structure. The matrix protein VP40 contains more beta than alpha-helical structure,[48] but the surface glycoprotein, which is responsible for receptor binding and membrane fusion, contains significant amounts of helical structure.[45-47] This protein, however, is present in low amounts in the VLP preparations compared to NP and VP40. In contrast, the NP protein which is highly helical in nature and relatively abundant in the particles might be expected to dominate the protein signal in the CD spectrum. The CD studies clearly show major alternations in secondary structure at high temperatures and at lower pH (3-5). Both VLPs possess higher stability at neutral pH and much lower stability at pH 3 and 4 even at low temperature (10 ℃).

The tertiary structure of the VLPs was investigated by both intrinsic and extrinsic (Laurdan) fluorescence. The intrinsic fluorescence emission peak position of the eVLPs and mVLPs are around 332 nm and 333.5 nm, respectively. This observation suggests that the aromatic amino acid residues reside, on average, in a relatively apolar environment. This result could also reflect an effect of either the interior of the VLP proteins, and/or the hydrophobic regions of the lipid bilayer. The results from Laurdan fluorescence indicate that pH and temperature both affect the rate and extent of particle membrane hydration. As expected, the generalized polarization values decrease with increasing temperature. The initial generalized polarization values of the eVLPs are higher than those of the mVLPs at each pH value. This suggests that the eVLPs possess a more apolar interfacial region compared to mVLPs. This observation is consistent with the results obtained from the intrinsic fluorescence experiments, in which the initial peak positions of the eVLPs are smaller than mVLPs by 1-2 nm for all samples.

It is apparent that both VLPs have a strong tendency to aggregate at low pH and high temperature. This susceptibility to aggregation could potentially shorten the shelf life and decrease the biological activity of the VLP particles in inappropriate formulations. The sizes of the eVLPs and mVLPs are sensitive to changes in both pH and temperature. The VLPs aggregate more readily at lower pH. The DLS data clearly show that the eVLPs at pH 3 and 4 are highly aggregated and that the mVLPs at the same pH values also aggregate quickly with increasing temperature. In contrast to the DLS results, static light scattering data detected a lower intensity of scattered light for VLPs at pH 3 and 4 compared to samples under other pH

conditions. This discrepancy is presumably due to precipitation followed by particles settling. Particles at pH 7 and 8 again manifest the highest stability based on the light scattering data.

Stability optimization is an essential component of the vaccine-formulation process. Here, a combination of orthogonal physical techniques was employed to investigate the natural stability profiles of unformulated eVLPs and mVLPs as a function temperature and pH. The two VLPs show similar behavior in terms of their EPDs and have similar stability profiles. This study provides valuable information that could be used for the development of stable liquid formulations of VLP-based vaccines. More specifically, the EPDs constructed from the physical data facilitate the identification of formulation conditions for these vaccines and potential screening conditions for the identification of effective stabilizing excipients.

6.5 REFERENCES

1. Feldmann H, Klenk H 1996. Marburg and Ebola viruses. Advances in Virus Research 47:1-52.

2. Geisbert T, Hensley L 2004. Ebola virus: new insights into disease aetiopathology and possible therapeutic interventions. Expert Reviews in Molecular Medicine 6(20):1-24.

3. Sanchez A, Khan A, Zaki S, Nabel G, Ksiazek T, Peters C 2001. Filoviridae: Marburg and Ebola viruses. Fields virology 1:1279-1304.

4. Feldmann H, Jones S, Klenk H, Schnittler H 2003. Ebola virus: from discovery to vaccine. Nature Reviews Immunology 3(8):677-685.

5. Leroy E, Kumulungui B, Pourrut X, Rouquet P, Hassanin A, Yaba P, Délicat A, Paweska J, Gonzalez J, Swanepoel R 2005. Fruit bats as reservoirs of Ebola virus. Nature 438(7068):575-576.

6. Towner J, Amman B, Sealy T, Carroll S, Comer J, Kemp A, Swanepoel R, Paddock C, Balinandi S, Khristova M 2009. Isolation of genetically diverse Marburg viruses from Egyptian fruit bats.PLoS Pathog 5(7): e1000536.

7. Towner J, Pourrut X, Albariño C, Nkogue C, Bird B, Grard G, Ksiazek T, Gonzalez J, Nichol S, Leroy E 2007. Marburg virus infection detected in a common African bat. PLoS One 2(8).

8. Martini G 1973. Marburg virus disease. British Medical Journal 49(574):542.

9. Sullivan N, Yang Z, Nabel G 2003. Ebola virus pathogenesis: implications for vaccines and therapies. Journal of virology 77(18):9733.

10. Leffel EK, Reed DS 2004. Marburg and Ebola viruses as aerosol threats. Biosecurity and bioterrorism: biodefense strategy, practice, and science 2(3):186-191.

11. Borio L, Inglesby T, Peters C, Schmaljohn A, Hughes J, Jahrling P, Ksiazek T, Johnson K, Meyerhoff A, O'Toole T 2002. Hemorrhagic fever viruses as biological weapons: medical and public health management. Jama 287(18):2391.

12. Bray M 2003. Defense against filoviruses used as biological weapons. Antiviral research 57(1-2):53-60.

13. Peters C 2000. Are Hemorrhagic Fever Viruses Practical Agents for Biological Terrorism? Emerging infections:201-210.
14. Groseth A, Jones S, Artsob H, Feldmann H 2009. Hemorrhagic fever viruses as biological weapons. Bioterrorism and infectious agents: a new dilemma for the 21st century:169-191.
15. Sanchez A, Kiley M, Klenk H, Feldmann H 1992. Sequence analysis of the Marburg virus nucleoprotein gene: comparison to Ebola virus and other non-segmented negative-strand RNA viruses. Journal of General Virology 73(2):347.
16. Sanchez A, Kiley M, Holloway B, Auperin D 1993. Sequence analysis of the Ebola virus genome: organization, genetic elements, and comparison with the genome of Marburg virus. Virus research 29(3):215-240.
17. Geisbert T, Pushko P, Anderson K, Smith J, Davis K, Jahrling P 2002. Evaluation in nonhuman primates of vaccines against Ebola virus. Emerging Infectious Diseases 8(5):503-507.
18. Hart M 2003. Vaccine research efforts for filoviruses. International journal for parasitology 33(5-6):583-595.
19. Yang C, Ye L, Compans R 2008. Protection against filovirus infection: virus-like particle vaccines. Expert Review of Vaccines 7(3):333-344.
20. Warfield K, Deal E, Bavari S 2009. Filovirus infections. Journal of the American Veterinary Medical Association 234(9):1130-1139.
21. Bukreyev A, Collins P 2010. Filovirus vaccines: what challenges are left? Expert Review of Vaccines 9(1):5-8.
22. Warfield K, Swenson D, Demmin G, Bavari S 2005. Filovirus-like particles as vaccines and discovery tools. Expert Review of Vaccines 4(3):429-440.
23. McAleer WJ, Buynak EB, Maigetter RZ, Wampler DE, Miller WJ, Hilleman MR 1984. Human hepatitis B vaccine from recombinant yeast.
24. Garcea RL, Gissmann L 2004. Virus-like particles as vaccines and vessels for the delivery of small molecules. Current opinion in biotechnology 15(6):513-517.
25. Garland SM, Hernandez-Avila M, Wheeler CM, Perez G, Harper DM, Leodolter S, Tang GWK, Ferris DG, Steben M, Bryan J 2007. Quadrivalent vaccine against human

papillomavirus to prevent anogenital diseases. New England Journal of Medicine 356(19):1928.

26. Warfield K, Bosio C, Welcher B, Deal E, Mohamadzadeh M, Schmaljohn A, Aman M, Bavari S 2003. Ebola virus-like particles protect from lethal Ebola virus infection. Proceedings of the National Academy of Sciences 100(26):15889.

27. Warfield K, Swenson D, Negley D, Schmaljohn A, Aman M, Bavari S 2004. Marburg virus-like particles protect guinea pigs from lethal Marburg virus infection. Vaccine 22(25-26):3495-3502.

28. Warfield K, Olinger G, Deal E, Swenson D, Bailey M, Negley D, Hart M, Bavari S 2005. Induction of humoral and CD8+ T cell responses are required for protection against lethal Ebola virus infection. The Journal of Immunology 175(2):1184.

29. Swenson D, Warfield K, Negley D, Schmaljohn A, Aman M, Bavari S 2005. Virus-like particles exhibit potential as a pan-filovirus vaccine for both Ebola and Marburg viral infections. Vaccine 23(23):3033-3042.

30. Warfield K, Posten N, Swenson D, Olinger G, Esposito D, Gillette W, Hopkins R, Costantino J, Panchal R, Hartley J 2007. Filovirus like particles produced in insect cells: immunogenicity and protection in rodents. The Journal of infectious diseases 196:S421-S429.

31. Warfield K, Swenson D, Olinger G, Kalina W, Aman M, Bavari S 2007. Ebola virus like particle–based vaccine protects nonhuman primates against lethal Ebola virus challenge. The Journal of infectious diseases 196:S430-S437.

32. Sun Y, Carrion Jr R, Ye L, Wen Z, Ro Y, Brasky K, Ticer A, Schwegler E, Patterson J, Compans R 2009. Protection against lethal challenge by Ebola virus-like particles produced in insect cells. Virology 383(1):12-21.

33. Bavari S, Bosio C, Wiegand E, Ruthel G, Will A, Geisbert T, Hevey M, Schmaljohn C, Schmaljohn A, Aman M 2002. Lipid Raft Microdomains. The Journal of experimental medicine 195(5):593.

34. Swenson D, Warfield K, Kuehl K, Larsen T, Hevey M, Schmaljohn A, Bavari S, Aman M 2004. Generation of Marburg virus-like particles by co-expression of glycoprotein and matrix protein1. FEMS Immunology & Medical Microbiology 40(1):27-31.
35. Licata J, Johnson R, Han Z, Harty R 2004. Contribution of Ebola virus glycoprotein, nucleoprotein, and VP24 to budding of VP40 virus-like particles. Journal of virology 78(14):7344.
36. Ye L, Lin J, Sun Y, Bennouna S, Lo M, Wu Q, Bu Z, Pulendran B, Compans R, Yang C 2006. Ebola virus-like particles produced in insect cells exhibit dendritic cell stimulating activity and induce neutralizing antibodies. Virology 351(2):260-270.
37. Hartlieb B, Weissenhorn W 2006. Filovirus assembly and budding. Virology 344(1):64-70.
38. Boisgérault F, Moron G, Leclerc C 2002. Virus-like particles: a new family of delivery systems. Expert Review of Vaccines 1(1):101-109.
39. Kueltzo L, Ersoy B, Ralston J, Middaugh C 2003. Derivative absorbance spectroscopy and protein phase diagrams as tools for comprehensive protein characterization: A bGCSF case study. Journal of pharmaceutical sciences 92(9):1805-1820.
40. Ausar SF, Foubert TR, Hudson MH, Vedvick TS, Middaugh CR 2006. Conformational Stability and Disassembly of Norwalk Virus-like Particles. Journal of Biological Chemistry 281(28):19478.
41. Kissmann J, Joshi SB, Haynes JR, Dokken L, Richardson C, Middaugh CR H1N1 influenza virus like particles: Physical degradation pathways and identification of stabilizers. Journal of pharmaceutical sciences.
42. Watanabe S, Noda T, Kawaoka Y 2006. Functional mapping of the nucleoprotein of Ebola virus. Journal of virology 80(8):3743.
43. Noda T, Hagiwara K, Sagara H, Kawaoka Y 2010. Characterization of the Ebola virus nucleoprotein-RNA complex. Journal of General Virology 91(6):1478.
44. Mavrakis M, Kolesnikova L, Schoehn G, Becker S, Ruigrok RWH 2002. Morphology of Marburg virus NP-RNA. Virology 296(2):300-307.

45. Lee JE, Fusco ML, Hessell AJ, Oswald WB, Burton DR, Saphire EO 2008. Structure of the Ebola virus glycoprotein bound to an antibody from a human survivor. Nature 454(7201):177-182.
46. Malashkevich V, Schneider B, McNally M, Milhollen M, Pang J, Kim P 1999. Core structure of the envelope glycoprotein GP2 from Ebola virus at 1.9-Å resolution. Proceedings of the National Academy of Sciences of the United States of America 96(6):2662.
47. Watanabe S, Takada A, Watanabe T, Ito H, Kida H, Kawaoka Y 2000. Functional importance of the coiled-coil of the Ebola virus glycoprotein. Journal of virology 74(21):10194.
48. Dessen A, Volchkov V, Dolnik O, Klenk H, Weissenhorn W 2000. Crystal structure of the matrix protein VP40 from Ebola virus. The EMBO Journal 19(16):4228-4236.

Chapter 7 Conclusions

7.1 Summary and Conclusions

The current and projected rapid increase in the number of protein drug candidates in clinical development highlights the need for high throughput instruments and methods to be used in the development of stable protein formulations. Signature features of high throughput methods are used to analyze a large number of samples using small amounts of material over a short time with limited resource requirements.[1] The development of high throughput methods on currently available equipment is critical for the formulation development of protein drugs. High throughput methods can save material, time and resources, which are all typically constrained before and during a drug's clinical evaluation. They provide a quick and ideally comprehensive view of complex properties of protein molecules over a wide range of experimental conditions in a short time period. They will also add significant value to the success of product development, including less resource use, a shorter time to market and an increased chance of success over competitors. Thus, the development of high throughput methods can play a critical role in the development of protein-based therapeutics, and much recent attention and effort have been involved in this area.

In Chapter 2, I described the development of a reproducible, sensitive and robust method to investigate protein stability as a function of environmental stresses (pH and temperature in this case) by simultaneous data collection on a multifunctional instrument (the Chirascan-plus spectrometer).[2] The method was developed by using four model proteins, which have different molecular sizes, thermal transition temperatures and secondary structural components. The new method has the capability to acquire near- and far- UV CD, UV absorption and turbidity data simultaneously in a single sample. Fluoresence capability is

also demonstrated. The method allows us to get maximum protein structural information (secondary, tertiary and aggregation information) from a minimum amount of samples over a reduced experiment time. We estimated that the new method will save at least 40% of experimental samples and total data acquisition time will be substantially reduced compared to the same experiments performed on separate instruments. In combinaton with EPD data analysis, the method can be used to rapidly and comprehensively characterize the stability of biological systems in terms of their various structural levels with low sample requirements. The collection and evaluation of larger data sets of lower-resolution biophysical data by a high throughput method offers an alternative, more readily acessible and practical approach to rapidly evaluate protein structural integrity compared to higher resolution techniques such as X-ray crystallography and NMR. This new high throughput approach is useful for analysis of unknown proteins as well as screening for stable formulation conditions for protein drug candidates.

In Chapters 3 and 4, I applied the new method of Chapter 2 to characterize the conformational stability of anthrax rPA, its analogue 2-FHis rPA and its double mutant DNI. In these studies, the conormational stability of these three proteins were characterized comprehensively as a function of pH and temperature by employing the multimodal spectrometer. The stability profiles of 2-FHis rPA and DNI were created employing EPD data analysis. Similarities and differences in the propetries of rPA and the two mutants (2-FHis rPA and DNI) were also identified. Results showed that rPA and 2-FHis rPA had the most similar and the highest stability at pH 7 to 8. With decreasing pH, however, 2-FHis rPA was found to be more stable than rPA, especially at pH 4 and 5. Measurements of their dynamic

properties at pH 5 found that 2-FHis rPA was more dynamic under acidic pH conditions. For the DNI protein, results showed that the thermally stressed molecule completely retained its native structure up to temperatures as high as 70 ℃ for a month. The long-term stability of DNI was also demonstrated after refrigerated storage for about 8 years. More importantly, our collaborator's work (Solegenix.Inc) showed that animals vaccinated with an aluminum salt adjuvanted DNI-based vaccine developed high titer neutralizing antibodies that confer protection against anthrax infection.

PA is a protein antigen component in the currently used inactivated vaccine and provides a minimal level of protective immunity against anthrax infection. The current licensed U.S. anthrax vaccine (AVA, BioThrax) has a limited duration of protection, and requires multiple immunizations and yearly boosters.[3] The AVA is composed of PA inactivated with formaldehyde and an incompletely defined culture supernatant adsorbed to an aluminum salt adjuvant, so the purity of the vaccine is not easily determined. Therefore, there is a need to develop newer versions of anthrax vaccines such as those based on recombinant PA, which have a better defined composition and can produce longer-lasting immunity. Recombinant protein analogue of PA such as 2-FHis rPA and DNI are promising candidates. Previous research shows that both 2-FHis rPA and DNI can potentially provide therapeutic activity in antitoxic therapy because of their ability to inhibit cytotoxicity in cells.[4,5,6,7] In addition, DNI was also found to provide higher immunogenicity than PA in a mouse study.[7] The characterization data presented here provides enhanced information for the development of alternative, more stable and immunogenic anthrax vaccines using these two mutated anthrax protective antigens. In addition, the successful application of the new high

throughput method to characterize the stability of these proteins demonstrates the utility of this approach for the analysis of unknown proteins. The reproducibility, senstivity and robustness of the method are also demonstrated in these studies.

In Chapter 5, structural changes and aggregation behavior of the pneumolysin mutant (L460D) were monitored using various spectroscopic and light scattering techniques as a function of pH and temperature. Data were then summarized and analyzed by the empirical phase diagram method. The characterization data and EPD show that pneumolysin (L460D) is most stable in solution at pH 6- and loses its conformational integrity above about 48 ℃. Samples at pH 3 and 4, however, are much less stable and contain protein in a structurally altered state, even at low temperatures. In the following excipients screening study, potential stabilizers were identified and optimized by appropriate assays. Sugars such as trehalose and sucrose show stabilizing effects on pneumolysin with respect to improving thermal transition temperatures and minimizing its aggregation. Pneumolysin shows efficient binding to aluminum hydroxide. The stability of pneumolysin on the surface of alhydrogel does not seem to be affected by adsorption to the adjuvant, either with or without excipients. Finally, an optimal formulation containing 15% trehalose in 10 mM histidine buffer at pH 6 was identified.

The development of recombinant protein-based vaccines offers an alternative way to produce cheaper, robust and broader coverage pneumococcal vaccines in comparison to current polysaccharide and conjugate based vaccines. Pneumolysin is a lead vaccine candidate and has been long known to be immunogenic. The characterization and formulation studies described above provide valuable information to aid in the development of stable

formulation for a recombinant pneumolysin antigen (L460D) as a pneumococcal vaccine that has the potential to be potent against all pneumococcal serotypes and therefore provide broader protection.

In Chapter 6, the work focuses mainly on the preformulation development of eVLP-and mVLP-based vaccines. Preformulation stability data of VLPs aids in the design of a rational strategy to begin development of a final formulation. The VLPs examined in this study primarily contain the nucleoprotein (NP), glycoprotein and viral protein 40 (VP40) of the corresponding viruses. Therefore, several proteins contribute to the observed biophysical characterization results. The glycoprotein is present in low amounts in the VLP preparations compared with NP and VP40. Both NP and GP are primarily helical proteins containing coils, while VP 40 possesses approximately twice as much beta-sheet (30%) as helix (15%). The above properties of each protein need to be considered during the interpretation of the results obtained with the VLPS. The conformational stability of Ebola and Marburg VLPs was characterized by various techniques. Temperature/pH EPDs of the two VLPs were also constructed to analyze the large volume of data generated. The EPDs showed that both VLPs lost their conformational integrity above about 50-60 ℃, depending on solution pH. The VLPs were maximally thermal stable in solution at pH 7-8, with a significant reduction in stability at pH 5 and 6. They were much less stable in solution at pH 3-4 due to increased susceptibility of the VLPs to aggregation.

In summary, studies in Chapters 5 and 6 provide a description of the physical properties of a pneumolysin mutant (L460D) and Ebola and Marburg VLPs under a range of solution conditions (pH, temperature, ionic strength and solute). The information obtained

provides a basis for the rational design of long- term stable pharmaceutical formulations. The utility of the three step experimental design described in the Abstract is also illustated. Instead of collecting data from the individual, single-function instruments used in Chapters 5 and 6, the use of the multimodal spectrometer method developed in Chapter 2 should provide an alternative and effective way to characterize stability in the preformulation and formulation stages of development of protein-based drugs.

7.2 Future Directions

In Chapters 2, 3 and 4, a reproducible, accurate and sensitive method was developed and applied to characterize the stability of model and therapeutic proteins as well as to compare them in terms of various levels of macromolecular structure. In combination with EPD data analysis, a conformational stability profile of a protein as a function of pH (3-8) and temperature (10-87.5 ℃) can be obtained within 3 days by using only about a 200 μg of protein sample in each sample run.

The process required to collect data and generate an EPD for individual proteins still can be accelerated by developing improved instrument software, a new generation of multifunctional instruments, and automated EPD data analysis software. First, the major instrument parameter of sampling time can be further optimized by improving current instrument software. Because the peptide sensitive CD signals in the far-UV region are much stronger than the aromatic CD signals in the near-UV, a much shorter sampling time such as 1s or 0.5s can be applied in the far-UV CD measurements while retaining the longer optimized sampling time of 3s in the near-UV. The reproducibility of far-UV CD results is not compromised by reducing the sampling time (data not shown). The setting of different

sampling times in near- and far- UV regions can be achieved by further developments of the instrument's software. The capability of varying the sampling time can also save about 30% of total data acquisition time compared to the current method of data collection. Second, time and energy can also be saved by developing and using an improved multimodal spectrometer. The instrument company (Applied Photophysics Ltd, Leatherhead, UK) has developed a new generation of CD spectrometers called "Chirascan-plus ACD Auto CD spectrometer", which has an automated sampling system and a robotic work station. It employs a fully integrated, state-of-the-art robotic system providing unattended automation for up to 4x96 well plates. Applying the new method (Chapter 2) in this new instrument, it should be straightforward and permits the analysis of unattended overnight samples instead of switching batches manually during each day.

Lastly, the new method can be improved by using automated EPD data analysis software. Our lab is developing a software tool to perform such automated analysis of large combined data sets. This new software can perform mathematical, graphical and file operations effectively.[8] Use of the new method with the Chirascan and automated EPD data analysis will offer an efficient approach that provides comprehensive biophysical data of a protein with minimal sample and experiment time requirements. The new method has currently primarily been used for the characterization of the physical stability of proteins. This approach can also be used as a high-throughput analytical strategy to screen for stabilizing agents and thus more efficiently design optimally stable formulations for protein therapeutic drug candidates in the future. It should be applicable to more complex systems such as viruses as well as nucleic acids.

In Chapters 5 and 6, the preformulation and formulation work of Ebola and Marburg VLPs and the pneumolysin (L460D) provide some key stability data that can be of significant aid in the design of final liquid-formulations for these candidate vaccine antigens. The influence of various factors such as solution pH, temperature, buffer ion, salt, protein concentration and excipients on physical stability of these macromolecules was identified. Other formulation studies that need to be performed in the future are photostability, cavitation/shaking, freeze-thaw cycling, preservatives and material compatibility. All of these studies are used to address different aspects of protein stability in solution formulations and enable the rational development of a final liquid formulation. The accelerated stability studies provide rapid identification of formulation conditions and an improved understanding of the physicochemical characteristics of the protein molecule. They also provide information concerning which formulation conditions would be most suitable to maintain the stability of the protein. Long term stability studies, however, still need to be performed under the selected storage conditions over the desired storage period (1-3 years).[9] In this period, the toxicity and immunogenicity studies will also need to be evaluated.

In this dissertation, I presented my work on (1) Development and application of the high throughput method for the biophysical characterization of protein stability; and (2) Stability characterization and formulation of a pneumolysin (L460D) and Ebola and Marburg VLPs. Characterization and formulation of protein-based drugs and vaccines is a complex process, which requires the selection and combination of appropriate analytical methods. For the first part of my work, the new high throughput method employing the multifunctional instrument provides an effective approach to rapidly evaluate protein structural integrity with

low sample requirements. There is, however, still room to further improve the efficiency of the method with the new automated sampling system of instruments and the new EPD data analysis software. For the second part of my work, other future experiments are necessary to conduct studies such as freeze-thaw, shaking, photostability, material compatibility and long-term stability in order to develop stable final vaccine formulations of these protein antigens.

7.3 References

1. Samra, H. S.; He, F., Advancements in High Throughput Biophysical Technologies: Applications for Characterization and Screening during Early Formulation Development of Monoclonal Antibodies. *Molecular Pharmaceutics* **2012,** 9(4), 696-707.
2. Hu, L.; Olsen, C. M.; Maddux, N. R.; Joshi, S. B.; Volkin, D. B.; Middaugh, C. R., Investigation of Protein Conformational Stability Employing a Multimodal Spectrometer. *Analytical chemistry* **2011,** 83(24), 9399-9405.
3. Wright, J. G.; Quinn, C. P.; Shadomy, S.; Messonnier, N., Use of anthrax vaccine in the United States. *Morbid Mortal Wkly Rep* **2010,** *59*.
4. Wimalasena, D. S.; Cramer, J. C.; Janowiak, B. E.; Juris, S. J.; Melnyk, R. A.; Anderson, D. E.; Kirk, K. L.; Collier, R. J.; Bann, J. G., Effect of 2-fluorohistidine labeling of the anthrax protective antigen on stability, pore formation, and translocation. *Biochemistry* **2007,** *46* (51), 14928-14936.
5. Wimalasena, D. S.; Janowiak, B. E.; Lovell, S.; Miyagi, M.; Sun, J.; Zhou, H.; Hajduch, J.; Pooput, C.; Kirk, K. L.; Battaile, K. P., Evidence that histidine protonation of receptor-bound anthrax protective antigen is a trigger for pore formation. *Biochemistry* **2010,** 49, 6973-6983.
6. Sellman, B. R.; Mourez, M.; Collier, R. J., Dominant-negative mutants of a toxin subunit: an approach to therapy of anthrax. *Science* **2001,** *292* (5517), 695-697.
7. Aulinger, B. A.; Roehrl, M. H.; Mekalanos, J. J.; Collier, R. J.; Wang, J. Y., Combining anthrax vaccine and therapy: a dominant-negative inhibitor of anthrax toxin is also a potent and safe immunogen for vaccines. *Infection and immunity* **2005,** *73* (6), 3408-3414.
8. Maddux, N. R.; Rosen, I. T.; Hu, L.; Olsen, C. M.; Volkin, D. B.; Middaugh, C. R., An improved methodology for multidimensional high‐throughput preformulation characterization of protein conformational stability. *Journal of pharmaceutical sciences* **2012,** 101(6), 2017-2024.
9. Arakawa, T.; Prestrelski, S. J.; Kenney, W. C.; Carpenter, J. F., Factors affecting short-term and long-term stabilities of proteins. *Advanced drug delivery reviews* **2001,** *46* (1-3), 307-326.